Numerical Modelling of Drying Processes in a Mixed-flow Grain Dryer Based on Coupled Discrete Element and Computational Fluid Dynamics Method

by

Xinyi Wu

A Thesis submitted to the Faculty of Graduate
Studies ofThe University of Manitoba
in partial fulfillment of the requirements of the degree of

DOCTOR OF PHILOSOPHY

Department of Biosystems Engineering
University of Manitoba
Winnipeg

Abstract

The main objective of this research was to develop a numerical model to simulate the transport phenomena involved in the grain drying processes in mixed-flow grain dryers by coupling the discrete element method (DEM) and computational fluid dynamics (CFD), and utilize the proposed model for the design assessment and optimization of mixed-low grain dryers. The formation of the grain bed and the movement of the grain kernels were simulated by the proposed DEM model which was developed using a commercial software package PFC^{3D} (Particle Flow Code in Three Dimension, Itasca Consulting Group, Inc. Minneapolis, MN). Heat and mass transfer, as well as the air flow pattern were solved in the proposed CFD model, which was developed in ANSYS Fluent 2022. The coupling between the DEM and CFD models was realized by custom-coded algorithms in Matlab (Version 8.4) following a quasi-static fashion, i.e., each simulation was run incrementally in the time domain and the simulation results (data) were transferred between the CFD and DEM models after each time increment. The coupled CFD-DEM, as well as component DEM and CFD models, was validated against experimental data extracted from the literature in terms of grain temperature and moisture content distribution, as well as grain movement and airflow pattern. Close agreements were achieved between simulated results of the coupled CFD-DEM model and published experimental data, with an average difference of 4.3% for grain temperature and 2.5% for grain moisture content.

The model revealed the detailed distribution patterns of grain movement, temperature and moisture content. Specifically, the grain movement was slowed down by the air ducts and dryer walls, causing nonuniform distribution of grain velocity across the dryer, with the lowest velocity at about 43% of the highest velocity. The low-velocity zones were found underneath the air ducts. This nonuniform distribution of grain velocity resulted in large disparities in the residence time of drying, with the longest residence time (66 min) being 3.3 times the shortest one (20 min) while the median time was 36 min. There were considerable variations in grain temperature within the drying column, with the highest grain temperature underneath the inlet air ducts, while “cold zones” existed in the near-wall region. The grain moisture content was not uniform across the dryer, with the lowest moisture content underneath the inlet air duct and the higher moisture near the dryer walls.

Using empirical models in the literature, the potential reduction in grain quality during drying was estimated in terms of risks of germination reduction and fissure (stress cracking) of grain kernels, which were predicted based on the grain temperature and moisture simulated by the coupled CFD-DEM model. A valuable function of the model was the ability to predict the zones within the dryer where grain could potentially experience quality losses. These zones were generally located underneath the inlet air ducts.

The model was also applied to assessment of different duct designs and layouts in mixed-flow grain dryers. It was found that the air ducts with 60-degree angles resulted in the best drying performance among the five duct geometries that were simulated. The best layout had the ratio of vertical distance to duct height of 1.35 and the ratio of horizontal distance to duct width of 1.5.

Acknowledgements

I would like to express my special appreciation and thanks to my advisors Dr. Qiang Zhang and Dr. Stefan Cenkowski, not only for their advice, continuous guidance and constant encouragement, but for the room for me to grow freely and to nurture my independent research ability throughout my PhD program. I would also like to thank my committee members: Dr. Fuji Jian and Dr. Filiz Koksel for their valuable suggestions during committee meetings. I would like to thank Dr Ying. Chen for giving me access to the PFC^{3D} software.

I also wish to thank all my lab members: Dr. Xiaojie Yan, Dr. Amy La-Guzman and Mr. Chenchen Sun for their technical assistance and friendship.

I wish to express my deep gratitude to my parents for their unconditional love and support. Without their support, I could not have been here and finished my study.

Also, thanks are due to everyone not mentioned but most important not forgotten.

Dedication

To all the researchers who devoted their heart, sweat and tears to the study of grain drying and grain storage.

Table of Contents

List of Tables

List of Figures

1. Introduction

The purpose of grain drying is removing moisture from grain down to a specific moisture content for safe storage; this process is governed by the combined effects of heat and mass transfer both within grain kernels and between grain kernels and (hot) drying air. In typical grain dryers, hot air is blown through the grain bulk and exposure to heat may cause biological and chemical changes in grain such as nutritional loss, enzymatic reactions, aroma and color changes, fat oxidation and microbial degradation, which are critical attributes of grain quality. Improperly-designed grain drying systems can result in severe energy waste, degradation of grain quality, and shortened storability (Keppler et al., 2012; Mao et al., 2016; Mellmann et al., 2011). According to a report of Food and Agriculture Organization of the United Nations, the losses of cereal grain and beans in drying operation were estimated to be 8% of the total production globally in 2019 (FAO, 2019). Optimizing the design of mixed-flow grain dryers is necessary to prevent grain losses and maintain grain quality in drying operations. Prototyping new designs in the optimization process can become very time consuming and expensive, which is undesirable. An alternative method is to incorporate numerical simulations into the design process as they are not only fast and cost-effective, but they can also provide deeper insights into the heat and mass transfer phenomena, as well as airflow behavior during drying.

1.1 Problem statement

Grain drying is a well-established unit operation and the research into grain drying could be dated back to 1920s (Hall, 1987). However, the design of commercial grain dryers has been mostly based on empirical formulas and experiences. For example, mixed-flow grain dryers are the most widely used around the world, but our understanding of heat and mass transfer within the flowing grain mass is still limited and most published studies are focused on dynamic or smart control of drying process (Menshutina and Kudra, 2001; Zhang et al., 2006). In addition, as drying processes consume substantial amount of energy, it stands to gain significantly from enhancements in current

dryer design in terms of cost reduction. Thus, there is a strong need in advancing the knowledge and technologies to optimize the design of mixed-flow grain dryers.

The typical approach to solving grain drying problems involves conducting physical experiments and developing empirical models based on the collected data (Thompson, 1968; Valença and Massarani, 2000; Wang and Singh, 1978). However, performing grain drying experiments is challenging and resource-intensive, requiring significant time, financial investment, and labor. Furthermore, many existing empirical models lack robustness because many factors, such as airflow rate, air temperature, grain characteristics, and air duct design, may significantly impact the drying process (Dai and Cao, 1965), and it is almost impossible to include all these factors and their interplays in experiments. With rapid advances in computer technology, mathematical (computer-based) modelling has the potential to provide a tool for analyzing grain drying processes.

1.2 Objectives

This thesis research attempted to use the DEM (discrete element method) to model the grain movements and the pore structures of moving grain beds in mixed-flow dryers, and based on the proposed DEM model, CFD (computational fluid dynamics) was used to predict airflow and heat and mass transfer during drying.

The main objective of this research was to develop an integrated numerical model to simulate the transport phenomena involved in grain drying process in mixed-flow grain dryers by coupling DEM and CFD, and utilize the proposed model for the performance assessment and optimization of mixed-flow grain dryers. The specific objectives were:

1) to develop a DEM model to simulate the grain kernel movements in mixed-flow grain dryers,
2) to develop a CFD model to simulate airflow, and heat and moisture transfer in mixed-flow grain dryers,
3) to couple the CFD and DEM models, as well as empirical grain quality models to predict drying processes in mixed-flow grain dryers and changes in grain quality during drying,

4) to validate the DEM, CFD and coupled CFD-DEM models based on experimental data extracted from published experimental studies,
5) to use the coupled DEM-CFD model to perform parametric studies to evaluate the designs of air ducts in mixed-flow dryers, and
6) to explore the potential of using the coupled DEM-CFD to assess grain quality changes during drying.

1.3 Research contributions and applications

Mathematical models of grain drying grounded in the physical principles of fluid flow through porous media have the potential to integrate the effects of the key draying parameters on airflow and heat and mass transfer. However, when simulating grain drying, existing CFD models were usually limited by their assumptions of grain bulk homogeneity in terms of pore distribution and treating the moving grain bed as a stable porous medium (Langrish and Fletcher, 2001; Turgut et al., 2021). In reality, the grain bulk within dryers is non-homogeneous, with varying porosity as the grain moves through the dryer. Airflow and heat and mass transfer depend on the interstitial pore structure of grain bulk, which is intricate, heterogeneous, interconnected, and highly tortuous. The assumption of a simple homogeneous pore structure can significantly impact the accuracy of simulated airflow, as well as heat and mass transfer in grain drying processes, such as air velocity and static pressure distributions (Nwaizu and Zhang, 2021). DEM models are capable of simulating complex variability in pore structures of porous materials, such as bulk grains. Considering the complex variability in pore structure is crucial for modelling the drying processes. The coupled CFD-DEM method proposed in this study combined the strengths of DEM in modeling pore structures and CFD in modelling airflow and heat and mass transfer in porous media. The coupled DEM and CFD model had the potential to improve prediction of grain drying.

The proposed model could also be applied for dryer design optimization or performance assessment. As prototyping new designs and conducting drying experiments for performance assessment could be very costly in time, money and labour. Incorporating numerical simulations into the design processes is not only fast and cost-effective but may also provide deeper insights into the heat and mass transfer phenomena during drying. The proposed DEM-CFD method had the capability

to simulate the movement, moisture and temperature of every grain kernel in the dryer, as well as the airflow distribution within the dryer. Such information is important for assessing the performance of a design (whether zones with extreme grain temperature or grain velocities exist) in contrast to conducting design optimization and performance evaluation with experimental methods, where the measurement of moisture content and temperature is usually only taken at several sampling points (Cenkowski, 1985; Dai and Cao, 1965; Valença and Massarani, 2000).

Coupled DEM and CFD modelling opens a new pathway for investigating the mass and energy transport phenomena in grain drying, as well as for the design optimization and performance evaluation of mixed-flow grain dryers.

1.4 Thesis structure

Chapter 1 outlines the problem revolving around mixed-flow grain dryers and the limitations of existing studies of grain drying. The objectives of the proposed study are introduced, followed by the expected research contributions and applications.

Chapter 2 first summarizes different types of commercial grain dryers. A review grain drying models is also presented in this chapter, which included general models for describing heat and mass transfer phenomena, semi-empirical and empirical thin-layer drying models, and numerical models for describing grain drying.

Chapter 3 is focused on the methodology for modelling of the drying processes in a mixed-flow grain dryer based on coupled DEM and CFD. This chapter starts with introducing the configurations of the simulated mixed-flow grain dryer and the physical properties of grain which were needed for the simulations. The DEM model for modelling grain kernel movement, the CFD model for modelling heat and mass transfer, and coupling CFD and DEM models are presented, followed by the methods for model validation with published experimental data. Finally, this chapter ends with a description of methods for analyzing the grain kernel damage during drying.

Chapter 4 is dedicated to the presentation and discussion of results produced by the proposed DEM-CFD models. This chapter starts with the results of mesh optimization tests, followed by the model validation results where simulated results were compared with published experimental data. In this chapter, the distribution of airflow, grain velocity, residence time of drying, grain moisture content and

temperature simulated by the proposed DEM-CFD models are discussed in detail based on parametric studies. Influence of duct design and layout on dryer performance is discussed by comparing the variation and uniformity of grain temperature, moisture content and residence time in different dryer designs. Case-studies are presented to demonstrate the potential of the coupled DEM-CFD model in assessing the grain quality degradation during drying, as well as the influence of duct design and layout.

Chapter 5 presents the summary and conclusions of this study.

Chapter 6 summarizes recommendations for future work based on findings in this study in terms of model assumptions, model validation, the impact of drying on grain quality and dryer operation.

2. Literature Review

2.1 Grain dryers

Grain drying operation is a common practice on-farm or at large grain storage depots to lower grain moisture content for safe storage of grain. Depending on the mode of drying operation, grain dryers can be divided into two types, continuous grain dryers and batch grain dryers. The choice of dryer is usually determined by the production capacity and the drying characteristics of the product. Batch dryers are suitable for slow-drying or heat-sensitive grains, and they are smaller in scale compared to continuous dryers, thus are commonly adopted for on-farm usage (Kerr, 2013). In batch dryers, grain is loaded into the drying chamber and left until drying is complete (Kerr, 2013). Large-scale, high efficiency dryers are generally continuous drying systems, in which moist grain is fed to the dryer continuously from the top of drier and dried grain is collect at the bottom of dries, while drying air is forced through the moving grain bed in the drier. Based on the relative directions of air flow and grain flow, grain drying systems can be divided into cross-flow, concurrent-flow, counter-flow and mixed-flow grain dryers.

2.1.1 Cross-flow grain dryers

Cross-flow grain dryers are named, because of the “cross-wise” direction of grain flow relative to the direction of air flow. In a typical cross-flow grain dryer, grain flows under gravity between two perforated metal screens comprising the drying columns, while heated air is forced by an axial or centrifugal fan and then heated by a burner using direct combustion of propane or natural gas, before entering the drying column in the direction perpendicular to the direction of air flow. The height of the drying column in an on-farm cross-flow drying system is around 4 m, while commercial cross-flow drying systems could be as tall as 30 m; unloading feed-roll augers, which are located at the bottom of the dryer columns, mix and convey the grain out (Mukhopadhyay et al., 2019). In the United States, cross-flow column dryers are the most widely used rice dryers, because of its simplicity in structure and reliability (Mukhopadhyay and Siebenmorgen, 2018). Manufacturer of cross-flow grain dryers include Berico, Zimmerman, Airstream, Superb, Behlen, FF, GSI, M-C etc. One main drawback of this type of dryers is the non-uniformity: the grain moisture content at the far end from the inlet of hot air could be considerably higher than the grain close to the inlet, which may lead to the damage in grain quality (Thompson, 1969). It is also

worth noting that this type dryers usually require more than one round of drying operation to achieve the final moisture content for safe storage, and tempering process usually needs to be considered to maintain grain quality (Thompson, 1969).

Research related to cross-flow grain dryers are mainly focused on tackling the grain "non-uniformity" in four possible ways:

a. Circulating the grain

Circulation devices could be installed between the two perforated metal screens to allow for better grain mixing. This approach can not only reduce the variation in the moisture content of the final product but reduce the variation in grain temperature as well. It is reported that applying one to three sets of circulation devices to a grain bed of 31cm can reduce the variation in grain moisture content by 53 to 63 percent at the cost of a higher energy consumption rate (Thompson, 1969).

b. Applying a differential unloading rate

Two sets of feed-roll augers could be installed at the bottom at drying column and set to different rates so that the grain close to the entrance of hot air has experience shorter time of drying. Blount Inc. adopted a differential unloading rate of 4:1 and a noticeable improvement in uniformity was achieved ("Oregon Tools," 2023).

c. Applying a multi-stage system

The drying column could be divided into two or more stages. Each level may apply a different hot air temperature and/or a different air flow direction. This prevents the overheated grain from moving near to the hot air inlet (Bakker-Arkema et al., 1969).

d. Grain tempering

Tempering is a standard practice in most commercial rice drying processes (Dong et al., 2009; Mukhopadhyay et al., 2019; Tolaba et al., 1999). It was reported that for heated air drying, tempering at the drying air temperature for a sufficient duration is important for intra-kernel material state equilibration which contributes to uniformness of final product (Mukhopadhyay et al., 2019).

2.1.2 Concurrent-flow grain dryers

In concurrent-flow grain dryers, grain flow and heated air flow are in the same direction. In a typical commercial concurrent-flow grain dryer, grain flows downwards under gravity while air

flows downwards. The thickness of grain bed is typically between 0.6 to 0.9 m.; as heated air with the highest temperature is in-contact with grain of the highest moisture content, a relatively high drying temperature (65 ~ 120℃) could be employed without affecting grain quality (Valença and Massarani, 2000). Research was conducted to study the optimal tempering parameters for tempering in concurrent-flow grains and the effect of number of stages of multi-stage concurrent-flow grain dryers (Li et al., 2020; Valença and Massarani, 2000). One main disadvantage of this type of dryers is the low energy efficiency; as a result of thicker grain bed, the air-flow resistance in concurrent-flow grain dryers is higher than that of other dryers (Tsotsas and Mujumdar, 2007). Two methods could be adopted to improve energy efficiency, i.e. optimizing the structural design and applying insulation material at the entrance of the grain flow (Thompson, 1969). Fire safety should also be considered as the drying temperature for concurrent-flow grain dryers is high.

2.1.3 Counter-flow grain dryers

Counter-flow grain dryers are named because grain flow and heated air flow are in the opposite direction. In this type of dryer, heated air with the highest temperature is in contact with the grain of the lowest moisture content, thus drying temperature cannot be too high because air with the lowest temperature and highest RH is in contact with grain of the highest moisture content and lowest temperature, thus saturation is usually easily achieved. A typical design of counter-flow grain dryer usually consists of a round bin and a perforated floor. Studies of this type dryers are mainly focused on optimizing the structural design to achieve a better mixing of grain and a more uniformed drying medium (Li et al., 2020; Thompson, 1969; Valença and Massarani, 2000).

2.1.4 Mixed-flow grain dryers

Mixed-flow grain dryers are the most widely-used grain dryers around the world owing to their high adaptivity, high energy efficiency and high quality of the final product (Mellmann et al., 2008). In a typical mixed-flow grain dryer, multiple rows of air ducts are arranged in a staggered pattern, forming the pathways for heated air to enter and exit, while grain flows downwards under gravity and is in contact with heat air in “cross-flow”, “concurrent” and “counter-flow” directions at different locations. For the optimal performance, the shape of air ducts is usually selected based on the type of grain. Also, the layout of air ducts plays an important role in determining the condition of grain flow and the uniformity of drying (Cao et al., 2007).

Optimization on this type of dryers could be summarized in the following aspects:

a) Adopting a pulsatile system to unload the grain.

The grain unloading system plays an important role in deciding whether the grain could flow downwards through the drying column at a uniformed rate. In a conventionally designed mixed-flow grain dryer, the unloading system includes a hopper and augers with blades. A severe disadvantage of this design is that the speed of grain flow at the center of the dryer is much higher than at the edge, resulting in uniformity in the final product (Santeramo and Lamonaca, 2021). Adopting pulsatile unloading systems would allow a lower unloading speed at the center than the loading rate around the edge of the dryer, and thus improve the evenness of grain flow.

b) Applying variable-temperature or adopting a cooling system

The drying temperature along the direction of grain flow could be set to a decreasing pattern, so that grain flows gradually from a hotter area to a cooler area. The advantage of this method is that grain quality could be better maintained because overheating is avoided, and the energy efficiency is higher than constant temperature drying (Bakker-Aekema et al., 1969).

c) Adopting energy harvest systems

To make better use of the thermal energy (Weigler et al., 2017), energy harvest systems were included in mixed-flow grain dryers by many manufacturers including Svegma, Stela, Law, etc. It was done by harvesting the energy from the exit air, because the temperature of exit air is still higher than ambient temperature, reusing exit air will save the energy used to heat air to drying temperature.

d) Optimizing the design of air ducts

Studies have shown (Cao et al., 2007) that the performance of mixed-flow grain dryers, including drying efficiency, energy consumption and quality of final product, was influenced by the size, and layout of airducts. It was found that for drying columns of the same height, using designs with smaller air ducts can improve the drying rate.

e) Optimizing the residence time distribution

It was found (Mellmann et al., 2011) that the residence time of grain at different locations of mixed-flow grain dryers could be different, which is an important factor contributing to the non-uniformity of the final product. However, no published study has tried to optimize residence time of drying.

2.2 Modelling grain drying

2.2.1 Modelling heat and mass transfer

Models for describing temperature and moisture transfer for single kernels can be divided into two groups, (i) distributed models and (ii) lumped parameter models. Distributed models describe temperature and moisture transfer rate as a function of drying time and the position within the kernel. Most lumped models were adapted from distributed models based on simplifying assumptions; thus, they are simple in form and simulate temperature and moisture transfer as a function of drying time.

a) Distributed models

Heat and mass transfer were solved simultaneously in distributed models; the advantage of this type of models is that both the internal and external heat and mass transfer are considered, thus resulting in a better prediction of the temperature and the moisture gradients (Erbay and Icier, 2010). Generally, these models are built on the Luikov equations that come from Fick's second law of diffusion shown as Eq. 2.2.1-1 or their modified forms (Luikov, 1975).

$$\frac{\partial M}{\partial t} = \nabla^2 K11 \cdot M + \nabla^2 K12 \cdot T + \nabla^2 K13 \cdot P \quad (2.2.1\text{-}1)$$

$$\frac{\partial T}{\partial t} = \nabla^2 K21 \cdot M + \nabla^2 K22 \cdot T + \nabla^2 K23 \cdot P \quad (2.2.1\text{-}2)$$

$$\frac{\partial P}{\partial t} = \nabla^2 K31 \cdot M + \nabla^2 K32 \cdot T + \nabla^2 K33 \cdot P \quad (2.2.1\text{-}3)$$

where, K11, K12, K13, K21, K22, K23, K31, K32 and K33 are experimentally derived coefficients (Brooker et al., 1974), M is moisture content, T is temperature (°C) and P is pressure (kPa). For most drying processes, the pressure effect is negligible compared with the temperature and the moisture effect, so the Luikov equations are simplified as (Brooker et al., 1974):

$$\frac{\partial M}{\partial t} = \nabla^2 K11 \cdot M + \nabla^2 K12 \cdot T \quad (2.2.1\text{-}4)$$

$$\frac{\partial T}{\partial t} = \nabla^2 K21 \cdot M + \nabla^2 K22 \cdot T \quad (2.2.1\text{-}5)$$

However, due to the complexity of real drying mechanisms, the modified form of the Luikov equations (Eq. 2.2.1 -4) cannot be solved analytically and numerical methods, such as the finite element method (FEM) have to be used (Özilgen and Özdemir, 2001).

b) Lumped parameter models

In lumped parameter models, the temperature gradient in the product is neglected, and it is assumed that the temperature of the drying product is equal to the temperature of drying medium and there exists no temperature difference within the drying product (Erbay and Icier, 2010). Based on the above assumptions, the Eq. 2.2.1-4 could be written as:

$$\frac{\partial M}{\partial t} = \nabla^2 K11 \cdot M \tag{2.2.1-6}$$

$$\frac{\partial T}{\partial t} = \nabla^2 K21 \cdot T \tag{2.2.1-7}$$

Coefficient K11 is known as the effective moisture diffusivity (D_{eff}) and K22 is known as thermal diffusivity (α). For constant values of D_{eff} and α, Equations 2.2-3 can be rearranged as:

$$\frac{\partial M}{\partial t} = D_{eff}\left[\frac{\partial^2 M}{\partial x^2} + \frac{a1}{x} \cdot \frac{\partial M}{\partial x}\right] \tag{2.2.1-8}$$

$$\frac{\partial T}{\partial t} = \alpha\left[\frac{\partial^2 T}{\partial x^2} + \frac{a1}{x} \cdot \frac{\partial T}{\partial x}\right] \tag{2.2.1-9}$$

where, parameter $a_1 = 0$ for planar geometries, $a_1 = 1$ for cylindrical shapes and $a_1 = 2$ for spherical shapes (Ekechukwu, 1999).

This type of model assumes uniform temperature distribution and equal temperature of the ambient air and product. The error caused by such assumptions occurs only at the beginning of drying and it may be reduced to acceptable range with reduced the thickness of the product (Henderson and Pabis, 1961). With this necessity, thin layer drying gains importance and thin layer equations are derived.

2.2.2 Thin-layer drying models

The American Society of Agricultural and Biological Engineering (ASABE) described “thin layer” as a layer of material exposed fully to an airstream during drying process and the thickness of the layer should be uniform and should not exceed three layers of particles (ANSI/ASAE, 2014). The temperature distribution of thin layer drying can be safely assumed to be uniform along its thickness, and thus is very suitable for applying lumped parameter models.

Thin-layer drying equations are fundamental to the modelling of drying agricultural products, and are widely used due to their ease of use and requirement of less data compared to complicated distributed models (such as phenomenological and coupling coefficients) (Madamba et al., 1996; Özilgen and Özdemir, 2001). These equations represent the moisture exchange between a thin

layer of the drying product with the drying medium. From the mathematical point of view, a thin layer represents the "spatial thickness (dx) that is infinitely small within which changes in humidity and temperature of the air can be assumed linear" (Wang et al., 2004).

Thin layer equations may be theoretical, semi-theoretical, or empirical. A detailed review of thin-layer drying equation could be referred to the study by Jayas et al. (1991). Theoretical thin-layer drying equations take into account only the internal resistance to moisture transfer (Bruce, 1985; Henderson, 1974a; Parti, 1993; Suarez et al., 1980), while the others consider only the external resistance to moisture transfer between the product and the drying air (Fortes and Okos, 1981; Özilgen and Özdemir, 2001; Parti, 1993; Whitaker et al., 1969). Theoretical models provide a clear explanation of product drying behaviors and can be applied across all process conditions. However, they come with a significant drawback as they rely on numerous assumptions, leading to substantial errors. The most commonly employed theoretical models are based on adaptations of Fick's second law of diffusion. Similarly, semi-theoretical models are typically derived from Fick's second law and its simplified forms with some modifications (alternatively, some semi-theoretical models draw inspiration from Newton's law of cooling). These models offer the advantage of being more straightforward and requiring fewer assumptions since they incorporate experimental data to a certain extent. Nevertheless, they have a limitation in that they are only valid within the specific process conditions in which they are employed (Fortes and Okos, 1981; Parry, 1985). Empirical models share similar drawbacks with semi-theoretical models, as these models rely heavily on the specific experimental conditions under which they are developed and provide only limited insights into the drying behavior of the product (Keey, 1972). Below is a summary of assumptions of thin-layer drying models:

a) the grain particles are homogenous and isotropic;
b) the material properties of grain are constant, and particle shrinkage is neglected;
c) the variation of air pressure is minimal, and is thus neglected;
d) evaporation only takes place at the surface of grain kernels;
e) the distribution of moisture content is uniform within the grain kernel at the beginning of drying and remains symmetrical during the drying process;
f) the inner-kernel moisture equilibrium was assumed, and diffusion only happen on the surface on the kernel;
g) temperature distribution is uniform within the grain kernel and the temperature of grain kernels is

always equal to the temperature of drying medium;

h) the heat transfer is done by conduction within the grain kernel, and by convection outside of the grain kernel; and

i) effective moisture diffusivity stays constant and does not change with respect to changing moisture content during drying

Based on the above assumptions, the analytical solution for a sphere for Eq. 2.2.1-7 could be given as (Crank, 1975):

$$MR = A1 \sum_{i=1}^{\infty} \frac{1}{(2i-1)^2} \exp\left[-\frac{(2i-1)^2 \pi^2 D_{eff}{}^{t}}{A2}\right] \quad (2.2.2\text{-}1)$$

where t is time (s), *A1 and A2* are geometric constants, D_{eff} is the effective moisture diffusivity (m^2/s), and MR is defined as moisture ratio $MR = \frac{M_t - M_e}{M_i - M_e}$, M_t is the real-time moisture content at time t, M_i is the initial grain moisture content and M_e is the equilibrium moisture content.

2.2.2.1 Semi-empirical models

a. Lewis model

The Lewis model was adapted from Newton's law of cooling, thus is also called Newton model. This model was based on the assumption that the thickness of material to be dried was thin enough, and the airflow rate was high enough that the temperature and relative humidity of the hot air stayed constant and unaffected by the heat and moisture exchange due to drying. It was found that in the falling drying-rate period, the rate of moisture change is proportional to the difference between real-time moisture content and the anticipated equilibrium moisture content (Lewis, 1921).

$$\frac{dM_t}{dt} = -K \cdot (M_t - M_e) \quad (2.2.2\text{-}2)$$

where t is time, M_t is the real-time moisture content at time t, M_e is the equilibrium moisture content, and K is the drying constant. Grain drying rate (K) is an important property for describing transport phenomena during drying; it could be determined experimentally and is affected by drying conditions (Mujumdar, 2007). If we define moisture ratio (MR) as $\frac{M_t - M_e}{M_i - M_e}$, then Eq. 2.2.2-2 could be re-arranged as:

$$MR = \frac{M_t - M_e}{M_i - M_e} = \exp(-kt) \quad (2.2.2\text{-}3)$$

where M_i is the initial moisture content of grain.

b. Page model

In order to more accurately describe the drying behavior of shelled corn, Page (1949) made modification to the Lewis model by adopting another empirical constant (n).

$$MR = \frac{M_t - M_e}{M_i - M_e} = \exp(-kt^n) \quad (2.2.2\text{-}4)$$

where n is the experimentally-determined dimensionless model constant.

c. Modified Page model

Similar to the Page model, different modifications were made to the Lewis model for better describing the drying characteristics of different grains. A summary of drying models adapted from Page model is as shown in Table 2 -1.

Table 2-1 Summary of modified Page models

Drying models	Grain/crop type	Equations	Source
Modified Page-I model	Shelled corn	$MR = \frac{M_t - M_e}{M_i - M_e} = exp(-kt)^n$ (2.2.2 -5)	(Overhults et al., 1973)
Modified Page-II model	Soybean	$MR = \frac{M_t - M_e}{M_i - M_e} = exp - (kt)^n$ (2.2.2 -6)	(White et al., 1980)
Modified Page-I model	Sweet potato slices	$MR = \frac{M_t - M_e}{M_i - M_e} = exp - k(t/l^2)^n$ (2.2.2 -7) where l is an experimentally determined dimensionless empirical constant	(Diamante and Munro, 1993)

d. Henderson and Pabis model

To effectively predict the drying behavior of corn, the Henderson and Pabis model (1961) was developed based on Fick's second law of diffusion, and it was found that if drying time was

sufficiently long, Eq. (2.2.2 -1) could be solved using only one term (i=1) with small error. Based on such finding, Eq.2.2.2-1 could be written as:

$$MR = \frac{M_t - M_e}{M_i - M_e} = A1 \sum_{i=1}^{\infty} \frac{1}{(2i-1)^2} \exp\left[-\frac{(2i-1)^2 \pi^2 D_{eff}{}^t}{A2}\right] \quad (2.2.2\text{ -8})$$

Assuming D_{eff} remains constant over the whole drying process, then:

$$MR = \frac{M_t - M_e}{M_i - M_e} = a \exp(-kt) \quad (2.2.2\text{ -9})$$

where a is a dimensionless geometric constant affected by the shape of grain kernels, and k is the drying constant (s^{-1}).

e. Logarithmic model

A model was adapted from the Henderson and Pabis model by introducing another empirical constant for describing the drying behavior of laurel leaves (Chandra and Singh, 1995), the equation is as follows:

$$MR = \frac{M_t - M_e}{M_i - M_e} = a \exp(-kt) + c \quad (2.2.2\text{ -10})$$

where c is an experimentally determined constant

f. Midilli model

In 2002, Midilli and colleagues (2002) introduced a new model by augmenting the Henderson and Pabis model with an additional empirical component that incorporates the influence of drying time (t). This model comprises both an exponential and a linear term. They subsequently utilized this model to analyze the drying processes of pollen, mushrooms, and shelled/unshelled pistachios using various drying techniques. The equation for Midilli model is as follows:

$$MR = \frac{M_t - M_e}{M_i - M_e} = a \exp(-kt) + b^* \cdot t \quad (2.2.2\text{ -11})$$

where b^* is an experimentally determined empirical constant (s^{-1})

g. Modified Midilli model

To describe the drying behavior of flax fiber, Ghazanfari et al. (2006) underscored the importance of setting the shape term (a) in the Midilli model (as defined by Equation 2.2.2 -11) to be equal to 1.0 at t = 0. To address this, they put forward a modification as follows:

$$MR = \frac{M_t - M_e}{M_i - M_e} = \exp(-kt) + b * t \quad (2.2.2\text{ -}12)$$

h. Demir et al. Model

Inspired by the modifications by Overhults et al. (1973), Henderson and Pabis (1961), Chandra and Singh (1995), and Ghazanfari et al. (2006), a new model was introduced by Demir et al. (2007). The equation for **Demir et al. Model** is as follows:

$$MR = \frac{M_t - M_e}{M_i - M_e} = a \exp\left[-(kt)\right]^n + b \quad (2.2.2\text{ -}13)$$

i, Two-Term Model

In 1974, Henderson (1974) suggested an improvement to the Henderson and Pabis Model (1961) by utilizing the first two terms (i=2) of the general series solution of Fick's second law of diffusion (as represented by Eq. 2.2.2 -14). Subsequently, Glenn, in 1978, applied this proposal to the context of grain drying. As a result of this approach, a new model was developed as follows:

$$MR = \frac{M_t - M_e}{M_i - M_e} = a \exp(-k_1\, t) + b \exp(-k_2\, t) \quad (2.2.2\text{ -}14)$$

where a and b are dimensionless geometric constants affected by the shape of grain kernels, and k_1 and k_2 are the experimentally determined drying constants (s^{-1}).

j. Two-Term Exponential Model

In 1980, Sharaf-Eldeen and colleagues (1980) made modifications to the Two-Term model by reducing the number of empirical constants used in the equation and redefining the shape constant (b) associated with the second exponential term (as defined by Equation 2.2.2 -15). They highlighted the significance of setting the value of b in the Two-Term model to be equal to (1 - a) in order to achieve MR = 1 at t = 0. They then proposed a modification to the model as follows:

$$MR = \frac{M_t - M_e}{M_i - M_e} = a \exp(-k\, t) + (1 - a) \exp(-ka\, t) \quad (2.2.2\text{ -}15)$$

k. Verma Models

To describe the drying behavior of rice, Verma and colleagues (1985) made adjustments to the Two-Term Exponential model by introducing an additional empirical constant to the second exponential term.

$$MR = \frac{M_t - M_e}{M_i - M_e} = a \exp(-k\, t) + (1 - a) \exp(-g\, t) \quad (2.2.2\text{ -}16)$$

where g is the experimentally determined drying constants (s^{-1}).

l. Diffusion Approach model

In 1998, Kassem (1988) restructured the Verma model by separating the drying constant term (k) from the parameter (g) and introduced a revised form as follows:

$$MR = \frac{M_t - M_e}{M_i - M_e} = a \exp(-k\,t) + (1 - a) \exp(-kb\,t) \quad (2.2.2\text{ -}17)$$

m. Modified Henderson and Pabis (Three Term Exponential) Model

In order to improve the performance of the Henderson and Pabis model and the two-term models, a new model was developed based on the solution to Fick's second law of diffusion (as represented by Eq. 2.2.2 -18) adopting the first three terms (i=3) of the general series (Karathanos, 1999). Karathanos concluded that the first term accounts for the final segment, the second term describes the middle section, and the third term elucidates the initial part of the drying curve in terms of the rate of moisture removal over time.

$$MR = \frac{M_t - M_e}{M_i - M_e} = a \exp(-k\,t) + b \exp(-g\,t) + c \exp(-h\,t) \quad (2.2.2\text{ -}18)$$

where a, b and c are dimensionless geometric constants affected by the shape of grain kernels, and k, g and h are the experimentally determined drying constants (s^{-1}).

2.2.2.2 Empirical models

1) Thompson model

Thompson et al. (1968) proposed the below empirical equation based on experimental results of drying shelled corns in the temperature range of 60–150°C

$$t = a\ln(MR) + b[\ln(MR)]^2 \quad (2.2.2\text{ -}19)$$

where a and b are empirical constants in s^{-1}

This model was also applied by other researchers to describe the drying characteristics of green peas, blueberries (Shi et al., 2008) and (Pardeshi et al., 2009), and agreeable results were reached.

2) Wang and Singh model

Based on thin-layer drying data of rough rice, Wang and Singh (1978) proposed a new quadratic equation as below

$$MR = 1 + at + bt^2 \quad (2.2.2\text{ -}20)$$

where a and b are empirical constants in s^{-1} and s^{-2} respectively.

This model was also test on drying of banana (Kadam and Dhingra, 2011), parsley leaves (Akpinar, 2011), and bamboo shoot slices (Bal et al., 2010), and satisfying results were reached.

3) Wang et al. models

Three different empirical models were developed by Wang and colleagues by a visual method based on MATLAB tool (2004), the equations were as below:

$$MR = a\exp(b\ k\ t) + 1 - a \quad (2.2.2\text{-}21)$$

$$MR = (1 - a)\exp(b\ k\ t) + b\exp(c\ k\ t) \quad (2.2.2\text{-}22)$$

$$MR = (1 - a - b)\exp(c\ k\ t) + a\exp(d\ k\ t) + b\exp(f\ k\ t) \quad (2.2.2\text{-}23)$$

where a, b and c are dimensionless empirical constants, and k is the experimentally determined drying rate (s^{-1})

4) Jena and Das model

This model includes two exponential terms related to drying time. The exponents in the first and second terms of the model are maintained at constant values of 1.0 and 0.5, respectively, for the sake of simplicity. This model was developed to mitigate the adverse impact of varying diffusivity on moisture content and has proven effective in the drying of coconut presscake, as demonstrated in a study by (Jena and Das, 2007).

$$M_R = a\exp\left(-k\ t + b\sqrt{t}\ \right) + c \quad (2.2.2\text{-}24)$$

where M_R is the moisture ratio, a and c are dimensionless empirical constants, and k and b are the experimentally determined drying constants

5) Demir et al. model

To describe the drying characteristics of green table olives, curve fitting procedure, similar to the work by Page (1949), and Midilli et al. (2002), Demir et al. (2007) proposed a new empirical model as below, and satisfying results were reached.

$$MR = a\ \exp[-(kt^n)] + b \quad (2.2.2\text{-}25)$$

where a, b and n are dimensionless empirical constants, and k is the experimentally determined drying rate (s^{-1})

6) Haghi and Angiz models

Based on experimental data from wool drying, Haghi and Angiz (2007) proposed three different empirical equations as stated below, and satisfying results were reached.

$$\mathrm{MR} = a\ exp\ (-b\ t)^c + \ d\ t^2 + e\ t + f \quad (2.2.2\text{-}26)$$

$$\mathrm{MR} = a + b\ t + c\ t^2\ + d\ t^3 \quad (2.2.2\text{-}27)$$

$$MR = \frac{a+b\ t}{1+c\ t+d\ t^2} \quad (2.2.2\text{-}28)$$

$$MR = \ a \exp\left[\frac{-(t-b)^2}{2c^2}\right] \quad (2.2.2\text{-}29)$$

where a is a dimensionless constant, and b, c, d, e and f are empirical constants

7) Hii et al. model

Hii et al. (2008) proposed a new model consisting of which was inspired by the Page model and two-term drying models. In their equation, a power term n was introduced to account for the effect of drying time

$$MR = a \exp(-kt^n) + c \exp(-gt^n) \quad (2.2.2\text{-}30)$$

where a, b, c and n are dimensionless empirical constants, and k and g are the experimentally determined drying rates (s^{-1}).

This model was developed based on previous observations, which revealed that the Page and two-term models, when applied individually, often provided satisfactory fits for drying data when tempering was included, as discussed in the work by Hii et al. in 2009. It has been successfully applied to various materials, including coffee (Varadharaju et al., 2001), carrot pomace (Kumar et al., 2012), and cocoa (Hii et al., 2008, 2009), yielding good results in these cases.

8) Vega-Galvez et al. models

Vega-Galvez et al. (2008) proposed three different empirical models to describe drying behavior of red pepper.

$$MR = n + k\sqrt{t} \quad (2.2.2\text{-}31)$$

$$MR = \exp(n + kt) \quad (2.2.2\text{-}32)$$

$$MR = (a + b\ t)^2 \quad (2.2.2\text{-}33)$$

where a, b and n are dimensionless empirical constants, and k is the experimentally determined drying rate (s^{-1})

The primary reason for wide adoption of the third model is its simplicity, which facilitates the calculation of drying time for the material. Additionally, this model utilizes two parameters that enhance its accuracy in fitting experimental data. It has been tested and validated for use with yellow squat lobster fishery waste (as demonstrated in Vega-Galvez et al., 2009) and pumpkin (as shown in the study by Guine et al., 2012).

9) Diamante et al. model

To describe the drying behavior of kiwi fruit and apricots, a quadratic equation was proposed by Diamante et al. (2010) based on curve-fitting of experimental data as stated below, and agreeable results were reached.

$$\ln\left[-\ln(MR)\right] = a + b\ln(t) + c\left[\ln(t)\right]^2 \quad (2.2.2\text{-}34)$$

where a, b and c are dimensionless empirical constants

10) Weibull distribution models

This particular model lacks a physical interpretation and is purely a statistical approach, the Weibull distribution, is presented below. This Weibull distribution model has been tested for figs (as demonstrated in (Babalis et al., 2006)) and jujubes (as shown in the study by Yi et al., 2012). There are three variations of the Weibull distribution models as follows

$$MR = a - \mathrm{b}\exp\left[-(kt^n)\right] \quad (2.2.2\text{-}35)$$

$$MR = a - \mathrm{b}\exp(-kt^n) \quad (2.2.2\text{-}36)$$

$$MR = \exp\left[-(t/a)^n\right] \quad (2.2.2\text{-}37)$$

where a, b and n are dimensionless empirical constants, and k is the experimentally determined drying rate (s^{-1})

11) Sripinyowanich and Noomhorm model

This model was created by combining a general grain-drying model, which is the Page model, with a straightforward linear equation. It effectively fitted to the moisture loss patterns observed during the final falling-rate drying period. This model has been applied successfully in the drying of rice, as demonstrated in the work by Sripinyowanich and Noomhorm (2011).

$$MR = \exp(-kt^n) + b\,t + c \quad (2.2.2\text{-}38)$$

where a, b and c are dimensionless empirical constants, and k is the experimentally determined drying rate (s^{-1})

12) Moomhorm and Verma model

To simulated the dying behavior of rough rice, an empirical model was developed as below (Moomhorm and Verma, 1986)

$$MR = a\exp(-k\,t) + b\exp(-g\,t) + c \quad (2.2.2\text{-}39)$$

where a, b and c are dimensionless empirical constants, and k and g are the experimentally determined drying rates (s^{-1})

13) Hasibuan and Daud model

An empirical drying model was developed by Hasibuan and Daud model (2007) for drying oil palm empty fruit bunches fiber, and it was found that this model could successfully fit the data of both increasing drying rate and the falling rate periods.

$$MR = 1 - a\,t^n\ \exp(-kt^m) \quad (2.2.2\text{-}40)$$

where a, m and n are dimensionless empirical constants, and k is the experimentally determined drying rate (s^{-1})

Later, this model was tested for predicting the thin-layer drying behavior of kenaf fibers, and agreeable results were reached (Hasibuan and Daud, 2007).

14) Sharaf-Eldeen et al. model

Sharaf-Eldeen et al. proposed an empirical model based on experimental data from the drying of ear corn (Sharaf-Eldeen et al., 1980 from Wang et al., 2004)

$$MR = a\exp(\,k\,t) + [1 - a\exp(-b\,k\,t)] \quad (2.2.2\text{-}41)$$

where a and b are dimensionless empirical constants, and k is the experimentally determined drying rate (s^{-1})

15) Henderson and Henderson models

These models are simplifications of the analytical solution of the diffusional model (Henderson and Henderson, 1968 from Barrozo et al., 2004).

$$MR = a\,[\exp(-\,k\,t) + \tfrac{1}{9}\exp(-9\,k\,t)] \qquad (2.2.2\text{ -}42)$$

where a is dimensionless empirical constants, and k is the experimentally determined drying rate (s^{-1})

16) Parabolic model

This model is in quadratic form and given as:

$$\mathrm{MR} = a + b\,t + c\,t^2 \qquad (2.2.2\text{ -}43)$$

where a, b and c are dimensionless empirical constants.

It was tested for African breadfruit seeds (Shittu and Raji, 2011), thyme (Doymaz, 2011a) and seedless and seeded grapes (Doymaz, 2011b), and successfully used for apple slices (Doymaz, 2010).

17) Geometric model

This model was tested for rice (Hacıhafızoğlu et al., 2008), mushroom (Celen et al., 2010), and onion (Jain and Pathare, 2004)

$$\mathrm{MR} = a\,t^n \qquad (2.2.2\text{ -}44)$$

where a and n are dimensionless empirical constants

18) Logistic model

This model is examined for parsley leaves (Soysal et al., 2006), bamboo sheet (Bal et al., 2010), and rice (Cihan et al., 2007)

$$MR = a0\,[1 + \exp(-\,k\,t)] \qquad (2.2.2\text{ -}45)$$

where a0 is the dimensionless empirical constants, and k is the experimentally determined drying rate (s^{-1})

19) Power law model

This power-law model is tested for sweet pepper (Vengaiah and Pandey, 2007) and pomegranate peel (Emam-Djomeh et al., 2007)

$$\mathrm{MR} = a\ t^{b} \qquad (2.2.2\text{ -}46)$$

where a and b are dimensionless empirical constants

20) Regression models

These models were tested for blueberries (Shi et al., 2008).

$$\mathrm{MR} = exp[-(\ a\ t^{2} + b\ t)] \qquad (2.2.2\text{ -}47)$$

$$\mathrm{t} = a\ (MR)^{2} + b\ (MR) + c \qquad (2.2.2\text{ -}48)$$

where a, b and c are dimensionless empirical constants

21) Chavez-Mendez et al. model

This is mentioned as logarithmic model and tested for chilli pepper (Tunde-Akintunde, 2011), banana (Sankat et al., 1996), and described as the best model for sweet pepper (Vengaiah and Pandey, 2007).

$$\mathrm{MR} = a + b\ln(t) \qquad (2.2.2\text{ -}49)$$

where a and b are dimensionless empirical constants

22) Aghbashlo model

This model has been validated with pistachio (Chayjan et al., 2012), tomato (Garavand et al., 2011), apple (Meisami-Asl and Rafiee, 2009), and demonstrated satisfactory performance in describing the drying characteristics of carrots (Aghbashlo et al., 2009).

$$MR = exp[-\ \frac{k_1 t}{1 + k_2 t}] \qquad (2.2.2\text{ -}50)$$

where k_1 and k_2 are the experimentally determined drying rates (s^{-1})

23) Modified Henderson and Perry model

This model was examined for the drying characteristics of mango fruits (Chottanom and Phoungchandang, 2005) and popcorn kernels (Taiwo et al., 2008).

$$MR = a\ \exp(-kt^n) \quad (2.2.2\text{ -}51)$$

where a and n are dimensionless empirical constants, and k is the experimentally determined drying rate (s^{-1})

24) Three-parameter model

This model demonstrated agreeable performance in predicting the drying process of popcorn kernels (Taiwo et al., 2008) and sweet basil seeds (Phoungchandang and Kongpim, 2012).

$$MR = a\ \exp[-(kt^n)] \quad (2.2.2\text{ -}52)$$

where a and n are dimensionless empirical constants, and k is the experimentally determined drying rate (s^{-1})

25) Asymptotic model

This model demonstrated satisfactory performance for describing the drying processes of onion slices (Jain and Pathare, 2004)

$$MR = a0 + \ \exp(-kt) \quad (2.2.2\text{ -}53)$$

where a0 is the dimensionless empirical constant, and k is the experimentally determined drying rate (s^{-1})

26) Alibas model

The Alibas model (2012) was derived by approximating the results from Midilli et al. model as follows:

$$\mathrm{MR} = a\ exp[(-k\ t)^n + b\ t] + g \quad (2.2.2\text{ -}54)$$

where a, b, g and n are dimensionless empirical constants, and k is the experimentally determined drying rate (s^{-1}).

27) Khazaei and Daneshmandi model

This model is examined by sesame seeds and presented as (Khazaei and Daneshmandi, 2007):

$$MR = a + \ \exp(-bt) - c\ t \quad (2.2.2\text{ -}55)$$

where a, b and c are dimensionless empirical constants.

28) Growth curve models

In a different study (Siatkowski et al., 2010), 37 different growth curve functions were tested to model corn kernels drying process. These equations were as detailed in Siatkowski et al.'s work (2010).

29) Kaleemullah Model

Kaleemullah (2002) proposed an empirical model that included *MR*, *T*, and *t,* which was adopted in describing the drying behavior of red chilli fruits (Kaleemullah and Kailappan, 2006).

$$\mathrm{MR} = \exp - c^* \cdot T + b^* \cdot t^{(p\,T+n)} \qquad (2.2.2\text{-}56)$$

where, constant c^* is in $^{o}C^{-1}$ s^{-1}, constant b^* is in s^{-1}, p is in $^{o}C^{-1}$ and n is dimensionless

2.2.3 Numerical modelling of grain drying

2.2.3.1 CFD models for grain drying

Computational fluid dynamics (CFD) is a powerful and advanced numerical method to solve governing partial differential equations of mass, momentum and energy conservation in fluid flow and heat and mass transfer problems (Norton and Sun, 2006). CFD was first used in the 1950s (Norton & Sun, 2006), and has increasingly been used in grain drying. A comprehensive review on CFD application in simulating and designing drying processes was given by Jamaleddine and Ray (Jamaleddine and Ray, 2010). Computational Fluid Dynamics (CFD) has found valuable applications in studying and optimizing drying processes, particularly in the food industry. Here are some notable examples of how CFD has been used:

Drying process optimization: Mathioulakis et al. (1998) used CFD to simulate air movement in an industrial batch tray air dryer. Their research revealed that the degree of dryness of fruit depends on its position in the dryer. CFD showed that non-uniform air velocities within the dryer were a major cause of variations in drying rates and moisture contents. This underscores the importance of spatial homogeneity in drying processes.

Spray dryer design: CFD has been instrumental in the design of spray dryers used in food production, such as milk and coffee powder. Spray dryer performance is strongly influenced by

the complex air and spray flow patterns within the dryer. CFD simulations have been used to optimize the design of these dryers and address operational challenges such as wall deposition (Langrish and Fletcher, 2001).

Airflow analysis: Researchers have used CFD to analyze airflow patterns in co-current pilot spray dryers (Kieviet et al., 1997) and to study the effects of air inlet geometry and spray cone angle on wall deposition rates (Langrish and Zbiciński, 1994). These studies demonstrated the potential of CFD for airflow analysis and its impact on drying processes.

Particle drying simulation: CFD can simulate airflow in spray dryers, calculate trajectories, and model the drying process of atomized particles. Models incorporating turbulence and gas flow fields have proven effective in optimizing product quality and drying performance in industrial dryers (Straatsma et al., 1999b, 1999a).

As dryer applications become more complex, the need for improved pilot plant testing increases, and CFD simulations become essential to provide rapid and valuable insight (Masters, 1994). CFD continues to be a powerful tool for understanding and optimizing drying processes in various industrial contexts.

The capability of modern CFD packages to couple the equations of fluid flow (drying medium) and existing empirical drying models for the solid had strengthened its application in drying. For example, various numerical models such as pore network models (Vorhauer et al., 2010; Yiotis et al., 2001), diffusion models (Elgamal et al., 2014; A. Erriguible et al., 2005), and macroscopic models (Nasrallah and Perré, 1988; Perré, 2010) were applied in the convective drying process coupled with the CFD codes. Coupling of the porous media models with the Navier-Stokes equations in the fluid medium was performed by introducing appropriate boundary conditions at the solid-fluid interface. Such coupled models were adopted by researchers for simulating high-temperature convective drying, superheated steam drying, and vacuum drying (Erriguible et al., 2005) where the classic boundary layer hypothesis could not be applied. Commercial CFD software packages, such as ANSY Fluent, ANSYS CFX, COMSOL, STAR-CD etc., have become a handy tool to simulate grain drying.

Numerical models utilizing CFD offer several advantages over empirical models when simulating drying processes:

- Accurate heat and mass quantification: CFD allows accurate quantification of heat and mass flow in both space and time, providing a detailed understanding of the drying process.

- Sensitivity Analysis: It is easy to evaluate how changes in operating conditions affect drying processes using CFD. This sensitivity analysis can be performed without the challenges associated with repeatability in experimental methods.
- Handling of transient flows: CFD provides strategies for managing transient flows, however, capturing random fluctuations in drying conditions, such as spray drying, can be demanding in both time and computational power.
- Safety and operating conditions: Numerical simulations in CFD are not constrained by safety concerns, making it possible to explore a wide range of operating conditions, including extreme temperatures.
- Scale and Configuration: CFD simulations can be performed at the actual scale of the drying equipment, which may not be possible with experimental-based modeling. In addition, CFD offers a 3D configuration that provides deeper insight into drying processes than traditional experiments.
- Versatility: CFD models are versatile and applicable to different sizes of solids undergoing drying, allowing researchers to model the drying process for different elements.

2.2.3.2 DEM models for grain drying

Drying grain in a dryer involves both airflow and grain movement. Mathematical models based on Discrete Element Method (DEM) could be an effective approach to study the grain kernel movement. The Discrete Element Method is a numerical technique used to simulate the movement of particles, encompassing various aspects like interactions between particles, interactions between particles and walls, particle behavior in a fluid environment, and the influence of external forces such as electromagnetic forces. In DEM, it explicitly computes the contact forces arising from particle collisions and interactions with walls (Cundall, 1988), and with sufficient computational power, it can simulate more than 10 million particles within a reasonable timeframe. The application of DEM is gaining popularity in modelling postharvest processing of grain and food products, because of its close characterization of actual conditions in predicting various processes. Pioneering work of the DEM was initially carried out by Cundall and Strack (1980) to model the behavior of dense solids assemblies in soil mechanics. They constructed an explicitly

numerical scheme in which the particle interaction is monitored at each contact and the particle motion is modeled particle by particle. The fundamental assumptions that form the basis of this model are as follows:

a. In the event of particle collisions, only particles in direct contact are affected the collision forces. Consequently, the impact of a particle collision is confined to its immediate neighbors (Cundall, 1988).

b. Deformation is managed by permitting particles to overlap when collisions occur. The degree of overlap is determined by the contact forces, with larger overlap distances corresponding to stronger repulsive forces.

These two basic assumptions are the foundation of the soft-sphere model. Since then, this method has been widely applied in the research of various disciplines. Due to the discrete and inhomogeneous nature of grain bulks, DEM has significant advantage over continuum techniques in simulating bulk materials at the particle level. Individual particle properties, such as size, shape and property variation, can be specified directly and the assembly (bulk) response is a direct output from the simulation. There is less need for global assumptions, such as uniform stress at a certain depth in the assembly. Certain phenomena such as particle size distribution can be simulated directly. This method is also able to take into account the simultaneous occurrence of various kinds of movements and interactions of the particles with each other and with the surfaces of the boundary. There is less than a hand full of investigations into the particle movement in mixed flow grain dryers. Cao, et al. (Cao et al., 2007) constructed a mathematical model based on DEM to study the grain flow and air flow in a mixed flow grain dryer, and the results was validated against experiments. In their study, the effect of structural parameters such as size and shape of air ducts, the spacing between air ducts, the number of rows of air ducts, and column height was analyzed. They found that ducts with smaller cross-section area have better performance compared to larger ones. Keppler et al. (Keppler et al., 2012) studied the grain velocity distribution in a mixed flow grain dyer, and they concluded side walls have a strong impact on the grain flow causing segregation which could result in over- or under drying. Changing the roof angle of the air ducts in case of wedge-shaped air ducts above sixty degrees does not result in more positive effect on the particle velocity distribution for the drying of wheat. Circular air ducts were not useful, because large velocity differences resulted by their use. Mellmann et al. (2011) found that for mixed-flow grain dryers, no matter whether they are in horizontal layout or diagonal layout, the moisture

content and temperature distributions of the grain bulk varied greatly across the cross section, resulting in inhomogeneous drying even with constant inlet moisture content over time.

2.2.3.3 Coupled CFD-DEM models for grain drying

Recently, the numerical coupling of CFD and DEM has emerged as a new research field to model complex processes with heterogeneous gas–solids interactions (Brosh and Levy, 2010; Li et al., 2003; Li and Mason, 2000; Zare and Ranjbaran, 2012). The theoretical foundation of the extended discrete element method (XDEM) was developed by Peters (2002), who described the incineration of a wooden moving bed on a forward acting grate and resolved the particulate phase by applying a thermodynamic model to each particle describing various conversion processes. The same concept was later employed by Simsek et al. (2009) to predict the process of a grate firing furnace system. XDEM was fist applied as a numerical simulation framework to predict the drying within a packed bed reactor in 2014 (Mahmoudi et al., 2014). Mahmoudi et al. (2016) presented a novel approach based on a volume averaging model implemented in the XDEM framework to simulate multi-phase systems of granular media in which solid phases are fully resolved while the surrounding gas phase is semi-resolved. Another group of researchers utilized XDEM to analyze the drying process of wet woody particles in a circulating cylinder, and the dynamics of moving particles was also investigated in their study (Mohseni and Peters, 2016).

Due to the fast increase in the performance of computational hardware, the application of this innovative method continues to grow and will bring new possibilities to investigate the “traditional” problems of grain drying in the future.

2.3 Summary of literature review

This chapter first summarized published literature about different types of commercial grain dryers, with respect to their working principle, advantages and disadvantages, and possible optimization methods. A review of necessary knowledge to model grain drying was also presented in this chapter, which included general models for describing heat and mass transfer phenomena, a summary of semi-empirical and empirical thin-layer drying models, and numerical models for describing grain drying.

It's worth mentioning that a subset of the 13 semi-empirical models and the 29 empirical models mentioned in section 2.2.2 may not be suitable for granular materials, making them unsuitable for modeling grain drying. Nonetheless, the primary goal of this chapter was to gain a comprehensive understanding of the current state of art in the modeling of food material drying, with emphasis on grain drying. Semi-empirical models faced a limitation in their applicability, as they were only valid within the particular process conditions for which they were designed (Fortes and Okos, 1981; Parry, 1985). Similar drawbacks were shared with empirical models, akin to semi-empirical models, as these models heavily depended on the specific experimental conditions in which they were formulated, offering restricted insights into the drying behavior of the product (Keey, 1972). Thus, developing a universal drying model that is unrestricted by particular drying conditions or materials would be beneficial for the industry.

The advances of CFD over the last decades provided possibility for developing such universal drying models. The development of CFD grain drying models is typically based on the continuum approach or the porous medium approach. In the continuum approach, the granular material is treated as a solid material, and it does not account for the effects of individual grain kernels, or neglects the discrete nature of bulk grain. Heat and mass transfer are modeled through conduction within the material. The porous medium approach considers the pores in the bulk grain and airflow through pores. Both conduction and convection heat transfer, as well as mass transfer within the porous structure are modeled. However, grain movement, which may lead to variable pore structures, is not accounted for in the porous medium approach. The coupled CFD-DEM approach presented in this study combines the strengths of DEM in modeling grain kernels movements and CFD in modelling airflow and heat and mass transfer in porous media. A general comparison of the three different approaches is presented in Table 2-2.

Most studies of grain drying have been focused on the general phenomena of heat and moisture transfer at the macroscopic scale. A significant advantage of the coupled DEM-CFD approach is that it is capable of simulating the drying processes by considering grain movement and its effects on heat and mass transfer and airflow.

Table 2-2 Comparison of different approaches for modelling grain drying

	Continuum approach	Porous medium approach	Coupled DEM-CFD approach
Assumed grain property	Continuum	Porous material	Discrete particles in DEM, porous material in CFD
Ability to simulate grain movement and variable pore structures	No	No	Yes
Mode heat and mass transfer	Conduction	Conduction and convection	Conduction and convection
Ability to simulate airflow	No	Yes	Yes

3. Methodology

3.1 Simulated drying system

A simulated (hypothetical) mixed-flow dryer was used in this study as a placeholder to develop and validate the coupled DEM-CFD model. The configuration of simulated mixed-flow dryer, as well as the physical properties of grain is detailed in this section.

3.1.1 Configurations of simulated mixed-flow dryer

A hypothetical mixed-flow dryer (numerical model) was created as a test case for developing and validating the proposed CFD-DEM model (Fig. 3-1). This simulated dryer represented a section (a single drying column) of a large-scale commercial mixed-flow grain dryer, but small enough to be accommodated in the DEM simulations, which normally have limits for the number of particles (grain kernels). In a mixed-flow dryer, air is usually heated by a heater, then blown into the duct by a fan, and finally enters the drying column through air inlets. The simulated dryer consisted of two full air inlets and four half air outlets. Hot air entered the drying column through inlet ducts #1 and #2, and then travelled through the grain bulk and exited through outlet ducts #3 to #6 (as presented in Figs. 3-1 and 3-2). The critical dimensions of the dryer include: the horizontal (X) and vertical (Y) distances between the inlet and the outlet, and the duct height (h) and apex angle (ϕ) (Fig. 3-2).

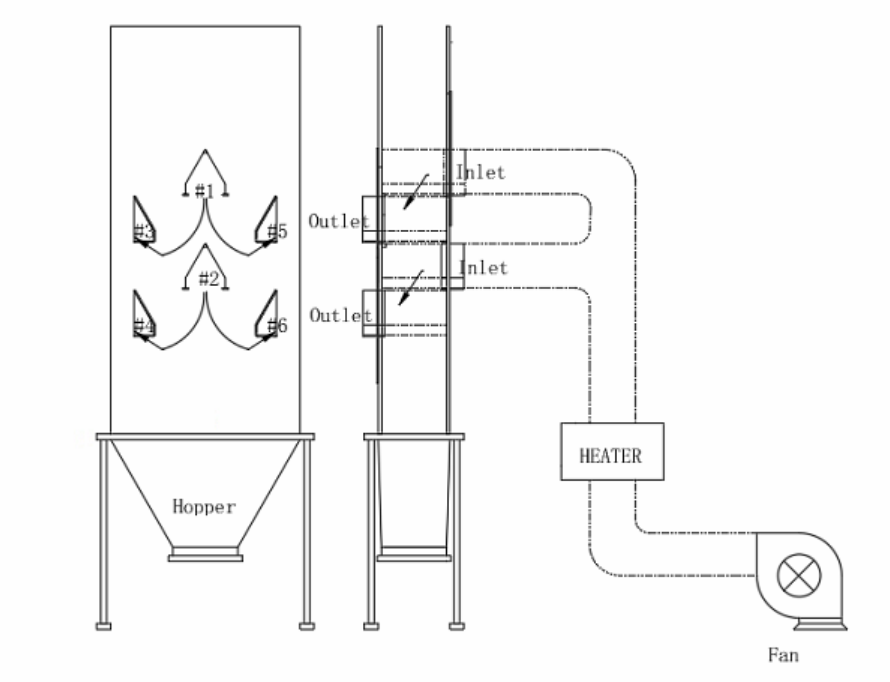

Figure 3-1 Schematic of a small-scale mixed-flow grain dryer used in simulations (#1 and #2 are air inlets and #3 - #6 are air outlets)

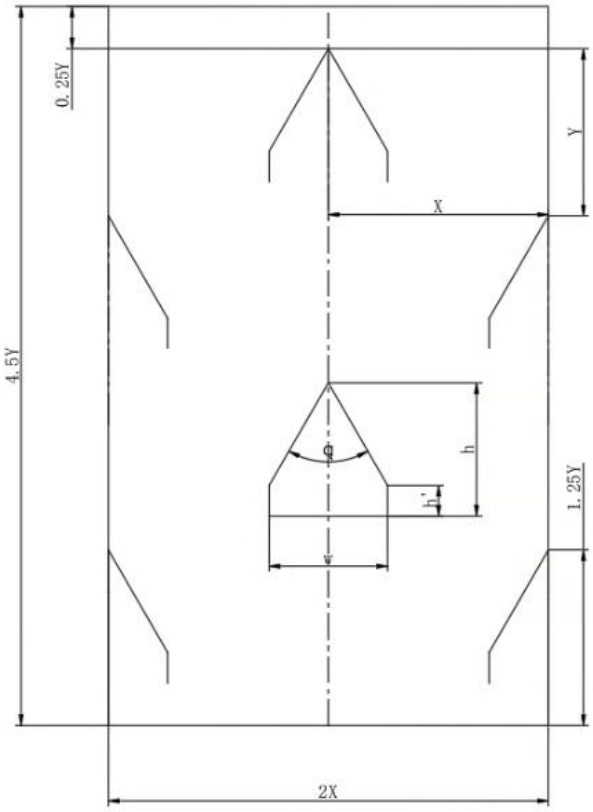

Figure 3-2 Critical dimensions of simulated dryer (dimensions in mm)

To study the effect of air duct design (geometric shape) and layout on dryer performance, different configurations were evaluated in simulations. Specifically, three configurations were simulated to study the effect of horizontal distance between the air inlet and outlet ducts (Table 3-1), three configurations for the vertical distance effect (Table 3-2), and four configurations for the duct shape effect (Table 3-3, Figure 3-3). These configurations covered the ranges commonly used in commercial dryers. When studying the effect of horizontal distance (denoted as X in Fig. 3-2), all other dimensions listed in Table 3-1 (h, h', w, ϕ and Y) were kept the same; in a similar vein, all other dimensions apart from vertical distance (denoted as Y in Fig. 3-2) were kept the same to study the effect of vertical distance.

Table 3-1 Configurations for studying the effect of horizontal distance between inlet and outlet ducts

Configuration	1	2	3
Vertical distance (mm)	210	252	294

Table 3-2 Configurations for studying the effect of vertical distance between inlet and outlet ducts

Configuration	4	5	6
Horizontal distance (mm)	165	213	260

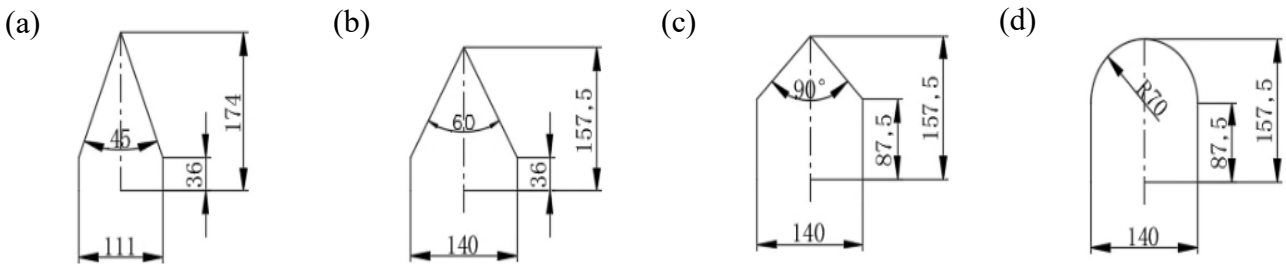

Figure 3-3 Configurations for studying effect of duct shape (a) air duct with 45-degree apex angle (b) air duct with 60-degree apex angle (c) air duct with 90-degree duct angle d) air duct with half-circle (all dimensions in mm)

Table 3-3 Configurations for studying the effect of duct shape

Configuration	7	8	9	10
h (mm)	174	157.5	157.5	157.5
h' (mm)	36	36	87.5	87.5
w (mm)	111	140	140	140
ϕ (°)	45	60	90	half circle
X (mm)	252	252	252	252
Y (mm)	213	213	213	213

3.1.2 Grain

Wheat was selected as a placeholder in this study for model development and simulations to study the drying processes in a mixed-flow grain dryers because more data is available in the literature for wheat than other grains for model validation. The mechanical properties of wheat needed in the study are discussed below. The values adopted for parameters mentioned in this section were as listed in Table 3-4 and 3-5.

a) Porosity

Porosity is defined as the ratio of the volume of voids or pore space divided by the total volume.

$$\varphi = \frac{Vv}{V_T} = \varphi = \frac{\rho_B}{\rho_P} \tag{3.1.2-1}$$

where φ is the porosity, Vv is the void volume, V_T the total volume, ρ_B the bulk density of grain and ρ_P the particle density of grain.

b) Moisture content

Moisture content on dry basis is used throughout CFD simulation because dry matter remains constant in drying. It is defined as the ratio of mass of water to the weight of dry matter.

$$m_{db} = \frac{m_w}{m_d} \tag{3.1.2-2}$$

where m_{db} is the moisture content on dry basis, m_w is the mass of water, and m_d is the mass

of dry matter. It could also be calculated as:

$$m_{db} = \frac{c_w M_w}{(1-\varphi)\rho_B - c_w M_w} \quad (3.1.2\text{-}3)$$

where c_w is the concentration of water (mol/m^3) and M_w is the molar mass of water in g/mol.

c) Bulk density

Bulk density, which is also called apparent density, is defined as the mass of an assembly of grain particles divided by the total volume. The total volume includes particle volume, inter-particle void volume, and the internal pore volume.

$$\rho_B = \frac{m}{V_T} \quad (3.1.2 - 4)$$

where m is the total mass of grain.

d) Specific heat capacity

Specific heat capacity (C_p) of a substance is the heat capacity of a sample divided by its mass, and it is equal to the amount of heat needed for one unit mass of substance to increase one unit in temperature. The SI unit for specific heat capacity is joule per kelvin per kilogram, J/(kg·K). According to ASABE standard, the specific heat capacity for hard wheat (moisture content 9.2% w.b.) is 1549 J/(kg·K)(ANSI/ASABE, 2022).

e) Thermal conductivity

Thermal conductivity of a material (k) is a measure of its ability to conduct heat. The defining equation is:

$$q = -k\nabla T \quad (3.1.2\text{ -}5)$$

where q is the heat flux and ∇T is the temperature gradient. The SI unit for thermal conductivity is watt per meter per kelvin (W/(M·K)). According to ASABE standard, the thermal conductivity for hard wheat (moisture content 9.2% w.b.) is 0.1402 (W/(M·K)) (ANSI/ASABE, 2022).

f) Intrinsic permeability

Intrinsic permeability (k_{in}) is a measure of ability of a porous material to allow fluids to pass through it. Intrinsic permeability needs to be determined experimentally, and it is calculated as:

$$k_{in} = v\frac{\eta \Delta x}{\Delta P} \quad (3.1.2\text{ -}6)$$

where v is the fluid velocity through the porous medium (m/s), η is the dynamic viscosity of the fluid (Pa·s), Δx is the thickness of the bed of porous material, and ΔP is the applied pressure difference (Pa).

Montross and McNeil (2005) reported that the intrinsic permeability for air to pass through a bed of wheat is between 1.15×10^{-8} and 7.29×10^{-9} m^2. There is no reported value for intrinsic permeability for water to pass through wheat, thus it is estimated based mathematical function developed by Urumović and Urumović (2014) to describe the dependency of permeability on porosity and grain size.

$$k_{in} = \frac{\varphi^3}{180(1-\varphi)^2} D_m^2 \quad (3.1.2\text{ -}7)$$

where φ is the porosity and D_m is the mean diameter (m).

g) Water activity

Water activity (a_w) of grain indicates the amount of water which is biologically available to microorganisms; it is defined as the partial vapor pressure in grain divided by the saturated vapor pressure under the same temperature. Water activity is equal to the equilibrium relative humidity (ERH) in decimal form at the same temperature, which could be calculated with modified Henderson equation as follows (ANSI/ASABE, 2021):

$$a_w = ERH = 1 - \exp\left[-K(T+C)\cdot(100M)^N\right] \quad (3.1.2\text{-}8)$$

where M is the grain moisture content on dry basis (decimal), T is the grain temperature (°C), and K, C, N are constants based on grain type.

3.2 Modelling of drying process in a mixed-flow grain dryer

In a mixed-flow dryer, grain moves downwards while drying (hot) air enters the moving grain bed from air inlets and exits from air outlets, and heat and moisture transfer occurs between moving grain kernels and flowing air. Therefore, the proposed drying model involved two sub-models: a DEM sub-model for grain movement, and a CFD sub-model for airflow, as well as heat and moisture transfer with CFD.

3.2.1 DEM modelling of grain kernel movement

A commercial DEM software package, PFC2D 6.0 (Itasca Consulting Group, 2019), was used to simulate the particle flow (movement of grain kernels) numerically with explicit time integration scheme for given boundary and initial conditions. Linear-elastic contact models were applied to simulate the particle-particle and particle-wall interaction because of its simplicity and effectives (Yue and Zhang, 2017). The simulation of grain kernel movement could be divided into two phases. Phase one was involved with the formation of grain bed; in phase one, grain was filled into the dryer from the top of dryer and flowed downwards into the dryer under gravity. Phase two marked the start of drying operation; in phase two, grain was discharged at a prescribed rate from the outlet at the bottom of the drying column, and in the mean while new (undried) grain was added to the top of the dryer to maintain a constant height of grain bed. The geometry of the dryer column shown in the Figure 3-4 was used to set up and test the models, while other configurations shown in Tables 3-1, 3-2, and 3-3 were simulated to study the effect of dryer configurations on drying performance.

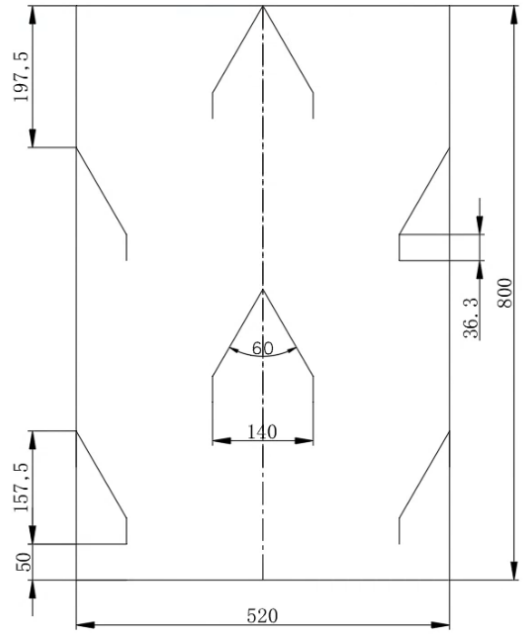

Figure 3-4 Domain geometry used in DEM model (dimensions in mm)

Two-dimensional disks were used to represent grain kernels in the DEM model because the drying column was treated as being two-dimensional, i.e., the variations of all simulated variables were assumed negligible in the z-direction. A two-dimensional model had to be used to reduce the total number of grain kernels in the DEM to run the model in a reasonable length of time. With this two-dimensional model, a total of 9871 particles was generated and a typical simulation took about 923 hours to be completed on a Windows computer with an i7-10700 2.90 GHz processor and 32.0 GB RAM. The assumptions involved in the simulation of particle flow are summarized as follows:

1) grain flow was uniform across the dryer (from the front to back); hence, a two-dimensional model was adopted;
2) the walls of dryers and air ducts were rigid, thus they did not have any deformation when subjected to pressure by the grain bulk;
3) the single grain kernel could be modelled as a round-shaped particle;
4) the particle sizes of grain kernels were large enough that van der Waals forces played no role;
5) grain was loaded evenly over the cross-sectional area from top of the dryer; and
6) grain was discharged evenly over the cross-sectional area from the bottom of the dryer.

The physical properties of wheat (mean diameter, equivalent spherical particle diameter and the bulk density) were taken from the literature (Boac et al., 2010; Mohsenin, 1970; Sokhansanj and Lang, 1996) (Table 3 - 4). It should be noted that instead of setting particle density and particle diameter as a fixed value, a normal distribution in the range from 75% to 125% of the reference value was adopted to mimic the differences in grain physical properties among individual grain kernels.

Simulations were also conducted to investigate the impact of particulate properties (i.e. particle density and particle diameter) on drying. To mimic the variation in particle density and particle diameter of grain kernels, the particle density and particle diameter of grain were set as a normal distribution in the range between 85% to 115% of the reference value (as shown in Table 3-4).

Table 3-4 Input parameters for the DEM model

Parameter	Value	Unit	Source
Wall normal stiffness	$1.8 \cdot 10^7$	N/m	Boac. et al., 2010
Wall shear stiffness	$9 \cdot 10^6$	N/m	Boac. et al., 2009
Particle elastic modulus	1422	MPa	Boac. et al., 2010
Particle shear modulus	501.05	MPa	Boac. et al., 2010
Friction coefficient between particles	0.5		Boac. et al., 2010
Friction coefficient between particles and wall	0.399		Boac. et al., 2010
Particle density	1287	kg/m^3	Sokhansanj and Lang, 1996
Bulk density (ρ_B)	772	kg/m^3	Sokhansanj and Lang, 1996
Porosity (φ)	0.4		Mohsenin, 1970
Particle diameter	3.85	mm	Mohsenin, 1970

Simulating grain kernel movements in the DEM model consisted of the repeated application of the law of motion to each particle, a force-displacement law to each contact, and a constant updating of wall positions (Itasca Consulting Group, 2019). The transition of each time step was determined for each particle. Thereby the particle equation of motion for translation and rotation was solved numerically. The equations of motion could be expressed as two vector equations: one related the resultant force to the translational motion; the other related the resultant moment to the rotational motion. The translational motion of the center of mass was described in terms of its position x_i, velocity $\dot{x}_i$, and acceleration $\ddot{x}_i$. The rotational motion of the particle was described in terms of its angular velocity ω, and angular acceleration $\dot{\omega}$. The equation for translational motion could be written in a vector form as shown in Equation 3.2.1-1 (Itasca Consulting Group, 2019).

$$F_i = m(\ddot{x}_i - g_i) \qquad (3.2.1-1)$$

where F_i is the resultant force, m is the total mass of the particle, and g_i is the body force acceleration vector.

For either a spherical or round particle, Euler's equation of motion could be simplified and referred to a global-axis system as Equation 3.2.1-1 (Itasca Consulting Group, 2019):

$$M = I\omega = \beta_m R^2 \omega \tag{3.2.1-2}$$

for rotational motion with $\beta = 0.4$ for spherical particles, where I is the principal momentum of inertia of the particle, R is the radius of particle, and ω is the angular velocity over the principal axes.

The equations (3.2.1-1) and (3.2.1-2) were integrated using a centered finite-difference procedure involving a time step of Δt. The accelerations were calculated as:

$$\dot{u}(\dot{t}) = \frac{t}{\Delta t} \times [u\left(t + \frac{\Delta t}{2}\right) - u\left(t - \frac{\Delta t}{2}\right)] \tag{3.2.1-3}$$

$$\dot{\omega}(\dot{t}) = \frac{t}{\Delta t} \times [\omega\left(t + \frac{\Delta t}{2}\right) - \omega\left(t - \frac{\Delta t}{2}\right)] \tag{3.2.1-4}$$

and velocities were solved as:

$$u\left(t + \frac{\Delta t}{2}\right) = u\left(t - \frac{\Delta t}{2}\right) - [\frac{F(t)}{m} + g_i]\Delta t \tag{3.2.1-5}$$

$$\omega\left(t + \frac{\Delta t}{2}\right) = u\left(t - \frac{\Delta t}{2}\right) - [\frac{M(t)}{I} + g_i]\Delta t \tag{3.2.1-6}$$

The velocities in Eq. (3.2.1-5) and (3.2.1-6) were used to update the position of the particle center as:

$$x(t + \Delta t) = x(t) + u\left(t + \frac{\Delta t}{2}\right)\Delta t \tag{3.2.1-7}$$

The values of $F(t + \Delta t)$ and $M(t + \Delta t)$to be used in the next time step were obtained by application of the force-displacement law. After determining the forces and momentums and the resultant displacements, the new positions of the particles were calculated. From the new positions followed new contacts after the next time step. Hence, new particle forces and momenta could be calculated. The DEM simulation results, including the particle ID, particle X-coordinate, particle Y-coordinate, particle X-velocity, particle Y-velocity, and particle density, were saved automatically in a series of matrices every 7500000 timesteps, which was equal to 1 minute (physical time in drying).

3.2.2 CFD modelling of heat and mass transfer and airflow in grain drying

A commercial CFD software package ANSYS FLUENT was utilized to simulate airflow, and heat and moisture transfer process in mixed-flow grain dryers. In line with the DEM modelling, the grain bed was simulated in a two-dimensional model. Moreover, the following assumptions were made to simplify the mathematical expressions:

- The grain bed was a porous medium and the pores were filled air, and water vapor.
- All phases (solid, liquid and gases) were continuous and local thermal equilibrium was assumed for all phases at the same location in grain bed.
- Shrinkage or expansion of grain kernels during drying process were minimal, thus were not considered.

The domain geometry of the CFD model was the same as that for DEM model (Fig. 3-5). Size of mesh and number of elements was selected based on mesh convergence test results. Six sampling points were selected to analyze the effect of meshing on simulated moisture content, which is the most important outcome of grain drying and the transport of moisture was influenced by other variable including temperature and air velocity. The layout of sampling points for mesh convergence test was as shown in Fig. 3-5. Each mesh convergence test was run for 15 minutes of drying time, and the moisture content of each test was compared to determine the adequacy of meshing.

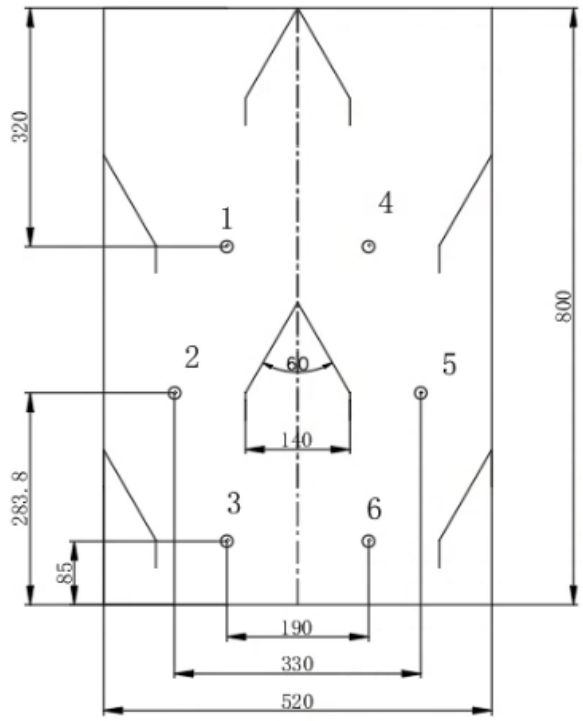

Figure 3-5 Layout of sampling points for mesh convergence test (dimensions in mm)

3.2.2.1 Specific equations used in CFD modelling

a) Mass and momentum transfer

The representative elementary volume (ΔV) for the domain consisted of the volume of different phases which are gas (ΔV_g), water in liquid state (ΔVw) and solid (ΔVs).

$$\Delta V=\Delta V_g+\Delta V_w+\Delta V_s \quad (3.2.2\text{-}1)$$

The apparent porosity (ϕ) is defined as the volume fraction of pores to total volume (Eq. (3.1.2-2)). The water saturation (S_w) and the gas saturation (S_g) are defined as the fraction of pore volume corresponding to these phases (Eq. 3.2.2-3 and 3.2.2-4). In this study, liquid water was assumed to be minimal in the pores of the grain bulk, thus was consider to be zero ($\Delta V_w = 0$).

$$\phi = \frac{\Delta V_g+\Delta V_w}{\Delta V} \quad (3.2.2\text{-}2)$$

$$S_w = \frac{\Delta V_w}{\Delta V_g+\Delta V_w} = \frac{\Delta V_W}{\phi \Delta_V} \quad (3.2.2\text{-}3)$$

$$S_w+S_g=1 \quad (3.2.2\text{-}4)$$

The concentration of liquid water (c_w), water vapour (c_v), and air (c_a) were described by the mass conservation equation given by (Schechter, 1961) (Eq. 3.2.2-5).

$$\frac{\partial c_i}{\partial_t} + \nabla \cdot (-Di \cdot \nabla c_i + u_i \cdot c_i) = \pm R_i \tag{3.2.2-5}$$

where c_i is the concentration of related phase (mol/m^3), Di is the diffusion coefficient (m^2/s), u_i is the velocity of the phase in the porous domain (m/s), and R_i is the reaction term describing the evaporation/condensation of water in liquid/vapor form (mol/m^{3}s). The "$\pm$" on the left side of the equation represents the state of water, with "-" for condensation into liquid water, "+" for evaporation of liquid water, and 0 for the balanced state (Eq. 3.2.2-6).

$$R_i = K(a_w c_{v,sat} - c_v) \tag{3.2.2-6}$$

where K is the evaporation rate constant (s^{-1}), a_w describes water activity of grain as a function of moisture content according to desorption isotherms (m_{db}, g water/g dry matter) (Kaymak-Ertekin and Gedik, 2004), and $c_{v,sat}$ is the saturated vapor concentration (mol/m^3).

The vapor and liquid water flux from the grain to the air could be calculated as follows:

$$n_{v,sur} = c_v u_{n,v} + h_m \phi S_g (c_v - c_{v,dryer}) \tag{3.2.2-7}$$

where S_g is the gas saturation defined as the fraction of pore volume corresponding to these phases, c_v is the concentration of vapor in porous domain, h_m is the mass transfer coefficient (m/s) and calculated using *Lewis number* from heat transfer coefficient (h_T) (Çengel and Ghajar, 2014), $c_{v,dryer}$ is the vapor concentration of heated drying air.

The first term on the right side of the above equation (Eq. 3.2.2-7) represented the removal of vapor from boundaries due to internal pressure and diffusion, and the second term represented the removal of vapor from boundaries due to external air flow.

b) Heat transfer

The conservation of energy in the domain was described using Eq. (3.2.2-8) (Schechter, 1961).

$$\rho_{eff} \cdot c_{p,eff} \cdot \frac{\partial T}{\partial t} + \nabla \cdot \left(-k_{eff} \cdot \nabla T + \rho_{eff} \cdot c_{p,eff} \cdot u_{eff} \cdot T\right) = \pm R_i \cdot M_w \cdot \lambda \tag{3.2.2-8}$$

where $c_{p,eff}$ is the specific heat capacity (J/kg·K), k_{eff} is the thermal conductivity (W/m·K), ρ_{eff} is the density (kg/m^3) of the porous domain, M_w is the molar mass of water in g/mol , *and* λ is the latent heat of evaporation (2.26 × 106 J/kg).

The effective density, thermal conductivity, and specific heat capacity of the porous material were calculated using the following mathematical expressions based on volume or mass fractions of different phases (Eq. 3.2.2-9 to 11) (Halder et al., 2007).

$$\rho_{eff} = \phi\left(S_g \cdot \rho_g + S_w \cdot \rho_w\right) + (1-\phi)\rho_s \quad (3.2.2\text{-}9)$$

$$c_{p,eff} = x_g\left(\omega_v \cdot c_{p,v} + \omega_a \cdot c_{p,a}\right) + x_w \cdot c_{p,w} + x_s \cdot c_{p,s} \quad (3.2.2\text{-}10)$$

$$k_{eff} = \phi[S_g\left(\omega_v \cdot c_{p,v} + \omega_a \cdot c_{p,a}\right) + S_a \cdot \rho_a] + (1-\phi)k_s \quad (3.2.2\text{-}11)$$

where ρ is density (kg/m^3), c_p is specific heat capacity (J/kg K), k is thermal conductivity (W/mK) of each phase defined by the subscripts, and the subscripts *g*, *v*, *a, w* and *s* correspond to gas, water vapour, air, water and solid fractions in a grain kernel, respectively. Density (ρ_i) of the gas was calculated using ideal gas law (Eq. 3.2.2-12)

$$\rho_i = \frac{\boldsymbol{p_i}}{\boldsymbol{RT}} M_i \quad (3.2.2\text{-}12)$$

where p_i is the partial pressure (Pa), R is the ideal gas constant (8.314 J/K·mol), T is the temperature (K), and M_i is the molar mass of the related phase (kg/mol).

The above heat and mass transfer equations were supplemented by a turbulence model. In the present case, the Shear Stress Transport (SST) k-ω model was used, as it combined the advantages of the k-e model in the far-field region and the k-ω model in the near-wall region(Menter, 1993). The boundary conditions and input parameters were listed in Table 3-5. The values adopted from published studies in this research were carefully selected to ensure that the simulated conditions closely matched those of the original studies. This was done to guarantee the applicability of the adopted values in the current study. It should be noted that a relatively high drying temperature (80°C) was adopted in the simulations to reduce computation time while still being able to observe an adequate amount of change in grain moisture content.

Table 3-5 Boundary conditions and other input parameters in CFD model

Parameter	Symbol	Value	Unit	Source
		Initial conditions		
initial moisture content	m_{db0}	0.25	g water/g dry matter	model assumption
water saturation	S_{w0}			Calculated from m_{db0} and ϕ_0
gas saturation	S_{g0}			Calculated from m_{db0} and ϕ_0
vapor concentration	c_{v0}	ideal gas law		Calculated from $P_{v,sat}$, S_{g0} and ϕ_0
air concentration	c_{a0}	ideal gas law		Calculated from $P_{v,sat}$, S_{g0} and ϕ_0
initial grain temperature	T_0	22	°C	model assumption
porosity	ϕ_0	40%		model assumption
heated air velocity (inlet)	u_0	0.6	m/s	model assumption
inlet temperature	T_a	80	°C	model assumption
		Density		
Bulk density of grain	ρ_s	772	kg/m^3	Mohsenin, 1970
water	ρ_w	998	kg/m^3	Mohsenin, 1970
		Specific heat capacity		
Grain	$c_{p,s}$	1275.5	J/kg·K	Sokhansanj and Lang, 1996
water	$c_{p,w}$	4178	J/kg·K	Sokhansanj and Lang, 1996
vapor	$c_{p,v}$	2062	J/kg·K	Sokhansanj and Lang, 1996
air	$c_{p,a}$	1006	J/kg K	Sokhansanj and Lang, 1996
		Thermal conductivity		
Grain	k_s	0.185	W/m·K	Sokhansanj and Lang, 1996
water	k_w	0.57	W/m· K	Sokhansanj and Lang, 1996
vapor	k_v	0.026	W/m·K	Sokhansanj and Lang, 1996
air	k_a	0.026	W/m·K	Sokhansanj and Lang, 1996
		Diffusion coefficient		
water	μ_w	$0.998 \cdot 10^{-3}$	Pa·s	Sokhansanj and Lang, 1996
gas	μ_g	$1.8 \cdot 10^{-5}$	Pa·s	Sokhansanj and Lang, 1996
latent heat of evaporation	λ	$2.26 \cdot 10^{6}$	J/kg	Sokhansanj and Lang, 1996

c) Airflow through porous media

The governing equations for flow through porous media formulation encompassed the continuity and momentum equations, which respectively represented the conservation of mass and momentum (Olatunde et al., 2016).

$$\frac{\partial p}{\partial t} + \frac{\partial(\rho u_i)}{\partial x_i} = 0 \tag{3.2.2-13}$$

$$\frac{\partial \rho}{\partial t} + \frac{\partial(\rho u_i)}{\partial x_i} = \frac{\partial P}{\partial t} + \rho g_i + \frac{\partial}{\partial x_j}(\mu + \mu_t)\left(\frac{\partial u_i}{\partial u_j} + \frac{\partial u_j}{\partial u_i}\right) + S_i \tag{3.2.2-14}$$

where ρ is the air density ($kg\ m^{-3}$), t is time (s), u_i and u_j are the average superficial velocity component respectively($m\ s^{-1}$), p is the static pressure (Pa), μ is the viscosity ($Pa.s$), g_i was the acceleration due to gravity (ms^{-2}). and S_i is the source term for the momentum equation.

The momentum source term S_i was expressed as follows (User's Guide, ANSYS Inc., Canonsburg, PA):

$$S_i = -\left(D_{ij}\mu u + C_{ij}\frac{1}{2}|u|u\right) \tag{3.2.2-15}$$

where D_{ij} is the viscous resistance coefficient, C_{ij} is the inertial resistance coefficient.

The terms D_{ij} and C_{ij} were represented as the inverse of the viscous loss coefficient α and the inertial loss coefficient C_2 respectively (ANSYS Inc., 2006). The viscous loss coefficient α and inertial loss coefficient coefficients C_2 were derived from Ergun's equation (Ergun and Orning, 1949; Lawrence and Maier, 2012)

$$\frac{\Delta P}{L} = \frac{150\mu(1-\varepsilon)^2}{d_p^2\varepsilon^3}u + \frac{1.75\rho(1-\varepsilon)}{d_p\varepsilon^3}u^2 \tag{3.2.2-16}$$

and

$$\alpha = \frac{150(1-\varepsilon)^2}{d_p^2\varepsilon^3} \tag{3.2.2-17}$$

$$C_2 = \frac{3.5(1-\varepsilon)}{d_p\varepsilon^3} \tag{3.2.2-18}$$

where d_p is the average particle diameter, ε is the porosity, μ is the viscosity $(Pa.s)$, $\frac{\Delta P}{L}$ is the static pressure drop.

Therefore, D_{ij} and C_{ij} could be solved as:

$$D = \frac{1}{\alpha} = \frac{d_p^2 \varepsilon^3}{150(1-\varepsilon)^2} \quad (3.2.2\text{-}19)$$

$$C = C_2 = \frac{3.5(1-\varepsilon)}{d_p \varepsilon^3} \quad (3.2.2\text{-}20)$$

It should be noted that when simulating grain drying, existing CFD models were usually limited by their assumption of grain bulk homogeneity in terms of porosity distribution (Langrish and Fletcher, 2001; Turgut et al., 2021). Pore structures of bulk grains are intricate, heterogeneous, and highly tortuous. Assuming a simple homogeneous pore structure can significantly impact the simulated airflow, as well as heat and mass transfer in grain drying processes, such as air velocity and static pressure distributions (Nwaizu and Zhang, 2021). DEM models are capable of simulating complex variability in pore structures. Therefore, coupling CFD and DEM may lead to improved prediction of grain drying.

3.2.3 CFD-DEM coupling

Coupling between CFD and DEM simulations followed a quasi-static fashion, i.e., each simulation was run incrementally in the time domain and alternatively at a given time, and the data was passed between the CFD and DEM models after each time increment (Fig. 3-6). The total drying time (to safe-storage moisture content) was divided into n timesteps with a time increment of Δt, where n was selected to match the experimental data extracted from the literature for model validation. The specific steps of coupling are outlined as follows and implemented in Matlab R2014b (Mathworks Inc.) (Fig. 3-6):

1) both CFD and DEM models were initialized, and corresponding boundary conditions and domain geometries were input into the models;

2) run the DEM model to simulate grain loading into the dryer and to form the initial grain bed. The drying time is set as t =0, an ID number was assigned to each particle (grain kernel) in the grain bed, and the initial coordinates of each particle were recorded in a matrix (P_0);
3) the information stored in matrix P0 was passed to the CFD model to define the domain for CFD simulation;
4) run the CFD model for a time period of Δt to solve for heat, mass and momentum transfer distributions;
5) the simulated moisture content and temperature were assigned to each particle (grain kernel) according to its location in the grain bed, and a matrix A0 was created to store the particle ID, coordinates, moisture content and temperature;
6) run the DEM model a time period of Δt to update the grain bed (new coordinates of each particle) and the information in matrix A0 was used to update the moisture content and temperature of each particle at the updated location, and the updated grain (particles) condition was stored in matrix A1;
7) the information stored in A1 was then passed to the CFD model and used as the initial condition for the next timestep simulation in CFD; and
8) steps 4 to 7 were repeated until the grain moved through the dryer.

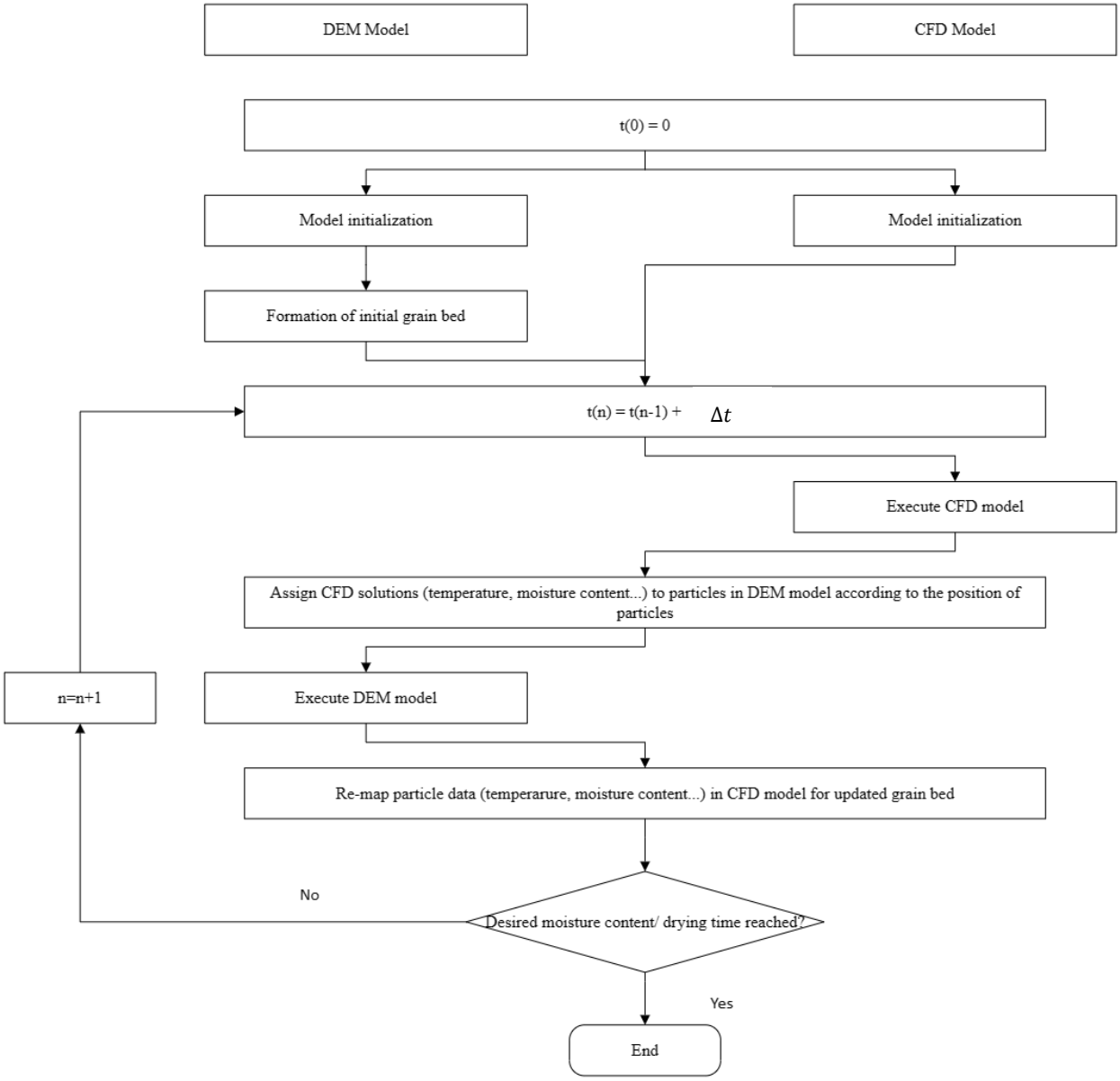

Figure 3-6 Schematic overview of DEM and CFD coupling process

3.3 Model Validation

The model-predicted results were compared with the experimentally-determined values extracted from the literature. Wilcoxon rank-sum tests were carried out to evaluate the difference between predicted and experimental results, in which the significance level (p-value=0.05) was calculated to quantify the statistical significance of differences in the distribution of predicted and experimental results. When using experimental data from peer-reviewed papers for model

validation, an algorithm was developed in MATLAB (R2014b, Mathworks Inc., USA) for automatically extracting data points if data were only presented in figures, and the R^2 between the reported value and extracted value was 0.99 with mean error at 0.01%.

Very few studies of mixed-flow dryers reported experimental data on both grain movement and drying performance (grain moisture and temperature). Given that modelling of drying process in this thesis involved DEM modelling of grain bed and CFD modelling of heat and mass transfer and airflow, model validation was carried out in two stages: validation of CFD and DEM models individually, and validation of the coupled DEM and CFD model. An advantage of the two-stage validation was the greater availability of data in the literature for each stage, which could be from studies of other drying systems. For example, data from a deep bed drying system without grain movement could be used for CFD model validation to verify the model adequacy in terms of heat and mass transfer. In addition, the two-stage validation would allow for identifying the problems at each stage of simulation to ensure the thoroughness of model validation. It should also be noted that it was extremely difficult to find the data in the literature that contained all necessary details to be compared with model simulations. An extensive literature search was conducted to find data that was deemed suitable for model validation.

3.3.1 CFD model validation

The function of the CFD model was to simulate heat and mass transfer and airflow through the grain bulk, the predicted variables were grain moisture content, grain temperature, and airflow distribution. An extensive literature search was conducted to find data for various drying systems that contained information on grain moisture content, grain temperature, or airflow. One set of data was selected for validation of grain moisture and temperature, and another set of data for airflow.

3.3.1.1 Validating for grain moisture content and temperature

The data from a deep bed grain drying study was used to validate the proposed CFD model in terms of grain moisture content and temperature distribution (Zhang, 2014). Corn was tested at an initial moisture content of 34.5% (db). The apparatus used 7 round trays (diameter of 35cm) stacking on top each other to form a drying column (grain bed) (Fig. 3-7). Each tray was filled with corn to a depth of 5 cm, and the weight of each tray was measured with a scale before drying and every 30 minutes during drying, so that the moisture content of corn at different times and bed

depth could be calculated. A temperature sensor was placed in the center of each tray for measuring the grain temperature. During the experiment, hot air at 45°C was blown from the bottom of the apparatus at a rate of 8.6 L/s. A 2-dimensional CFD simulation model was set up to predict the temperature and moisture content distributions in the middle cross-section of the drying column. According to the reported experimental conditions, the boundary conditions were established, and the physical properties of the test grain were determined (Table 3 – 6).

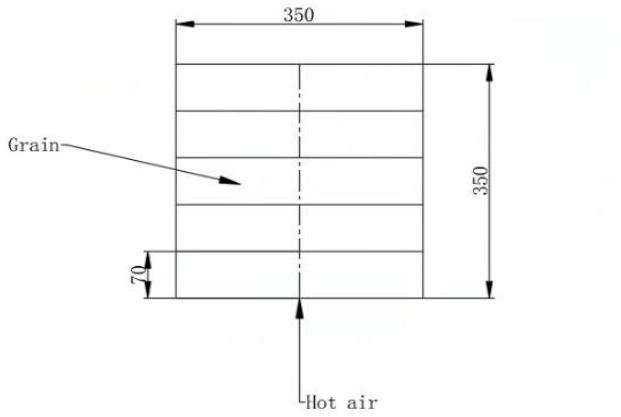

Figure 3-7 Schematic overview of the testing apparatus of the deep-bed experimental study (dimensions in mm)

Table 3-6 Boundary condition used in the deep-bed drying CFD simulation

Parameter	Value
Bed width	35 cm
Bed depth	35 cm
Initial grain temperature	11.75 ºC
Initial grain moisture content	34.5% (db)
Thermal conductivity of grain	0.185 W/m.K
Bulk density of grain	720 kg/m^3
Specific heat of grain	1684.8 J/kg.K
Dring medium temperature	45 ºC
Drying medium RH	35%
Inlet air velocity	0.7 m/s

3.3.1.2 Validating airflow

The experimental results from a study by Cenkowski et al. (1990) were utilized for validating the prediction of airflow pattern by the proposed CFD model. They conducted the experiment in a model mixed-flow dryer (Fig. 3-8). In their study, the static pressure was measured with a specially designed probe, and the static pressure was used to infer the velocity and direction of airflow.

A CFD model was set up according to the reported dimensions of the dryer used in the experimental study, with the boundary conditions shown in Table 3 - 7. The values adopted from published studies in this research were carefully selected to ensure that the simulated conditions closely matched those of the original studies. This was done to guarantee the applicability of the adopted values in the current study. Simulated static pressure was compared to the measured values from the experimental study at 9 sampling points at different heights in the drying column.

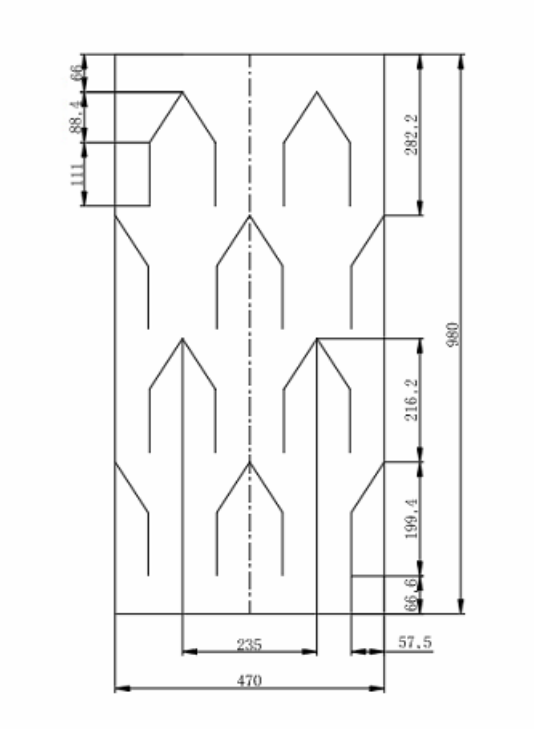

Figure 3-8 Geometry of the simulated drying column in CFD model (dimensions in mm)

Table 3-7 Boundary conditions of the CFD simulation

Parameters	Value	Source
Static pressure at inlet	40 Pa	Testing condition
Static pressure at outlet	0 Pa	Testing condition
Bulk density of grain (barley)	600 kg/m^3	Sokhansanj and Lang, 1996
Porosity of grain (barley)	0.43	Sokhansanj and Lang, 1996
Initial grain moisture content	26% (db)	Simulated condition
Initial grain temperature	22 °C	Simulated condition
Heated air temperature (inlet)	80 °C	Simulated condition

3.3.2 DEM model validation

The DEM model was validated from two aspects: grain bed formation and velocity of grain movement. The grain bed formation was validated with a characteristic variable – the bed angle and velocity validation were based on comparisons of simulated and measured velocity distributions.

3.3.2.1 Validating bed angle

The bed angle is the angle formed under the air ducts at the steady state (Fig. 3-9) (Weigler and Mellmann, 2014). The bed angle is an important characteristic of grain bed in mixed-flow dryers. Thus, a good agreement between experimental and simulated values would be an indication of adequacy of DEM modelling.

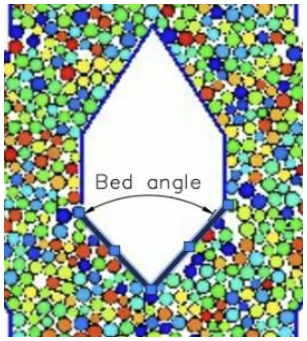

Figure 3-9 Bed angle under the air duct

The data from an experimental study by Weigler and Mellmann (2014) was used for validating the prediction of bed angle in the DEM model. The particle flow experiments were conducted in both the continuous and the interrupted flow modes. The measurements were performed in a test dryer, and the flow was controlled by a specially designed discharging device. Bed angles were measured from pictures taken with a digital video camera. For the continuous flow, images were recorded after the steady state of grain flow was attained, whereas for interrupted flow, images were taken when the discharging gate was closed.

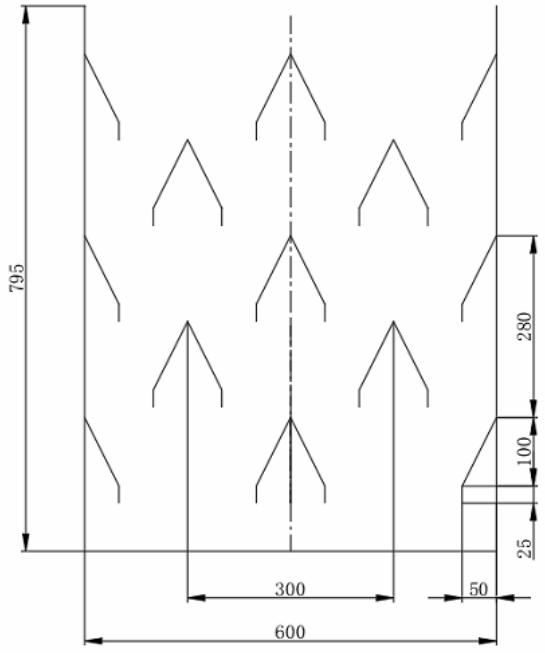

Figure 3-10 Domain geometry of the simulated test dryer in DEM model for bed angle validation (dimensions in mm)

A DEM model was set up according to the dimensions of test dryer used in the experimental study (Fig. 3-10), with boundary conditions summarized in Table 3 - 8.

Table 3-8 Boundary conditions of the DEM simulation for bed angle validation (values adopted from (Weigler and Mellmann, 2014))

Parameter	Value
Grain particle density	1300 kg/m^3
Grain friction coefficient	0.45
Wall friction coefficient	0.35
Particle normal contact stiffness	183000 Pa
Particle shear contact stiffness	183000 Pa
Wall normal contact stiffness	6800000 Pa
Wall shear contact stiffness	5960000 Pa
Shear viscous damping coefficient	0.7
Normal viscous damping coefficient	0.7

3.3.2.2 Validating grain velocity distribution

The velocity distribution data reported by (Iroba et al., 2011) from an experimental study on particle flow behavior in mixed-flow grain dryers was extracted for validating the DEM model. The design of the test dryer used in their experimental study was the same as the one used by Weigler and Mellmann (2014) that was discussed in the previous section for bed angle validation, thus the setup of the DEM model for simulating the grain velocity distribution followed the same procedure as described in Section 3.3.2.1. In the reported experimental study, the grain velocity at two different layers was determined with a digital video camera, thus the grain velocity at the same position was simulated and compared to the reported experimental values (Fig. 3-11). Six particles from each layer were selected for validation.

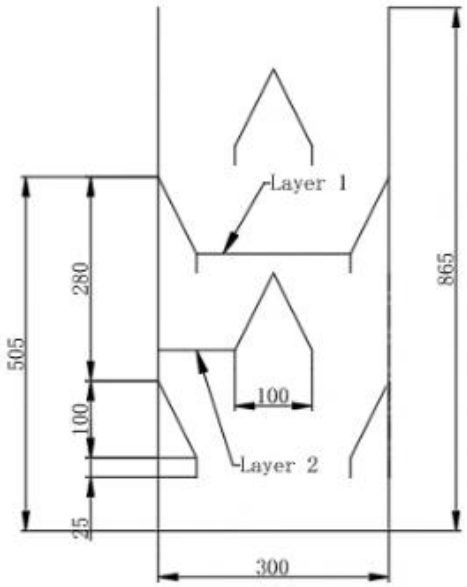

Figure 3-11 Position of two layers (1 and 2) of grain selected for velocity analysis (dimensions in mm)

3.3.3 Coupled CFD-DEM model validation

Validation of the coupled CFD-DEM model was based on the experimental data reported by (Cenkowski, 1988). The experimental setup consisted of three half ducts with positive pressure (+) as air inlets and three half ducts for the exhaust air (outlets) marked as (-) to simulate a drying column in a mixed-flow dryer, but only the top two pairs of half ducts were instrumented for data collection (Fig. 3-12). All inlet ducts were connected to a single fan and the average air flow rate was 0.00037 m^3/s. The air temperature entering the air duct was set to 80 ±1ºC. Grain was discharged from the dryer under the gravity using an airlock device that rotated at a constant speed, resulting in a grain discharge rate of 8 kg/h. Experimental conditions used in the experiment are summarized in Table 3-9.

Temperature measurements were taken with thermocouples at 32 different locations in the pilot dryer (including the inlet and outlet air ducts), and the location of thermocouples were detailed in Cenkowski's original paper (1988). Sixteen grain sampling ports of 1.5 cm in diameter were

positioned 1 cm from the side walls and air ducts for retrieving grain samples for moisture content measurement (Fig. 3-12). The 16 moisture measurement points corresponded to the 16 points of temperature measurements in the grain mass. Moisture content measurements was taken after the steady-state was reached.

Table 3-9 Experimental conditions for the mixed-flow dryer (Cenkowski, 1988)

Parameter	Value
Grain discharge rate	8 kg/h
Air temperature	80 ºC
Air flow rate	0.00037 m^3/s
Air humidity	0.0045 kg H_2O/kg dry air
Initial grain moisture content	0.254- 0.273 kg H_2O/kg dry mass
Initial grain temperature	13 - 17 ºC

The coupled CFD-DEM model was set up according to the reported dimensions of the test dryer, as well as the boundary conditions (Table 3-10). The values adopted from published studies in this research were carefully selected to ensure that the simulated conditions closely matched those of the original studies. This was done to guarantee the applicability of the adopted values in the current study.

Simulated data of temperature and moisture content corresponding to the 16 points of measurement in the drying column were selected for validating the proposed coupled CFD-DEM model.

Table 3-10 Boundary conditions and other input parameters in the CFD-DEM model

Parameter	Value	Unit	Source
	Initial conditions		
initial moisture content	0.256	g water/g dry matter	Model assumption
initial grain temperature	22	°C	Model assumption
porosity	40%		Model assumption
heated air velocity (inlet)	0.00037	m^3/s	Model assumption
inlet temperature	80	°C	Model assumption
Grain mass flow rate	8	kg/h	Model assumption
	Density		
Bulk density of grain	750	kg/m^3	Mohsenin, 1970
water	998	kg/m^3	Mohsenin, 1970
	Specific heat capacity		
Grain	2314	J/kg.K	Sokhansanj and Lang, 1996
water	4178	J/kg.K	Sokhansanj and Lang, 1996
vapor	2062	J/kg.K	Sokhansanj and Lang, 1996
air	1006	J/kg.K	Sokhansanj and Lang, 1996
	Thermal conductivity		
Grain	0.185	W/m.K	Sokhansanj and Lang, 1996
water	0.57	W/m.K	Sokhansanj and Lang, 1996
vapor	0.026	W/m.K	Sokhansanj and Lang, 1996
air	0.026	W/m.K	Sokhansanj and Lang, 1996
	Diffusion coefficient		
water	$0.998 \cdot 10^{-3}$	Pa.s	Sokhansanj and Lang, 1996
gas	$1.8 \cdot 10^{-5}$	Pa.s	Sokhansanj and Lang, 1996
latent heat of evaporation	$2.26 \cdot 10^{6}$	J/kg	Sokhansanj and Lang, 1996
	Grain particle properties		
Grain particle density	1300	kg/m^3	Weigler and Mellmann, 2014
Grain friction coefficient	0.45		Weigler and Mellmann, 2014
Wall friction coefficient	0.35		Weigler and Mellmann, 2014
Particle normal contact stiffness	183000	Pa	Weigler and Mellmann, 2014
Particle shear contact stiffness	183000	Pa	Weigler and Mellmann, 2014
Wall normal contact stiffness	6800000	Pa	Weigler and Mellmann, 2014
Wall shear contact stiffness	5960000	Pa	Weigler and Mellmann, 2014
Shear viscous damping coefficient	0.7		Weigler and Mellmann, 2014
Normal viscous damping coefficient	0.7		Weigler and Mellmann, 2014
Grain equivalent diameter	0.00348	m	Weigler and Mellmann, 2015

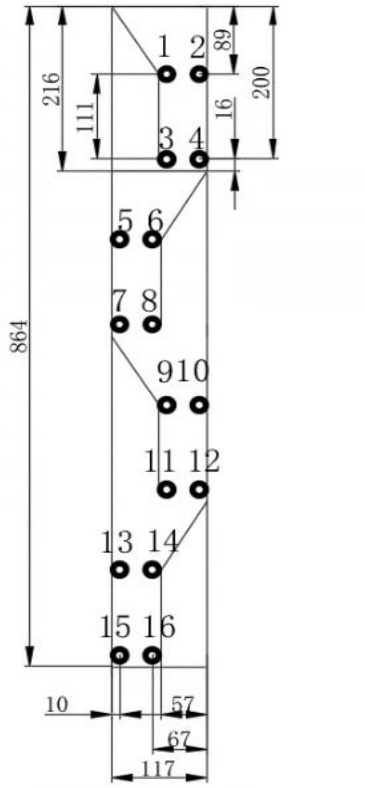

Figure 3-12 Dimensions of experimental mixed-flow dryer by (Cenkowski 1985). Numbers 1-16 indicate the moisture content sampling points(All dimensions are in mm)

3.3.4 Statistial analysis

3.3.4.1 Wilcoxon rank-sum test

In this study, Wilcoxon rank-sum tests were carried out with Python scripts to evaluate the difference between predicted and experimental results. The Wilcoxon rank-sum test, also known as the Mann-Whitney U test, is a non-parametric statistical test utilized to compare two independent samples to determine if their population distributions differ (Conover and Iman, 1981; Kasuya, 2001). The reason for adopting Wilcoxon rank-sum test was that it is a non-parametric, which means that it is unrestricted by the normal distribution assumption, which is required by other test, such as the paired-t test (Conover and Iman, 1981). The significance level (p-value=0.05) was calculated to quantify the statistical significance of differences between the simulated and

experimental results. The p-value calculation involved a series of methodical steps, as detailed below.

Step 1: Ranking of Observations

Initially, observations from both samples, simulated data (n=n_1) and experimental data (n=n_2), were merged into one single dataset. Each observation was then assigned a rank based on its value, with the smallest observation receiving a rank of 1, the next smallest a rank of 2, and so forth. In the presence of tied values, each tied observation was assigned the average rank of the positions they would occupy if there were no ties.

Step 2: Computation of Rank Sums for Each Sample

Subsequently, the ranks assigned in the previous step were summed separately for each sample. Let R_1 represent the sum of the ranks for the simulated data and R_2 represent the sum of the ranks for the experimental data.

Step 3: Calculation of the Test Statistic (U)

The test statistic, U, was calculated using the rank sums. For samples of sizes n_1 and n_2, the test statistic was determined as follows:

$$U_1 = n_1 n_2 + \frac{n_1(n_1+1)}{2} - R_1 \tag{3.3.4-1}$$

$$U_2 = n_1 n_2 + \frac{n_2(n_2+1)}{2} - R_2 \tag{3.3.4-2}$$

The smaller value of U_1 and U_2 was then employed for determining the p-value in the next steps.

Step 4: Determination of Mean and Standard Deviation of U

The mean (μ_U) and standard deviation (σ_U) of the test statistic, U, were computed as follows:

$$\mu_U = \frac{n_1 n_2}{2} \tag{3.3.4-3}$$

$$\sigma_U = \sqrt{\frac{n_1 n_2 (n_1+n_2+1)}{12}} \tag{3.3.4-4}$$

Step 5: Conversion of U to a Standardized Test Statistic (Z-score)

U was then converted into a Z-score utilizing the mean and standard deviation:

$$Z = \frac{U-\mu_U}{\sigma_U} \tag{3.3.4-5}$$

Step 6: Determination of the p-value

Finally, the p-value was determined based on the Z-score. For a two-tailed test, the p-value was calculated as twice the area under the standard normal curve to the right of the absolute value of the Z-score ($|Z|$):

$$p = 2 \times P(z > |Z|) \quad (3.3.4\text{-}6)$$

This approach provided a rigorous comparison of simulated and experimental data without presupposing a specific distribution for the data.

3.3.4.2 Relative differences between predicted and experimental values

To quantitively evaluate the goodness of prediction by the model, the relative differences between model-predicted values and experimental values extracted from published literature were calculated as follows:

$$Relative\ difference = \frac{predicted\ value - experimental\ value}{experimental\ value} \times 100\% \quad (3.3.4\text{-}7)$$

This equation was applied for the validation of grain moisture content, grain temperature, static pressure, grain bed angle and grain velocity.

3.4 Risk analysis of grain kernel damages during drying

Drying may cause damages to grain if the drying conditions are not controlled probably in grain dryers. For example, if the drying conditions are not uniform, grain in some localized areas could be exposed to excessively high temperature that could cause damage to the kernels. Since the coupled DEM-CFD model developed in this thesis could predict local conditions of grain during drying at the kernel level, it could be used to effectively estimate grain damage related to extreme drying conditions in localized areas. To explore the potential of using the coupled DEM-CFD model for risk analysis of grain damage during drying, two empirical models were used as the post

processors to estimate the germination rate and kernel cracking (fissure) rate, respectively. Specifically, after completing the DEM-CFD simulations, the simulated grain temperature and moisture data was fed to the two empirical models to calculate the germination and kernel cracking rates. It should be noted that the two empirical models used were developed for corn and rice, respectively, because no published studies were found for wheat. Although the coupled CFD-DEM simulations were performed using parameters for wheat, using the simulated data in empirical models to predict the germination rate for corn and kernel cracking rate for rice could still provide insights on the general patterns of how the germination and grain crack rates were affected by drying. The purpose was to illustrate the process of using the DEM-CFD simulations to assess grain quality.

In the empirical germination model (Wu et al., 2013), the decline in germination rate was estimated at a given time during drying as follows:

$$G_i = G_{i-1} \times \left(1 - \frac{1}{1+EXP\left(80.5-8.8{T_i}^{0.5}-1.3{t_i}^{0.5}-6.48M_i\right)}\right) \quad (i = 1, 2., \ldots) \qquad (3.4 - 1)$$

where G_i is the estimated germination rate at the end of time step i (fraction), T_i is the drying air temperature in time step i (C°), t_i is the duration of drying at time step i (min), M_i is the moisture content of grain kernel at time step i (%, wb).

Germination reduction risk was proposed herein to quantify the potential loss in germination rate of a grain kernel caused by a certain drying condition. This risk was defined as ratio of the accumulative decrease in germination rate up to time step i of drying to the initial germination rate (Eq. 3.4-2)

$$R_{Germ(i)} = \frac{G_1 - G_i}{G_1} \qquad (3.4 - 2)$$

where $R_{Germ}(i)$ is the estimated germination reduction risk of a grain kernel at time step i, and G_1 is the initial germination rate (assumed as 95%).

To quantify the kernel cracking risk, the cracking rate was first estimated as follows (Zheng and Wang, 1999):

$$C_i = C_{i-1}\,(7.649 + 0.453t_i + (6.749 + 0.150\,t_i)(1.746 - 0.039RH_i - \frac{57.974}{T_i}) \qquad (3.4 - 3)$$

where C_i is the estimated rate of kernel cracking at the end of time step i (fraction), and RH_i (%) is the relative humidity around the grain kernel at time step i.

Once C_i was calculated, the kernel cracking risk was determined as the ratio of accumulative increase in kernel cracking rate up to time step i of drying to the initial kernel cracking rate (Eq.3.4-4):

$$R_{Crack(i)} = \frac{C_i - C_1}{C_1} \quad (3.4 - 4)$$

where $R_{Crack\ (i)}$ is the estimated risk of cracking for a grain kernel time step i, and C_1 is initial kernel cracking rate. In this study, C_1 was assumed to be 5%. In post-harvest handling of rice, the percentage of broken kernels ranges from 1.5% to 46.3% (Phillips et al., 2024). By USDA standards, rice with 5% average broken percentage is classified as US No. 1 (Hardke and Siebenmorgen, 2009).

4. Results and discussion

4.1 Meshing optimization for CFD modelling

The hypothetical dryer configuration shown in Fig. 3-4 was used to conduct preliminary simulations to optimize CFD meshing. Given that the most important parameter in grain drying is grain moisture content, the simulated moisture content of the six sampling points at various locations in the dryer was used to optimize meshing in CFD modelling (Fig. 3-5). The predicted values converged gradually with the increase in number of elements, and stabilized at 15717 elements (cell size: 18.67 mm^2) (Fig. 4-1). Considering a safety factor of 1.5, meshing with 23576 elements (cell size: 12.45 mm^2) was adopted in CFD modelling. The final mesh of CFD-DEM model simulations was illustrated in Fig. 4-2.

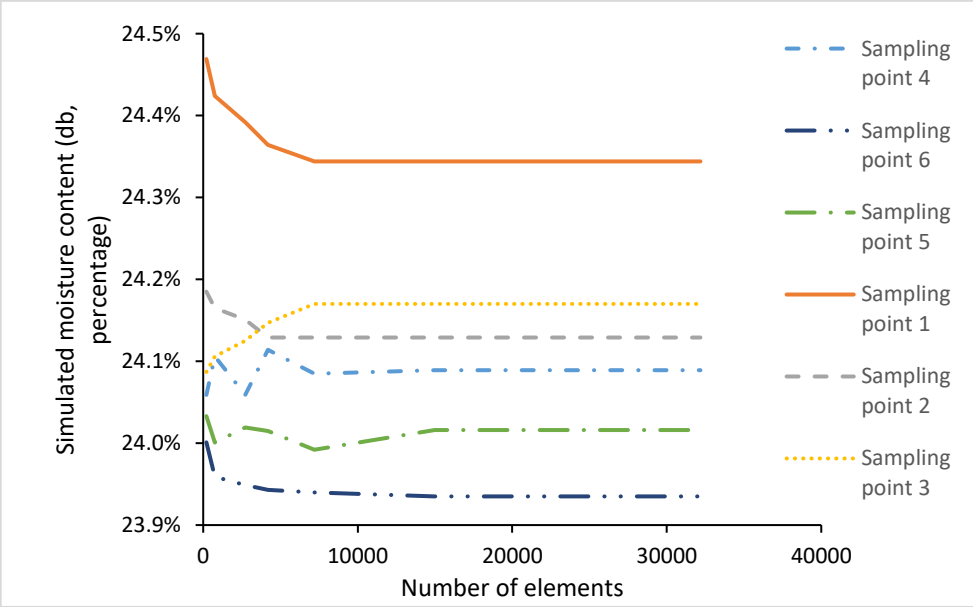

Figure 4-1 Meshing convergence results of simulated moisture content with different numbers of element

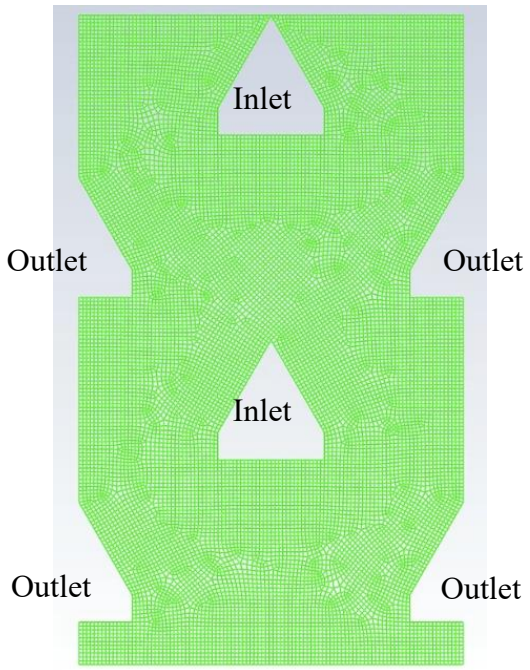

Figure 4-2 Final mesh of the proposed CFD-DEM model

4.2 Model validation

Model validation results are presented at two levels: validation of individual models (CFD and DEM were validated separately), and the coupled DEM-CFD model.

4.2.1 CFD model validation

CFD model validation was carried out by comparing three most import parameters in drying: grain moisture, grain temperature, and airflow, between model simulations and experimental data obtained from the literature.

4.2.1.1 Grain moisture content and temperature distributions

A good agreement was observed between simulated and experimental values of moisture content (Fig. 4-3). The minimum relative difference was 1.9% (0.56 percentage point) which was

found at the 10-15 cm layer while the maximum relative difference of 3.4% (1.55 percentage point) was found at the top layer. It seemed that grain in the top four layers (20-35 cm) was not dried at all in the experiment and the measured moisture content actually increased slightly, which was probably caused by condensation occurred when the warm drying air at high RH met the low-temperature grain in the top layers. However, this phenomenon of moisture gain by grain due to condensation was not considered in the CFD modelling. Therefore, the simulated moisture decreased slightly with drying time in the top layers (Fig. 4-3), resulting in greater relative differences between simulated and experimental moisture content values. In overall, Wilcoxon rank-sum test indicated that the differences between simulated and experimental values were statistically insignificant ($p>0.05$) in all layers during the entire drying period of 150 minutes (Table 4-1). Thus, it was concluded that the predictions of grain moisture content by the proposed CFD model were adequate.

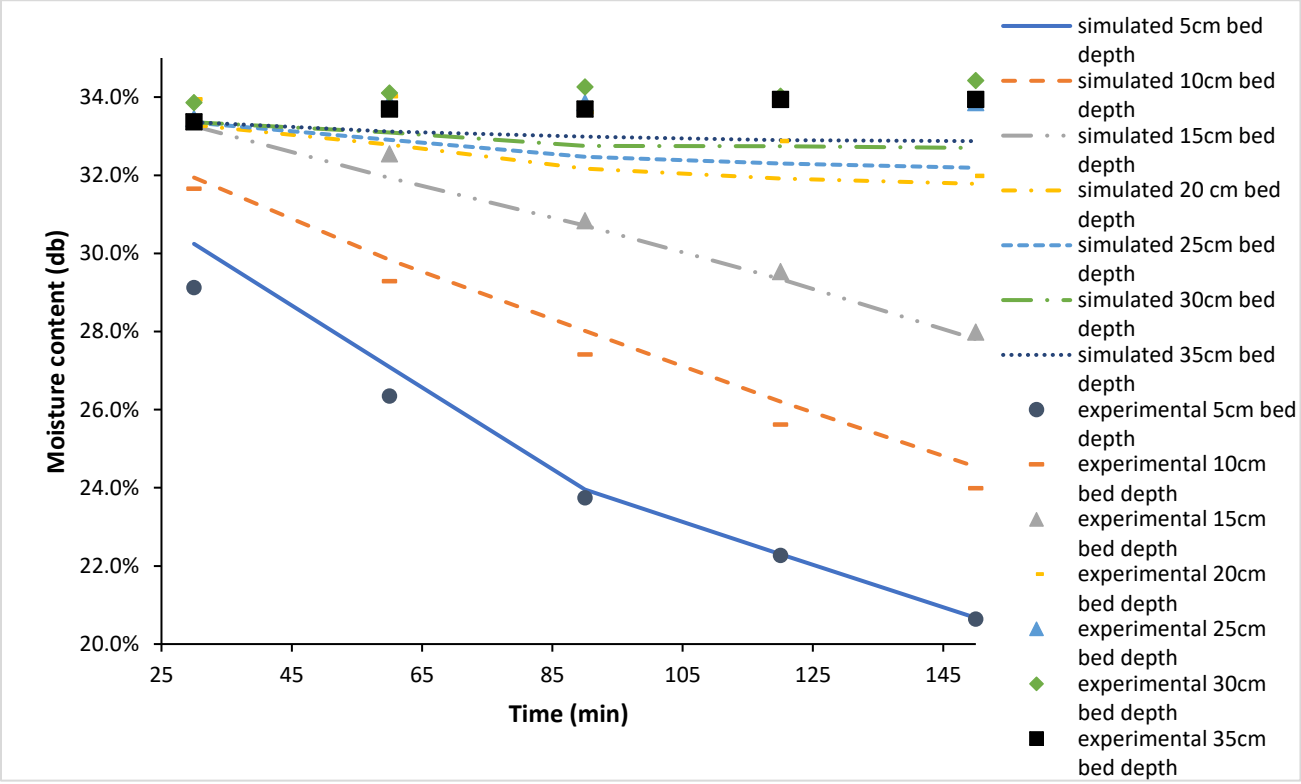

Figure 4-3 Simulated and experimental variations of grain moisture content at different bed depths (bed depth was measured from the bottom, experimental data extracted from Zhang, 2014)

Table 4-1 Wilcoxon rank-sum tests to compare simulated and experimental distributions of grain moisture content and temperature

Drying time (min)	p-value for moisture content comparison	p-value for temperature comparison
30	0.142	0.565
60	0.338	0.482
90	0.338	0.565
120	0.406	0.949
150	0.565	0.655

Excellent agreement between the experimental and simulated temperatures was observed for all layers, except the bottom (5 cm) layer (Fig. 4-4). In the bottom layer near the air inlet, the experimental temperature was higher than the simulated temperature, but the difference decreased as drying progressed. A possible explanation was that grain in the bottom layer was closer to the inlet of hot air, thus the measurement of grain temperature is more heavily affected by the incoming air (45 ^{o}C), which resulted in a higher reading. With the progress of drying, the influence of incoming air got smaller, as the grain temperature picked up and the temperature difference between incoming air and grain became smaller. The Wilcoxon rank-sum test considering all layers indicated that the differences between simulated and experimental temperatures were statistically insignificant ($p>0.05$) during the entire drying period of 150 minutes (Table 4-1). Thus, it was concluded that the predictions of grain temperature by the proposed CFD model were adequate.

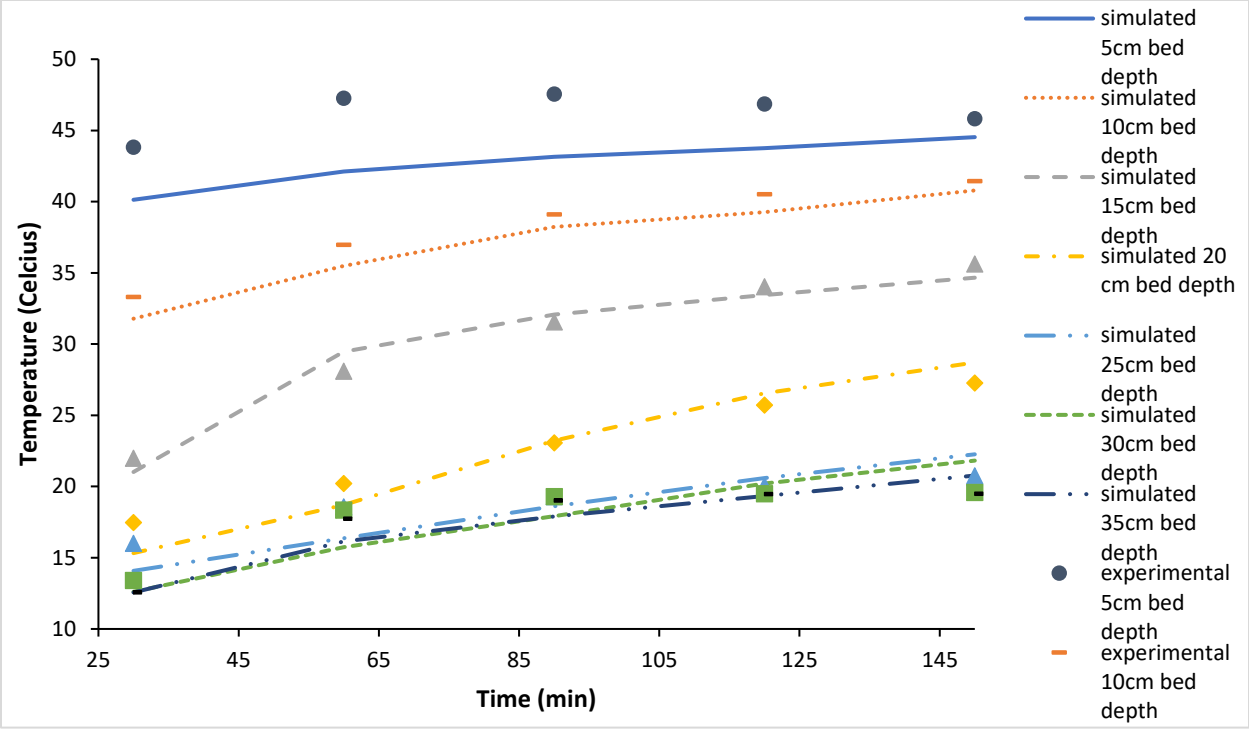

Figure 4-4 Simulated and experimental distribution of temperature at different bed depths (experimental data extracted from Zhang (2014))

4.2.1.2 Validation of air flow pattern

The simulated and experimental static pressure values at nine sampling points are tabulated in Table 4-2. The simulated static pressure showed an excellent agreement with the experimental values, with an average difference of 1.62%. Also, a Wilcoxon rank-sum test indicated that the difference between simulated and experimental values was statistically insignificant ($p>0.05$). Thus, it was concluded that the prediction of airflow pressure by the proposed CFD model was adequate.

Table 4-2 Comparison of simulated static pressure with experimental value reported by Cenkowski et al., (1990)

Sampling point	1	2	3	4	5	6	7	8	9
Experimental value (Pa)	22	27	33	38	40	44	46	41	37
Simulated value (Pa)	21	26	34	38	40	44	45	40	37
Relative difference	4.5%	2.6%	2.1%	1.3%	0.3%	0.2%	1.5%	1.5%	0.0%

4.2.2 DEM model validation

4.2.2.1 Validation of bed angles

The simulated value was in close agreement with the experimental values, with an average relative difference of 0.80% (Table 4-3). Wilcoxon rank-sum test also showed that the difference between simulated and experimental values was insignificant ($p>0.05$). Thus, it was concluded that the prediction of bed angle was adequate.

Table 4-3 Comparison of the experimental and simulated bed angle (experimental data extracted from Weigler and Mellmann, 2014)

Flow configuration	Bed angle (degree)		Relative difference
	Measured value	Simulated value (average)	
Continuous flow	105	104.3	0.67%
Interrupted flow	120	121.1	0.92%

4.2.2.2 Validation of grain velocity distribution

The simulated gain velocities were in good agreement with the experimental values for all 12 sampling points, with an average difference of 4.27% (Table 4-4). The highest relative difference was observed at sampling point 4 and 9, which were located in layer 2 and layer 1 respectively, and a possible explanation for higher differences at these two points could be the instantaneous fluctuation in grain particle velocity, which would be discussed with greater details in section 4.4. A Wilcoxon rank-sum test revealed that the difference between simulated and experimental values was statistically insignificant ($p>0.05$). Thus, it was concluded that the prediction of grain velocity in the proposed DEM model was adequate.

Table 4-4 Comparison of the experimental and simulated grain particle velocity (experimental data extracted from Iroba et al., 2011)

Sampling point	1	2	3	4	5	6	7	8	9	10	11	12
Layer	2	2	2	2	2	2	1	1	1	1	1	1
Distance from the left boundary (m)	0	0.01	0.04	0.06	0.08	0.1	0.25	0.23	0.2	0.15	0.13	0.1
Experimental value (m/s)	0.037	0.046	0.062	0.065	0.069	0.052	0.058	0.071	0.079	0.076	0.078	0.076
Simulated value (m/s)	0.035	0.045	0.063	0.059	0.073	0.052	0.057	$0.070	0.081	0.084	0.073	0.079
Relative difference	4.68%	2.56%	2.24%	9.23%	5.80%	0.30%	1.54%	1.54%	2.53%	10.53%	6.41%	3.95%

4.2.3 Coupled CFD-DEM model validation

An algorithm was developed in MATLAB (R2014b, Mathworks Inc., USA) for automatically extracting data points from the figures presented in Cenkowski's work (1985). It successfully retrieved the grain temperature from all sampling points (16/16) (as listed in Table 4-5), but due to the resolution of the original figure, it could only extract 14 out of 16 data points for grain moisture content (as listed in Table 4-6). Gain temperature and moisture content simulated by the coupled CFD-DEM model were compared with the experimental data reported by Cenkowski (1985) for a mix-flow dryer shown in Fig.3-12. A total of 2385 particles were generated in the simulation and the simulation was run until the steady-state was reached, which was equivalent to 33 minutes of physical drying time. The simulated average moisture content of discharged (dried) grain was 17.3% (db), while the experimental value was 18.9% (db).

The comparisons indicated an excellent agreement between the simulated and experimental results in both temperature and moisture content, with an average relative difference of 4.3% for temperature and 2.6% for moisture content (0.56 percentage points) as shown in Tables 4-5 and 4-6. The largest relative differences between simulated and experimental results were 9.1% for temperature and 8.5% and moisture content (1.6 percentage points) respectively. Wilcoxon rank-sum tests revealed that p-values exceeded 0.05, indicating that the discrepancy between the simulated and experimental values was statistically insignificant for both temperature and moisture content. Consequently, it was concluded that the coupled CFD-DEM model successfully predicted both temperature and moisture content distributions in a mixed-flow dryer.

Table 4-5 Comparison of simulated grain temperature with experimental data extracted from Cenkowski (1985)

Sampling point	Experimental (^oC)	Simulated (^oC)	Relative difference
1	46.7	43.8	6.3%
2	40.8	38.6	5.3%
3	51.9	48.0	7.6%
4	56.3	52.1	7.5%
5	80	80.0	0.0%
6	67.2	61.1	9.1%
7	60.5	55.3	8.6%
8	21.7	20.9	3.5%
9	22	21.5	2.4%
10	23.7	23.0	2.8%
11	24.1	23.8	1.1%
12	39.8	37.9	4.8%
13	34.1	32.7	4.1%
14	32.8	31.7	3.3%
15	30.3	29.6	2.4%
16	46.7	43.8	6.3%

Table 4-6 Comparison of simulated grain moisture content with experimental data extracted from Cenkowski (1985)

Sampling point	Experimental (%db)	Simulated (%db)	Relative difference
1	26.1	26.0	0.4%
2	25.9	26.0	0.4%
3	26.0	25.9	0.4%
4	25.5	25.8	1.2%
5	25.1	25.7	2.4%
6	24.9	25.6	2.8%
7	24.7	25.2	2.0%
8	26.1	26.0	0.4%
9	24.3	23.9	1.7%
10	23.5	23.1	1.7%
11	22.8	22.0	3.5%
12	22.3	21.5	3.6%
13	20.8	19.4	6.7%
14	18.9	17.3	8.5%

4.3 Simulated airflow distributions

Simulations were conducted to investigate airflow distributions in the hypothetical mixed-flow grain dryer shown in Fig. 3-4 for three inlet air velocities of 0.60, 0.45 and 0.30 m/s. These air velocities are commonly adopted in mixed-flow grain drying operations (Dai and Cao, 1965; Jia et al., 2000). The direction of air coming from an inlet duct into the surrounding ducts was as shown in Fig. 4-5. As the drying air came out of an inlet air duct, it was diverted into two directions, i.e., it either went up or down to the closest outlet air ducts. The highest velocity magnitude was found at corners of each air duct (Figs. 4-5 and 4-6), which could be explained by the local turbulence caused by the sharp angle of the flow path, while a near-zero-velocity zone could be found around the top of each outlet and inlet air duct (Fig. 4-6). It was observed that zones with highest static pressure were found under the inlet air ducts, and the static pressure gradually decreased until air exited through the outlet ducts (Fig. 4-7).

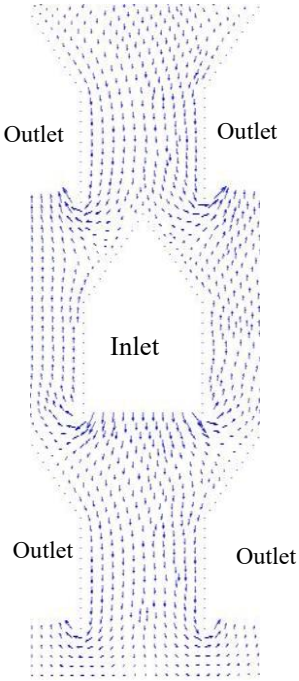

Figure 4-5 Simulated airflow distribution around an air inlet (the length of the arrows indicates the magnitude of air velocity) (The inlet air velocity was 0.60 m/s)

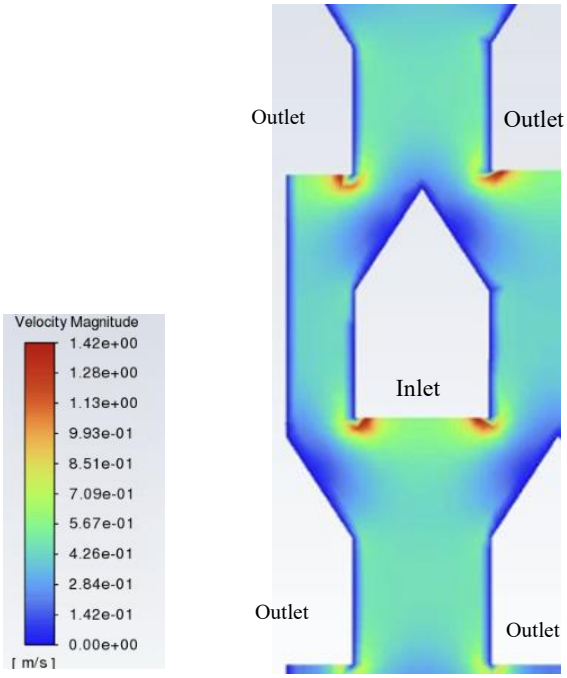

Figure 4-6 Zero air velocity zones (blue) and high velocity zones (red) (The inlet air velocity was 0.60 m/s)

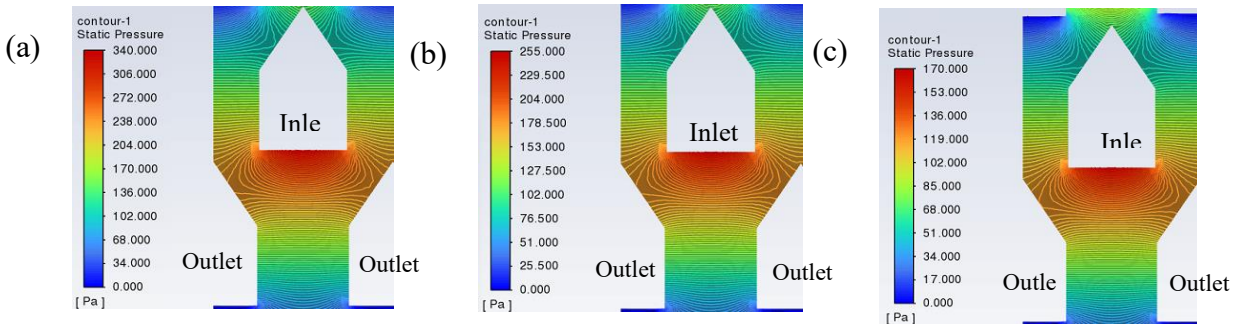

Figure 4-7 Static pressure distribution when inlet air velocity was at (a) 0.60 m/s, (b) 0.45 m/s and (c) 0.30 m/s

4.4 Simulated grain velocity distributions

4.4.1 General pattern of grain flow

When the flowing grain reached the tip of an air duct (inlet or outlet), it was divided into two "channels", one on the right and one on the left and few kernels crossed the channel boundaries into the other channel even when they reached the bottom the inlet (or outlet) (Fig. 4-8). The grain velocity in the center of each channel was higher than that near the boundaries, in particular near the wall. This was attributed to friction between grain and the surfaces of wall and air ducts or the encounter with grain kernels that were travelling at different velocities near the boundary between two channels. "Dead zones" existed under air ducts where the vertical velocity of grain was close to zero, and grain kernels in these zones had to move horizontally towards the channel boundary then move out the dead zones. The average velocity of grain kernels in the dead zone was 0.0047 m/s, which was 38.1% of the average velocity magnitude of all simulated grain kernels, thus these grain kernels would have higher risk of being over-dried or suffering from the heat-induced damage due to prolonged exposure to excessive heat.

Many researchers assumed that grain flow was symmetric about the dryer center line in modelling in order to use a simplified numerical model consisting of half of the dryer (Keppler et al., 2012). However, it was found in this study that the grain velocity distribution was not symmetrical, i.e., grain in the left and right sides of the dryer (referred as right and left flow

channels in this study) might move at different speeds and grain speed in both channels varied. Specifically, grain in one channel would sometimes move at a slower speed compared to the other channel, but after a short duration, grain in the slower channel could pick up speed and move faster than the other channel (Fig. 4-8). The instantaneous and random grain kernel velocity changes could be explained by instantaneous and random arch formation and collapse in the grain mass. Arching typically occurs in bulk solids storage systems when an undesirable hopper angle is adopted and/or the cohesion of material is too high. Grain is considered to be free-flowing material, i.e., no permanent arches would form to stop grain flow. However, air ducts acted as obstacles to grain movement by narrowing the flow channels and changing the flow direction, causing the formation of instantaneous formation of arches. But without cohesive forces, these arches could not sustain the gravity force from the grain mass above and they would collapse right away before they could stop grain flow. Cycling of arch formation and collapse caused the grain velocity to go down (arch formation) and up (arch collapse).

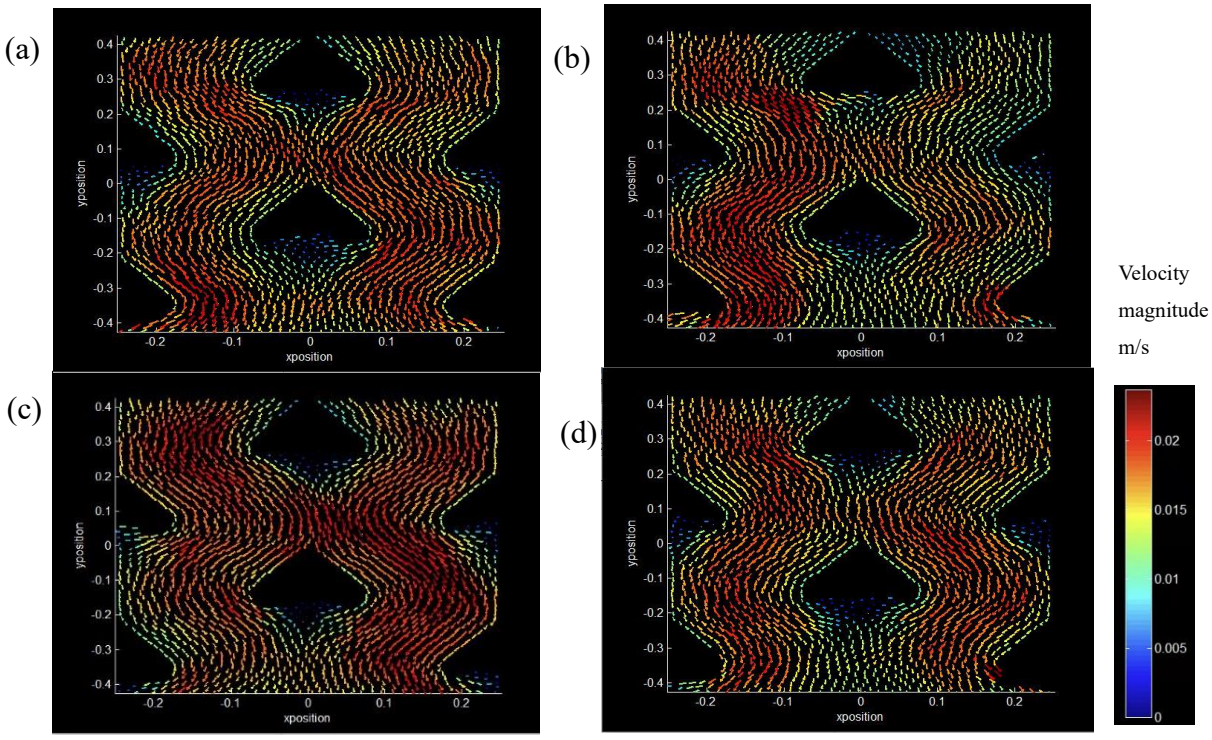

Figure 4-8 Grain velocity distribution at (a)7.5 minutes, (b) 15 minutes, (c) 22.5 minutes and (d) 30 minutes after the start of drying

4.4.2 Velocity variation

To analyze the influences of the wall and air ducts on grain velocity, two layers of grain were selected (Layer 1 and Layer 2) to represent the two critical locations in a grain flow channel on the left side of dryer (Fig. 4-9), and the vertical velocity (downward) profiles in these two layers are plotted (Fig.4-10). In Layer 1, the flow of grain kernels on the left was heavily affected by the air duct – there was a reduction of 42.8% in grain velocity. The similar effect by the dryer wall was observed on the right side: the velocity reduction from the channel center to the wall was about 24.5%. In Layer 2, the flow of grain on the right was heavily affected by the air duct, with a reduction in grain velocity of 41.4%. At the dryer center, the grain velocity decreased by about 11% due to: i) the air ducts along the centerline; and ii) the interaction with grain kernels in the left channel, in which grain might move slower. It should be noted that if grain in the left channel had flowed faster than the right channel, the grain near the centerline at Layer 2 could be higher than other locations. In overall, the simulation results indicated that air ducts had the strongest influence on grain velocity, followed by the wall surface, and then channel boundary. Therefore, the proper design and the design optimization of air ducts in mixed-flow grain dryers is of high importance.

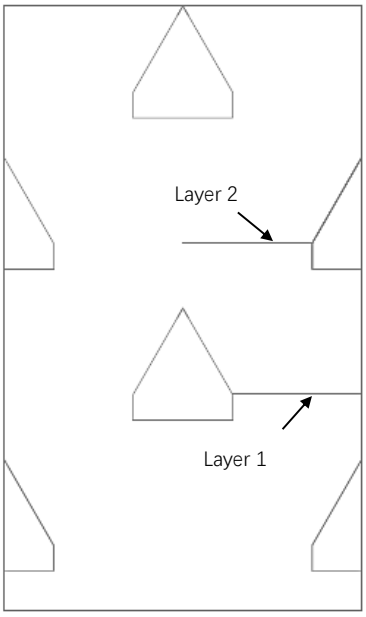

Figure 4-9 Position of two layers of grain selected for velocity analysis

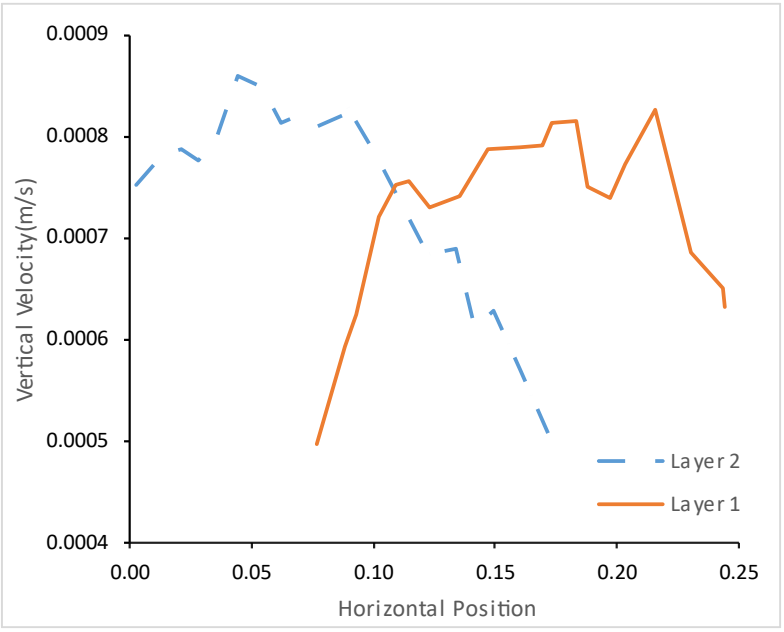

Figure 4-10 Vertical velocity of grain from two selected layers (the center of the drying column is the 0 horizontal position)

4.5 Residence time of drying

The residence time of drying is defined as the time it takes for a grain kernel to travel through the dryer. The uneven distribution of grain movement velocity causes a variation in grain residence time, which is eventually responsible for the uneven drying, thus studying the grain residence time distribution is of high importance for assessing the dryer performance.

4.5.1 Variation in residence time

To analyze the grain residence time, a layer of 73 grain kernels at the top of the drying column was marked as tracer particles (Fig.4-11), and their movements were tracked until they were discharged from the dryer.

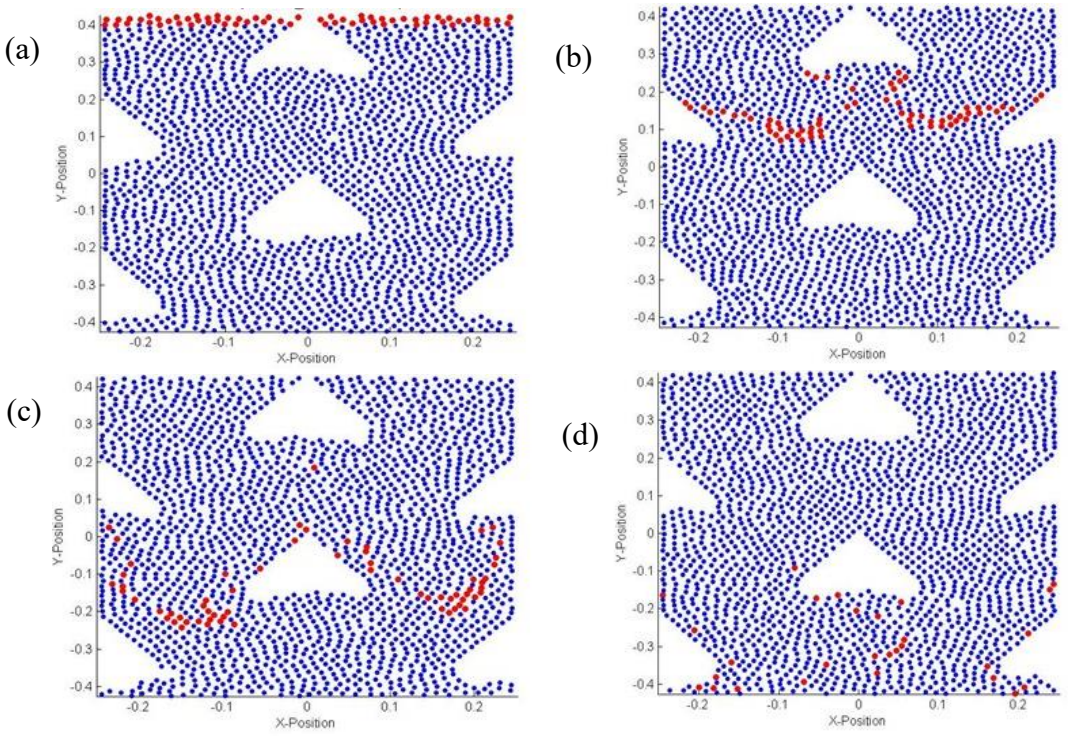

Figure 4-11 Position of tracer particles at (a)7.5 minutes, (b) 15 minutes, (c) 22.5 minutes and (d) 30 minutes after the start of drying

The simulation ran for 65 minutes until all tracer particles were discharged, which is 2.17 times of the grain throughput time (30 minutes). Grain kernels in the middle of the left and right flow channels took the shortest time to be discharged, while the kernels near the dryer walls, air ducts, and the dryer centerline experienced longer residence time of drying. The low-velocity zone underneath the air ducts had a strong influence on residence time of drying: kernels could be "trapped" for a longer time under the air ducts (Fig. 4-11(b)).

Variation of residence time across the dryer is shown in Fig. 4-12. The grain kernels near the dryer walls and at the center of the dryer experienced longer residence time because the effect of dryer walls and air ducts, with the highest residence time near the walls. This distribution of residence time was caused by friction of wall and obstacles to grain flow caused by air ducts that slowed down grain movement, as well as the possible effect of velocity difference along the boundary of two grain flow channels (Fig. 4-11). Thus, a possible way of optimizing the residence time distribution is to adopt a low-friction coating material inside the wall of the grain dryers and a narrower air duct design to minimize the effect of low-velocity zones under the air duct. The residence time distribution curve was not perfectly asymmetrical along the Y-axis, with the residence time on the left slightly lower that on the right side, indicating that grain in the left channel moved slightly faster than the right channel. It should be noted that the velocities of left and right channels were dictated by the random formation and collapse of instant arches in the grain mass, which was reflected by many small jumps in the curve shown in Fig. 4-12, and thus it is possible for either the left or the right side to have slightly shorter residence time.

The frequency distribution of residence time is shown in Fig. 4-13. The residence time of drying of all grain kernels ranged from 20 to 66 min, with a median of 36 min. The range of the highest frequency was from 31 to 36 min, followed by 25 to 31 minutes. The distribution did not follow the bell-shaped (normal) distribution, rather it had a longer tail, indicating that the more grain kernels experienced longer residence time. It should be mentioned that grain kernels were represented by discs in this study, i.e., the kernel shape effect on residence time was not considered in this study.

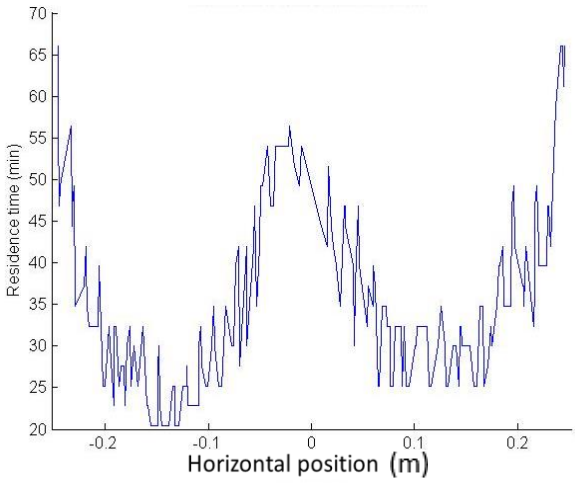

Figure 4-12 Residence time of tracer particles at different horizontal positions （0 in horizontal position represented the center of the dryer）

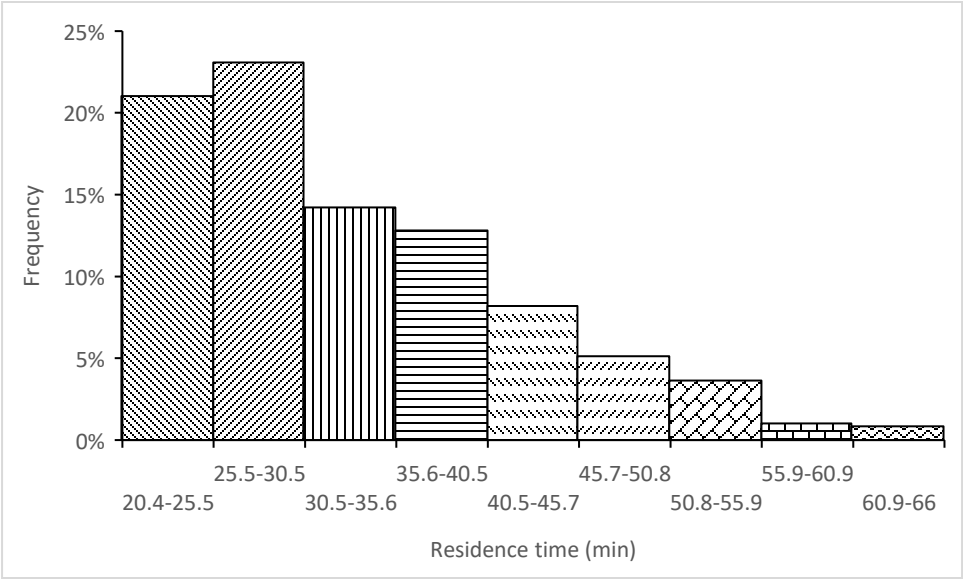

Figure 4-13 Frequency distribution of residence time of drying after steady state (based on 4991 grain kernels discharged after steady state)

4.5.2 Effect of kernel properties on residence time

The grain flow pattern is affected by the mechanical properties of the individual grain kernels, as well as foreign materials, such as dockage. In DEM modelling, grain particle density was set as a normal distribution in the range from 85% to 115% of the reference value (Table 3- 4) which

was adopted from the literature to study the influence of physical properties of individual particles on drying (Mohseni and Peters, 2016; Mohsenin, 1970). Residence times for grain kernels in four different density ranges were calculated from the DEM simulation results (Table 4-7).

Table 4-7 Average residence time of particles in different density ranges

Particle density range (kg/m^3)	1158 - 1223	1223 - 1287	1287 - 1351	1351 - 1415
Average residence time of drying (min)	38.4	35.19	34.51	34.31

The simulations revealed that the residence time decreased with density – the heavier grain kernels moved through the dryer faster and grain kernels in lower density ranges tended to experience longer residence time of drying. The relationship between the particle density and the residence time of drying could be expressed by a second-order polynomial function (R^2=0.72):

$$RTD = 0.002\,\rho^2 - 0.5208\rho + 407.17 \quad (4.5\text{-}1)$$

where RTD is the residence time of drying (min) and ρ the particle density (kg/m^3).

4.6 Moisture content distribution

The moisture content distributions after 7.5 minutes, 15 minutes, 22.5 minutes and 30 minutes of drying are shown in Fig. 4-14. Three general observations could be made: i) the grain moisture content decreased from the top to the bottom, as expected, ii) the moisture content distribution was not perfectly symmetrical about the dryer centerline; and iii) the grain moisture content was not uniform across the dryer, specifically a low moisture zone formed around the lower center inlet duct, with the lowest moisture content underneath the duct. Also, grain close to the wall of the dryers generally had higher moisture content than the rest of the grain bed.

On average discharged grain was dried to 20.7% (db) from the initial 25.0% (db) after 30 minutes. The instantaneous moisture content of discharged grain throughout the simulation process is plotted in Fig. 4-15. It could be seen that unevenness in moisture content started to show at 4.6 minutes after the start of drying and existed throughout the whole drying process. After 30 minutes of drying (the average throughout time), the moisture content ranged from 17.8% (db) to 22.0% (db) at the discharge point.

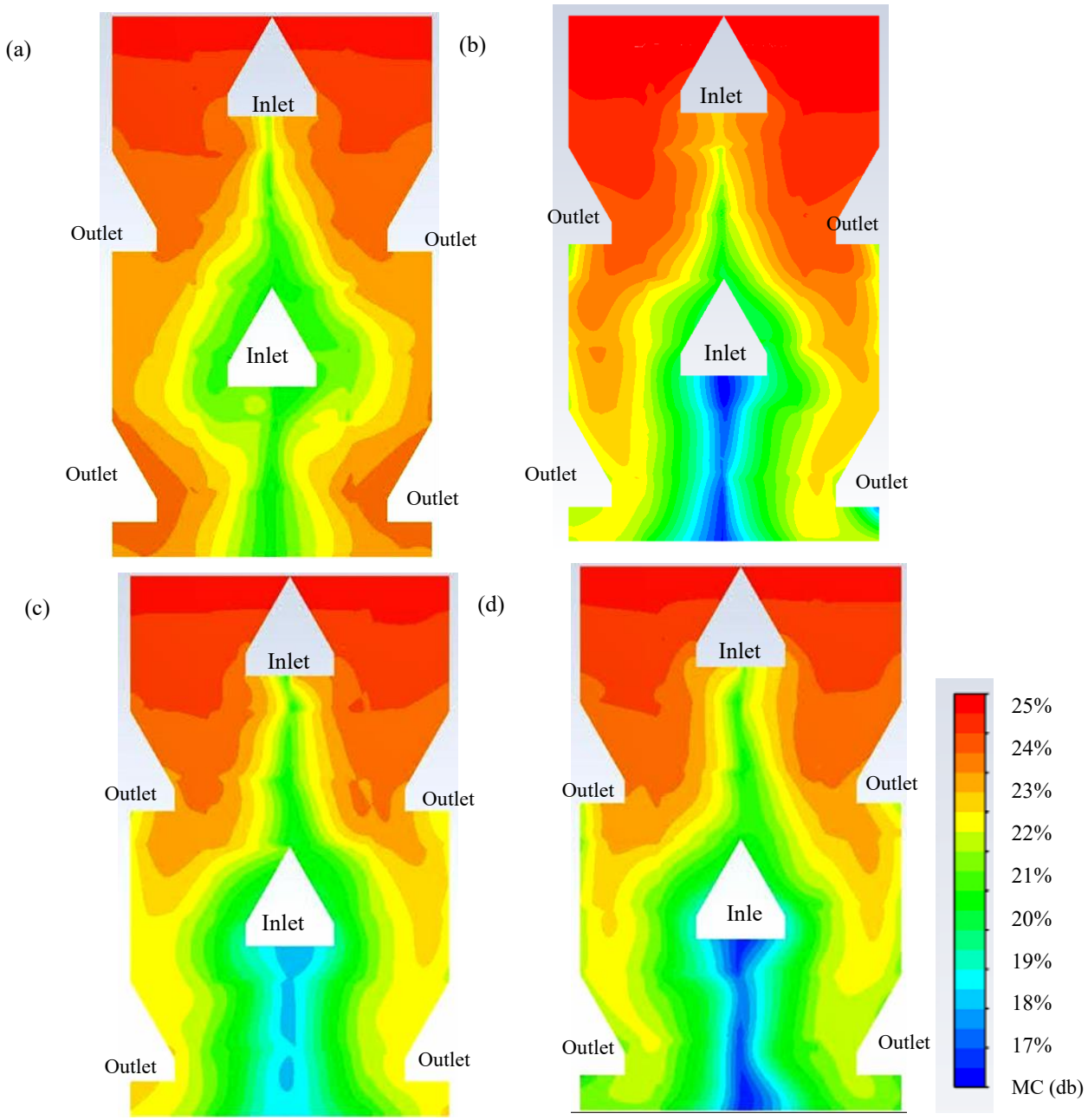

Figure 4-14 Moisture content (db, decimal) distribution in the drying column after (a) 7.5 minutes, (b) 15 minutes, (c) 22.5 minutes and (d) 30 minutes of drying

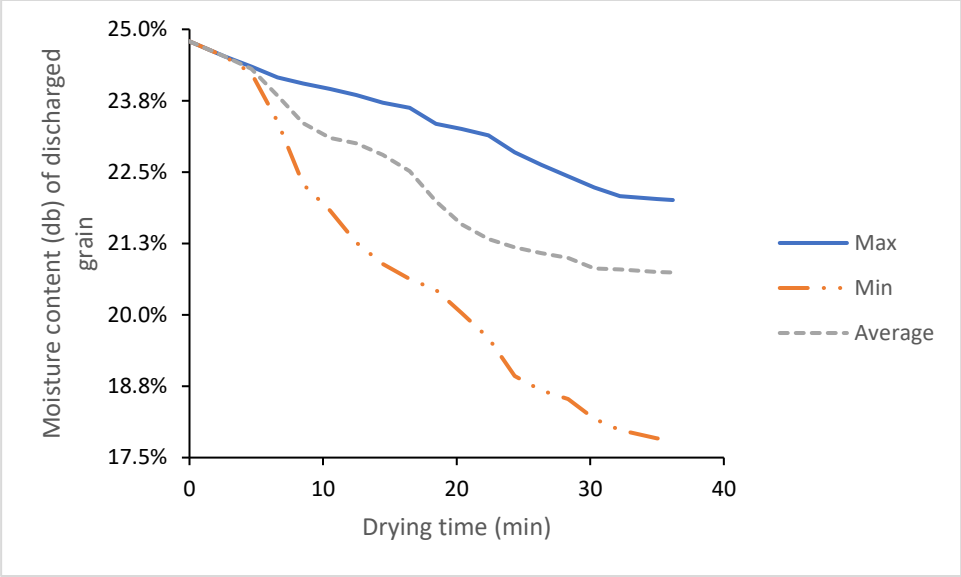

Figure 4-15 Simulated moisture content of discharged grain over time (initial moisture content: 25% (db), drying air temperature:80°C, nominal air velocity: 0.6m/s)

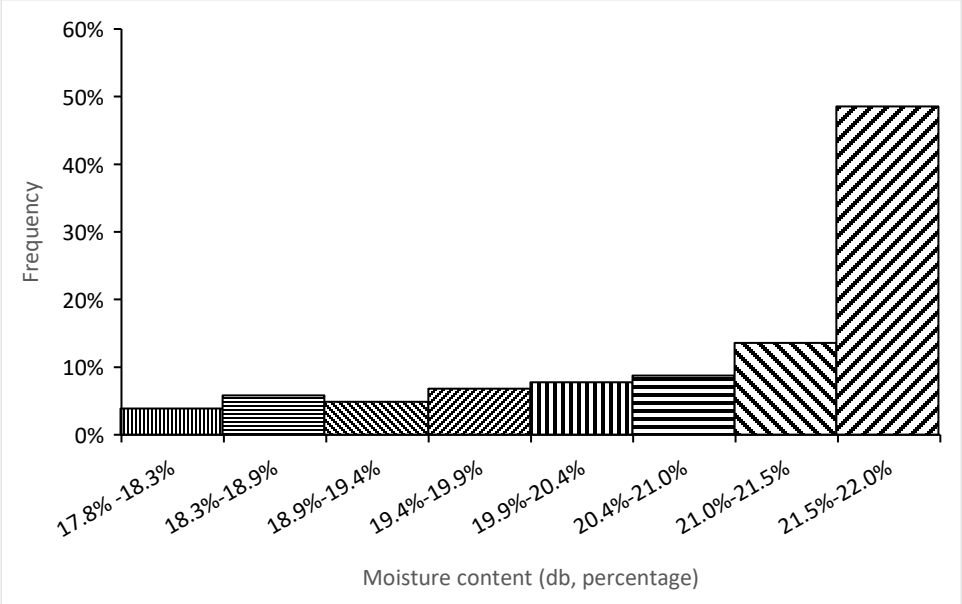

Figure 4-16 Frequency distribution of moisture content of discharged grain kernels after steady state (based on 4991 grain kernels discharged after steady state)

The frequency distribution of moisture content of discharged grain kernels was determined after steady state was achieved (Fig. 4-16). The moisture content of grain kernels did not follow the bell-shaped (normal) distribution, with the highest frequency at the moisture range of 21.5% -

22.0% (db) and a median value of 21.4% (db). This distribution pattern indicated that some grain kernels had lower moisture content, meaning that those kernels might have experienced prolonged residence time of drying.

A non-uniformity index was proposed in this study to assess the level of uniformity of the moisture content:

$$U_{MC(t)} = \sqrt{\frac{1}{N}\sum(MC_i - \overline{MC}_{(t)})^2} \tag{4.6-1}$$

where $U_{MC(t)}$ is the non-uniformity index of moisture content of discharged grain kernels at time t (db, percentage), N the total number of discharged grain kernels at time t, MC_i is the moisture content of kernel i (db, percentage), and $\overline{MC}_{(t)}$ is the average moisture content of grain kernels discharged at time t (db, percentage). $U_{MC(t)}$ physically measured how much the moisture content of grain kernels discharged at a given time (t) deviated from the average value. Although the variation in moisture content among kernels was not listed as a grading factors for grain quality (Dexter and D'Egidio, 2012) because most moisture content meters measure the bulk grain moisture, grain kernels of high moisture content could potentially cause local spoilage or fungi growth, while grain kernels of low moisture content could be directly linked to over-dried grain. There is no publication or standard that had quantitively defined a criterion for assessing the uniformity of grain moisture content among grain kernels, thus further study for evaluating post-drying uniformity of grain kernel moisture content is necessary. The non-uniformity index of moisture content (U_{MC}) predicted by the coupled DEM-CFD model could also serve as an indicator for evaluating the design of grain dryers in terms of their performance in maintaining post-drying grain quality. In the simulated dryer, the initial non-uniformity index $U_{MC}$was assumed to be zero at the start of drying, and it was observed to increase with time and plateaued (2.5%, db) at around 30 minutes, which suggested that moisture content distribution would remain in this range from this time onward (Fig.4-17). In this study, dryer designs yielding U_{MC} greater than 3% (db) at steady state was considered as to be unfavorable.

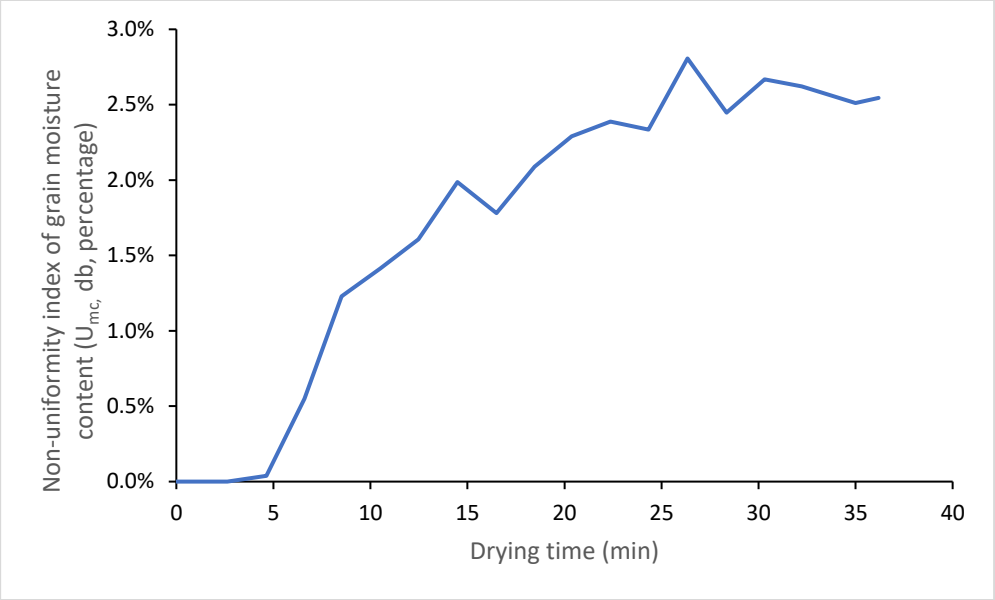

Figure 4-17 Non-uniformity index of moisture content (U_{mc}) of discharged grain kernels over time (initial moisture content: 25% (db), drying air temperature: 80°C, nominal air velocity: 0.6m/s)

4.7 Temperature distribution

The temperature distributions after 7.5 minutes, 15 minutes, 22.5 minutes and 30 minutes of drying are shown in Fig. 4-18. There were considerable variations in grain temperature in the drying column. The highest grain temperature was found underneath the two inlet ducts, while "cold zones" existed in the near-wall region. The temperature of discharged grain throughout the simulation process was plotted in Fig. 4-19. At the beginning of drying (until 8 minutes), there was a steep rise in grain temperature on average to around 45.9°C . Afterwards, grain temperature increased gradually until 28 minutes when the average temperature plateaued at 55.9°C. Individual grain kernels experienced temperature as high as 68.9°C , while the lowest discharged grain temperature fluctuated over time in the range of 31.9 – 36.9°C.

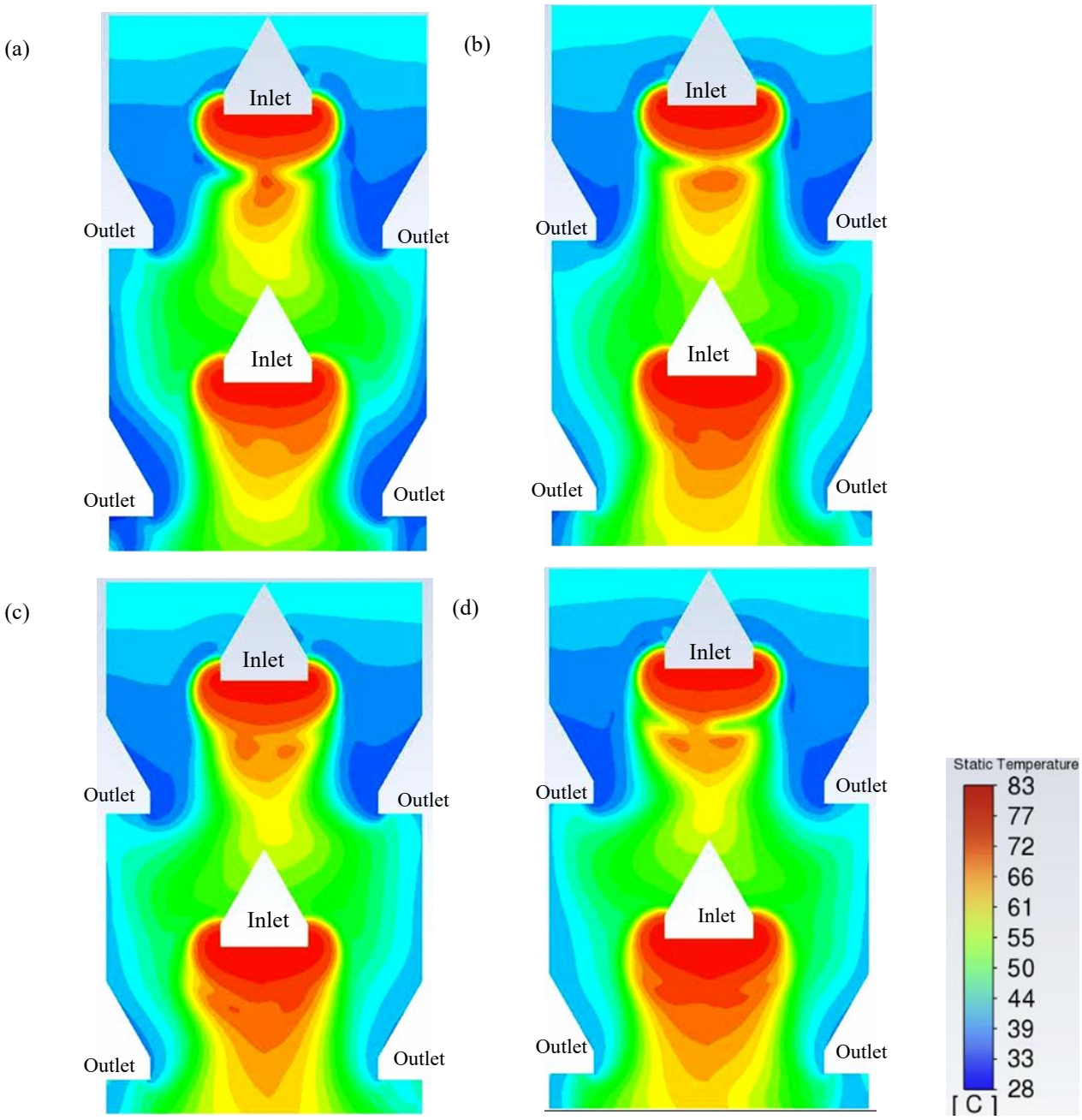

Figure 4-18 Grain temperature distribution in the drying column after (a) 7.5 minutes, (b) 15 minutes, (c) 22.5 minutes and (d) 30 minutes of drying

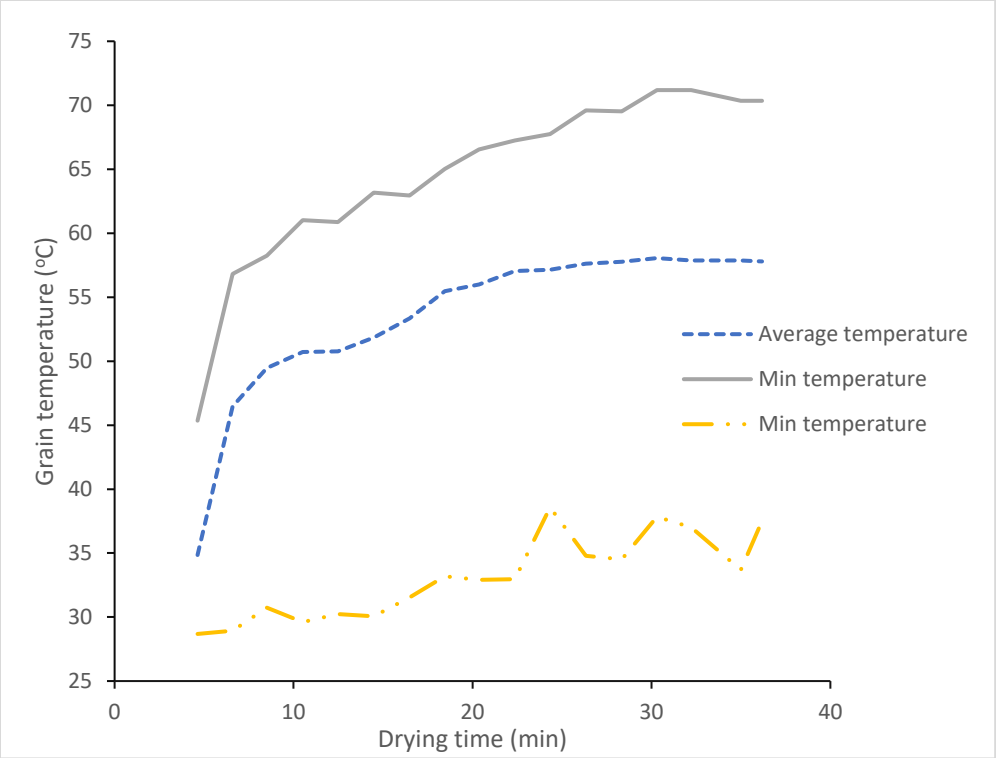

Figure 4-19 Simulated instantaneous temperature of discharged grain over time (initial moisture content: 25%db, drying air temperature: 80°C, nominal air velocity: 0.6m/s)

A non-uniformity index of temperature was proposed in this study to assess the level of uniformity of the temperature of discharged grain kernels as follows.

$$U_{T(t)} = \sqrt{\frac{1}{N}\sum(T_i - \overline{T_{(t)}})^2} \tag{4.7-1}$$

where $U_{T(t)}$ is the non-uniformity index of temperature of discharged grain kernels at time t (°C), N is the total number of discharged grain kernels at time t, T_i is the temperature of kernel i (°C), and $\overline{T_{(t)}}$ is the average temperature of grain kernels discharged at time t (°C). $U_{T(t)}$ physically measured how much the temperature of grain kernels discharged at a given time (t) deviated from the average value. High temperature grain kernels could potentially be linked to kernel cracking due to thermal stress, while grain kernels of low temperature could be directly linked to under-dried grain due to lack to heat exposure.

In the first 5-10 minutes of drying, there was a sharp increase in the unevenness of temperature, which was possibly because grain was partially heated initially, and then unevenness plateaued at around 12.5 minutes when the non-uniformity index fluctuated in the range of 9 to 11°C, which suggested a "steady" state was reached (as shown in Fig. 4-20). Since no publications or standards

had quantitively defined a criterion for assessing the uniformity of grain temperature, thus further study or evaluating post-drying uniformity of grain temperature is necessary. In this study, grain dryers yielding U_T lower than 10 °C at steady state was considered as to be favorable.

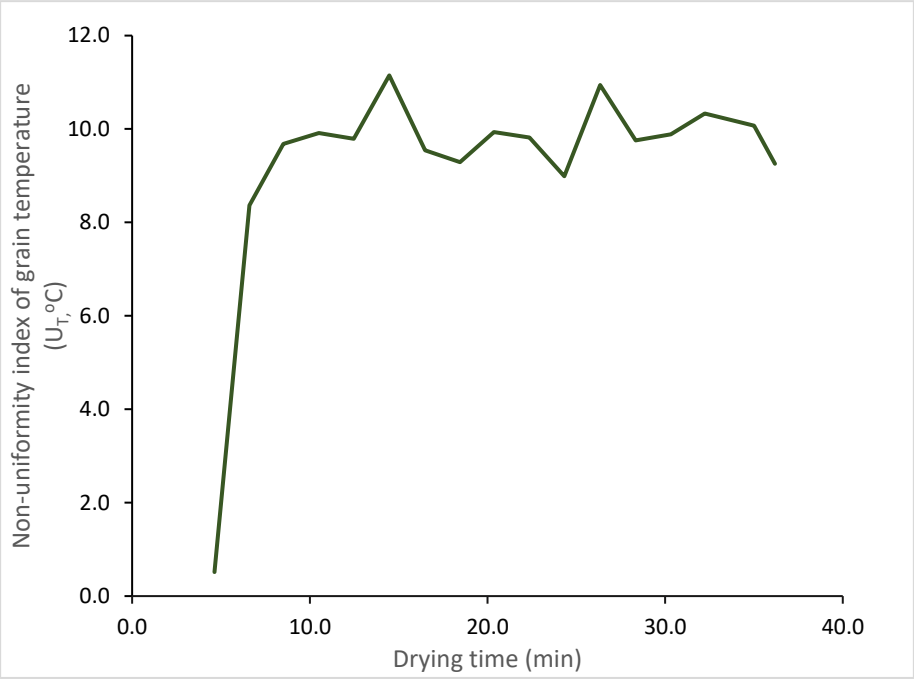

Figure 4-20 Non-uniformity index of discharged grain temperature (U_T) over drying time (initial moisture content: 25%db, drying air temperature: 80°C, nominal air velocity: 0.6m/s)

4.8 Influences of duct design and layout on dryer performance

Duct design and layout may affect grain flow and airflow. The performance of three triangular air ducts with 45°, 60° and 90° angles, respectively, and a half-circle duct (Fig. 3-3) were compared. These configurations are the most common designs in industry (Dai and Cao, 1965). The vertical velocity of grain movement was examined to assess the effect of duct shape on grain flow. A non-uniformity index of vertical velocity (U_v) was proposed to assess the level of uniformity of the grain velocity as follows.

$$U_{v(t)} = \sqrt{\frac{1}{N}\sum(v_i - \overline{v_{(t)}})^2} \quad (4.8\text{-}1)$$

where $U_{v(t)}$ is the non-uniformity index of grain velocity at time t (m/s), N is the total number of discharged grain kernels at time t, v_i is the magnitude of vertical velocity of kernel i (m/s), and $\overline{v_{(t)}}$ is the average magnitude of vertical velocity of grain kernels discharged at time t (m/s).

The maximum, minimum, average and non-uniformity index of vertical velocity were as listed in Table 4-8. Different duct designs didn't cause significant differences in the average vertical velocity ($p>0.05$). However, the ducts with 45° angles resulted in the highest variation in vertical velocity ($U_v = 0.000057$ m/s) followed by the design with half-circle duct ($U_v = 0.000040$ m/s), thus these two designs were deemed not ideal because of they resulted in uneven particle flow.

The influence of different duct designs on RTD was also analyzed, based on analysis of the maximum, minimum, average and non-uniformity index of RTD (U_{RTD}) of discharged grain kernel. The definition of non-uniformity index of RTD followed the same pattern as the definition of U_{MC}, U_T and U_v:

$$U_{RTD(t)} = \sqrt{\frac{1}{N}\sum(RTD_i - \overline{RTD_{(t)}})^2} \tag{4.8-2}$$

where $U_{RTD(t)}$ is the non-uniformity index of residence time of discharged grain at time t (min), N is the total number of discharged grain kernels at time t, RTD_i is the residence time of drying of kernel i (min), and $\overline{RTD_{(t)}}$ is the average RTD of grain kernels discharged at time t (min).

The analysis yielded similar findings to the analysis on vertical velocity. While different duct designs didn't cause significant differences in the mean value grain residence time of drying, they caused a difference in the non-uniformity factor (Table 4-9). The half-circle ducts resulted in the highest variation in RTD ($U_{RTD} = 7.83$ min) followed by the 45° triangular ducts ($U_{RTD} = 5.97$ min), while the 60° triangular ducts caused the least variation in residence time of drying ($U_{RTD} = 4.49$ min). It should be noted that the evenness in moisture content is not solely determined by the residence time, it is necessary to comprehensively consider the distribution of grain temperature and flow behavior to gain a full picture of the performance of air duct design.

To analyze the influence of duct design on grain temperature and moisture content distributions, their non-uniformity indexes of grain temperature (U_T) and moisture content ($\boldsymbol{U_{MC}}$) were compared. The maximum, minimum, average and non-uniformity index of discharged grain temperature (U_T) and moisture content ($\boldsymbol{U_{MC}}$) at steady state were as shown in Table 4-10 and 4-11. Half-circle air ducts created the highest variations in grain temperature ($U_T = 12.5$ °C),

followed by the 90° duct ($U_T = 11.3$ °C), thus these two designs were not ideal because they resulted in higher unevenness of temperature distribution. The analysis of the moisture content yielded the similar results: the 60° duct resulted in the least variation in discharged grain moisture content and temperature ($U_{MC} = 2.5\%$ (db)), thus it was considered to be the best design among all duct designs compared in this study.

Table 4-8 Maximum, minimum, average and non-uniformity index of vertical velocities at steady state with different duct designs (negative value indicated the downward direction)

Duct design	45°	90°	60°	Half circle
Max vertical velocity (m/s)	-0.00018	-0.00017	-0.00022	-0.00014
Min vertical velocity (m/s)	-0.00036	-0.00030	-0.00032	-0.00030
Average vertical velocity (m/s)	-0.00026	-0.00024	-0.00026	-0.00024
Non-uniformity index of vertical velocity (U_v, m/s)	0.000057	0.000032	0.000026	0.000040

Table 4-9 Maximum, minimum, average and non-uniformity index of residence time of drying of discharged grain kernels at steady state with different duct designs

Duct design	45°	60°	90°	Half circle
Average residence time of drying (min)	35.68	35.62	35.58	35.43
Max residence time of drying (min)	68.8	67.2	70.3	72.8
Min residence time of drying (min)	23.0	22.7	21.9	23.1
Non-uniformity index of residence time of drying ($\boldsymbol{U_{RTD}}$, min)	4.81	4.49	5.97	7.83

Table 4-10 Maximum, minimum, average and non-uniformity index of temperature of discharged grain kernels at steady state with different duct designs

Duct design	45°	60°	90°	Half circle
Average temperature (Celsius)	59.1	57.4	59.3	64.8
Max temperature (Celsius)	70.6	70	69.5	68.8
Min temperature (Celsius)	37.8	37.2	34.6	35.1
Non-uniformity index of temperature ($\boldsymbol{U_T}$, Celsius)	9.7	9.1	11.3	12.5

Table 4-11 Maximum, minimum, average and non-uniformity index of moisture content of discharged grain kernels at steady state with different duct designs

Duct design	45°	60°	90°	Half circle
Average moisture content (db, percentage)	20.8%	20.7%	20.4%	20.3%
Max moisture content (db, percentage)	23.3%	22.0%	22.6%	23.1%
Min moisture content (db, percentage)	18.1%	17.8%	17.3%	16.4%
Non-uniformity index of moisture content ($\boldsymbol{U_{MC}}$,db percentage)	3.1%	2.5%	2.7%	3.4%

Simulations were also performed to assess the influence of the horizontal and vertical distances between air ducts on dryer performance. As shown in Tables 4-12 and 4-13, it was observed that while larger horizontal and vertical distances resulted in more even grain flow (resident time), but less even temperature and grain moisture content distribution. Among all proposed designs, the best performance was layout #4 (U_{MC}= 2.5%), in which the ratio of vertical distance to duct height was 1.35 and the ratio of horizontal distance to duct width was 1.5.

Table 4-12 Effect of vertical distance on dryer performance

Configuration No.	1	2	3
Ratio of vertical distance to duct height	1.05	1.35	1.65
Non-uniformity index of residence time ($\boldsymbol{U_{RTD}}$, min)	5.88	4.49	3.71
Non-uniformity index of discharged grain temperature ($\boldsymbol{U_T}$, Celsius)	9.91	10.60	12.85
Non-uniformity index of discharged grain moisture content ($\boldsymbol{U_{MC}}$,db, percentage)	2.8%	2.6%	3.1%

Table 4-13 Effect of horizontal distance on dryer performance

Configuration No.	4	5	6
Ratio of horizontal distance to duct width	1.5	1.8	2.1
Non-uniformity factor of residence time ($\boldsymbol{U_{RTD}}$, min)	4.91	4.49	3.56
Non-uniformity factor of discharged grain temperature ($\boldsymbol{U_T}$, Celsius)	10.11	10.60	14.77
Non-uniformity factor of discharged grain moisture content ($\boldsymbol{U_{MC}}$,db, percentage)	2.5%	2.6%	2.8%

4.9 Risk analysis based on predicted germination rate and kernel cracking rate

The average value of predicted germination rate of discharged (dried) grain kernels G_i in each time step (i) was determined with Eq.3.4-1 based on the coupled CFD-DEM simuations (Fig.4-21). It could be seen that the average predicted germination rate decreased gradually with time from the assumed initial rate of 95% and a stabilized value of 83%, which was reached at around 30 minutes, i.e., a 12% reduction in germination rate. Reducton in generminaiton rate could be explained by the exposure to unfavorable drying conditions.

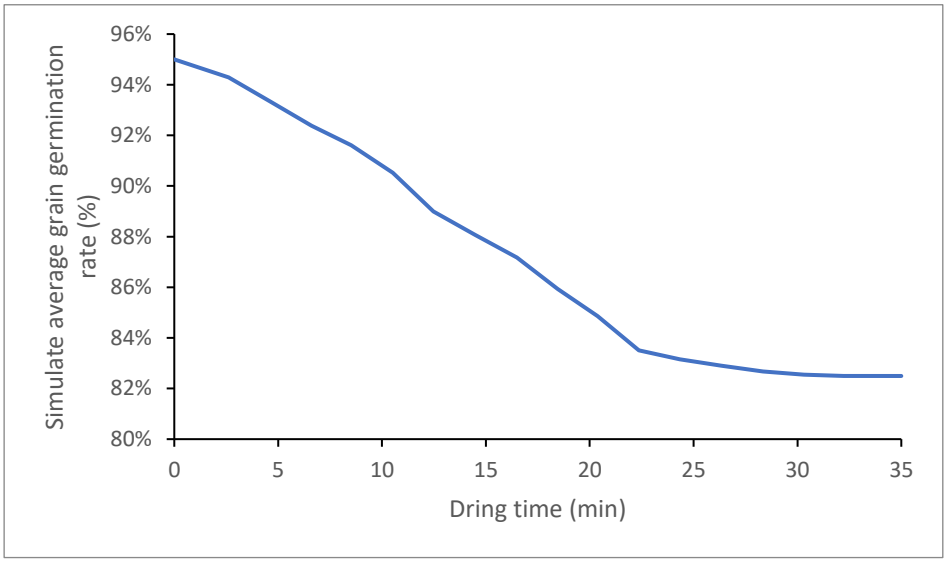

Figure 4-21 The average simulated germination rate of discharged grain kernels (initial moisture content: 25% db, drying air temperature: 80°C, inlet air velocity: 0.6m/s)

While most studies about the relationship between drying conditions and grain germination rate in the literature dealt with in the average reduction in gemination rate during drying, the proposed DEM-CFD model provided a tool to explore the locations where and when the drying conditons led to reduction in gemination rate. Based on simulated grain temperature and moisture content, the germination reduction risk of each grain kernel (R_{Germ}) in the simulated dryer was determined with Eq.3.4-2, and the distributions of germination reduction risk at different stages of drying is plotted in Fig. 4-22. It was observed that grain kernels underneath the air inlets experienced most reduction in germination rate, and of the two inlets in the simulated dryer, the worst location was underneath the lower inlet. Some kernels had the risk of 100% reduction in germination rate (Fig. 4-22). This distribution pattern could be explained by slow grain movement, high temperature, and low grain moisture under the inlet air ducts, where grain kernels experienced prolonged exposure to excessive heat. In this study, the grain kernels whose germination rate reduction risk was higher than 0.2 were considered as under germination loss risk. On average, 18.8% of the grain kernels in the dryer was at risk of germination loss during the simulated steady-state drying period.

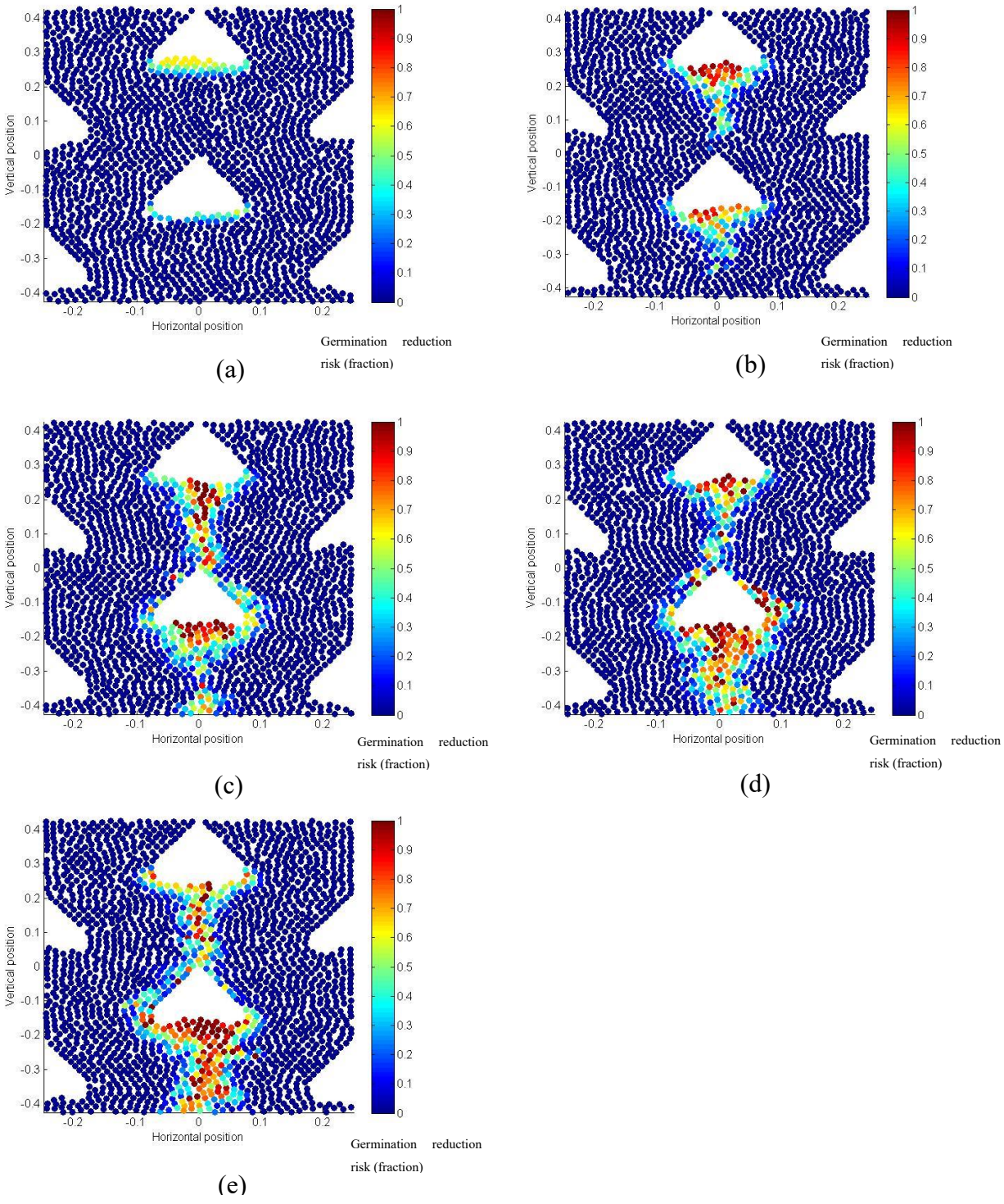

Figure 4-22 Simulated germination reduction risk (R_{Germ}) after drying for (a) 2.5 minutes, (b) 10.5 minutes, (c) 18.5 minutes, (d) 26.5 minutes and (e) 34.5 minutes

The average value of predicted rate of kernel cracking (fisure) of discharged grain kernels (C_i) in each time step (i) was determined with Eq. 3.4-3 based on the results of DEM-CFD simulations. It was observed that the simulated cracking rate increased gradually from 5% (the assumed initial cracking rate) with time and a stabilized value of 8.5% was reached at around 30 minutes (Fig.4-23). This represented a 46% increase in kernel cracking rate from the assumed initial cracking rate. The cause of increase in kernel cracking rate was similar to the reduction of germination rate, i.e. unfavorable dying conditions (temperature and moisture content).

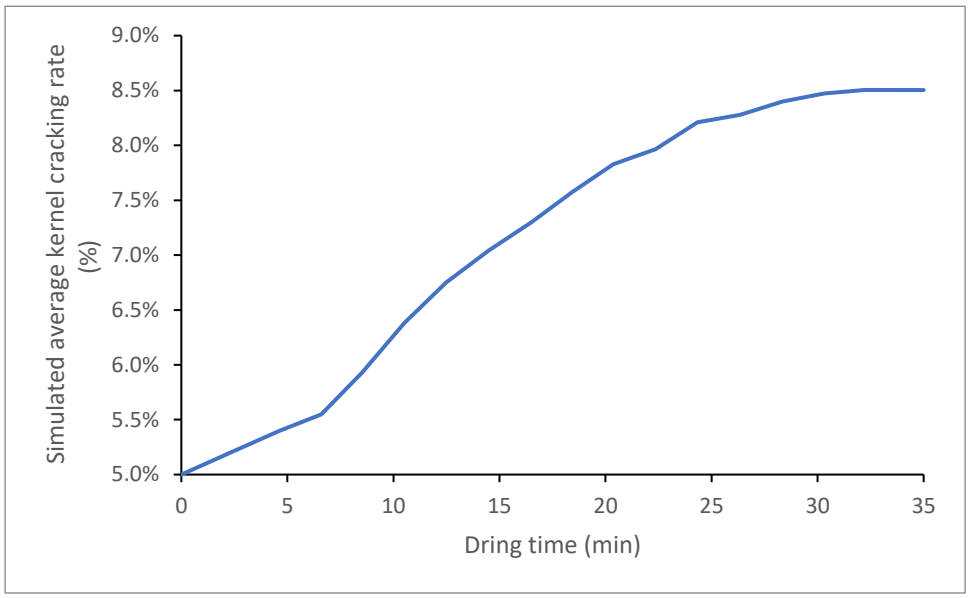

Figure 4-23 The average predicted kernel cracking rate of discharged grain kernels during drying (initial moisture content: 25%db, drying air temperature: 80°C, nominal air velocity: 0.6m/s)

The kernel cracking risk (R_{Crack}) in the simulated dryer was determined with Eq.3.4-4, and the distributions of kernel cracking risk at different stages of drying was as plotted in Fig. 4-24. In this study, the grain kernels whose cracking risk were higher than 0.6 were considered to be at risk of cracking, because the grade of grain with kernels at 0.6 cracking risk would be lowered by one grade (Mercier, 1989). According to this criterion, 11.2% of grain kernels in the dryer would be subjected to the risk of cracking at the end of drying (Fig. 4-24). Similar to gemination rate reduction, grain kernels at cracking risk were mainly located underneath the two air inlet ducts and the worst location was under the lower inlet duct. This distribution pattern could be explained by slow grain movement, high temperature, and low grain moisture under the inlet air ducts, where grain kernels experienced prolonged exposure to excessive heat.

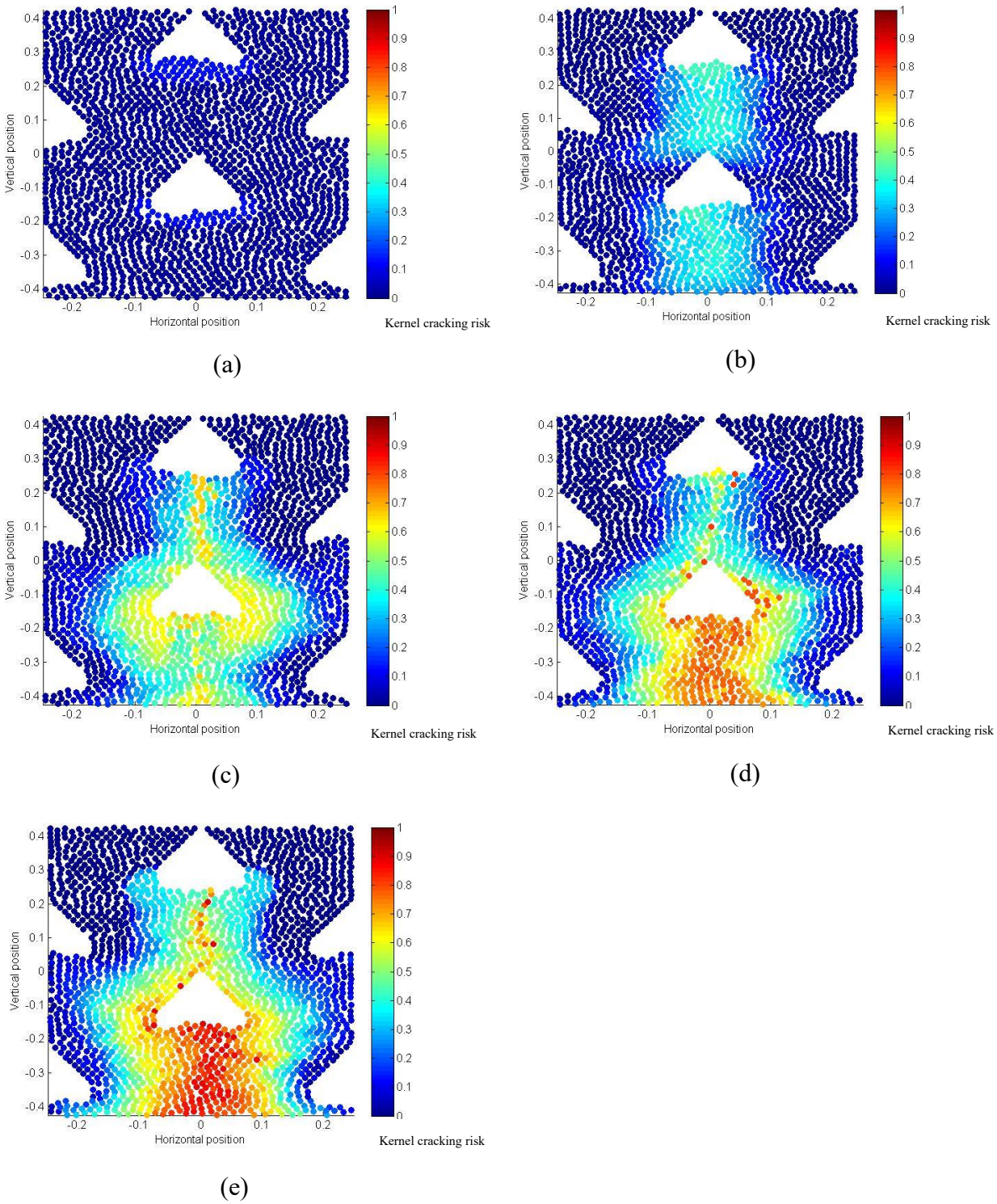

Figure 4-24 The distribution of kernel cracking risk (R_{Crack}) in at drying time of (a) 2.5 minutes, (b) 10.5 minutes, (c) 18.5 minutes, (d) 26.5 minutes and (e) 34.5 minutes

4.10 Influence of duct design and layout on grain germination rate and kernel cracking rate

The average germination reduction risk (R_{Germ}) and kernel cracking risk (R_{Crack}) for discharged grain kernels at steady state (i.e., all grain kernels that traveled from the top of the drying column to the bottom) were simulated for different air duct designs and layouts, as described in Figs. 3-2 and 3-3. It was observed that the triangular duct with 60° angle resulted in the least germination rate reduction (about 12%), while the half circle duct created the highest risk of germination loss (19%) (Table 4-15). The predicted average kernel crack rate (based on an assumed initial rate of 5%), percentage of kernels at crack risk, and average crack risk of discharged grain from dryers at steady state were determined for different air duct designs. It was observed that the duct of 60° angle created the least crack risk, while the half circle duct experienced the highest crack risk.

Simulations were also performed to assess the influence of horizontal and vertical distances between ducts on the germination rate and crack rate of discharged grain. Based on the predicted germination reduction risk ($\boldsymbol{R_{Germ}}$) and kernel cracking risk ($\boldsymbol{R_{Crack}}$), it could be seen that the layout #1 with vertical of 213 mm and horizontal distance of 252 mm showed the best performance in maintaining the germination rate and preventing cracking among all simulated designs, yielding only 10.3% reduction in germination rate, and 5.3% increase in kernel cracking rate.

Table 4-14 Influence of different duct designs on the germination reduction risk ($\boldsymbol{R_{Germ}}$) of discharged grain at steady state

Duct design	45°	60°	90°	Half circle
Average simulated reduction in germination rate (%)	12.5%	12.1%	16.1%	18.9%
Percentage of discharged (dried) grain at germination loss risk (%)	21.1%	18.8%	33.7%	36.3%
Average simulated germination reduction risk of discharged (dried) grain ($\boldsymbol{R_{Germ}}$)	0.132	0.127	0.170	0.199

Table 4-15 Influence of different duct designs on the cracking risk ($\boldsymbol{R_{Crack}}$) of discharged grain in steady state

Duct design	45°	60°	90°	Half circle
Average simulated kernel cracking rate of discharged (dried) grain (%)	7.7%	7.3%	8.4%	8.6%
Percentage of discharged (dried) grain at crack risk (%)	12.1%	11.2%	17.3%	18.7%
Average simulated cracking risk of discharged (dried) grain ($\boldsymbol{R_{Crack}}$)	0.433	0.420	0.478	0.491

Table 4-16 Influence of duct vertical distance on the germination reduction risk (R_{Germ}) and risk of kernel cracking ($\boldsymbol{R_{Crack}}$) of discharged grain at steady state (horizontal distance was 252mm)

Configuration number (dimensions as listed in Table 3-1)	1	2	3
Vertical distance (mm)	165	213	260
Ratio of vertical distance to duct height	1.05	1.35	1.65
Average simulated germination rate of discharged grain at steady state (%)	84.7%	82.9%	81.5%
Average simulated germination reduction risk of discharged grain (R_{Germ})	0.108	0.127	0.142
Percentage of discharged grain at germination loss risk (%)	17.2%	18.8%	23.7%
Average simulated kernel cracking rate of discharged grain at steady state (%)	7.0%	7.3%	7.92%
Percentage of discharged grain at cracking risk (%)	10.3%	11.2%	14.3%
Average simulated kernel cracking risk of discharged grain ($\boldsymbol{R_{Crack}}$)	0.391	0.420	0.453

Table 4-17 Influence of duct vertical distance on the germination reduction risk (R_{Germ}) and risk of kernel cracking ($\boldsymbol{R_{Crack}}$) of discharged grain at steady state (vertical distance was 213mm)

Configuration number (dimension as listed in Table 3-2)	4	5	6
Horizontal distance (mm)	210	252	294
Ratio of horizontal distance to duct width	1.5	1.8	2.1
Average simulated germination rate of discharged grain at steady state (%)	81.8%	82.9%	84.2%
Percentage of discharged grain at germination loss risk (%)	17.7%	18.8%	20.1%
Average simulated germination reduction risk of discharged grain (R_{Germ})	0.139	0.127	0.113
Average simulated kernel cracking rate of discharged grain at steady state (%)	7.1%	7.3%	7.75%
Percentage of discharged grain at crack risk (%)	10.8%	11.2%	13.6%
Average simulated kernel cracking risk of discharged grain ($\boldsymbol{R_{Crack}}$)	0.407	0.420	0.441

5. Conclusions

5.1 Model development and validation

In this study, an integrated numerical model was successfully developed and validated to simulate the transport processes in mixed-flow grain dryers. A DEM model was developed and validated to simulate grain movement, while CFD model was developed and validated for simulating heat and mass transfer, as well as airflow. These DEM and CFD models were coupled to simulate the drying process within the mixed-flow grain dryers, The couple model was validated against experimental data from the existing literature. Additionally, two empirical models were incorporated into the coupled DEM-CFD framework to predict the risks of germination loss and grain kernel cracking (fissuring) during the drying process.

5.2 Model simulations of grain flow, airflow, grain moisture and temperature

The coupled DEM-CFD model was employed to simulate the drying processes in a hypothetical mixed-flow grain dryer with a drying column containing two air inlets (full duct) at the center and two air outlets (half duct) on either side. Model simulations revealed that the drying air from each inlet was split into two streams—one moving towards the upper outlet and the other towards the lower outlet. High-velocity zones were observed at the corners of the air inlet ducts, while zero-velocity zones were located atop both the outlet and inlet ducts. The grain flow in the drying column was divided into two channels by the central air inlets, with grain kernels primarily traveling downwards within their respective channels and minimal cross-channel movement was observed. The highest kernel velocity occurred at the center of each channel, while dead zones with near-zero vertical velocity were found beneath the air ducts. Grain velocity distribution was asymmetrical along the dryer's centerline, with alternating higher velocities in either the right or left channel occurring randomly. The residence time distribution (RTD) of individual grain kernels varied considerably ranged from 20.4 to 66.0 minutes, with an average of 35.6 minutes for a targeted (normal) drying time 30 minutes. The most frequent residence times were between 30.5

and 35.6 minutes, with kernels in this range located centrally within their flow channels. Lower-density kernels experienced longer residence times, while kernel size had no significant effect on RTD (grain kernels were approximated as discs).

Grain moisture distribution was non-uniform, with values ranging from 17.8% to 22.0% (db) after 30 minutes of drying. A low-moisture zone formed around the lower inlet duct, with the lowest moisture content beneath it, while grain near the dryer walls generally retained higher moisture. Furthermore, the moisture distribution was not perfectly symmetrical about the dryer centerline. Similarly, grain temperature distribution was non-uniform during drying, with the maximum temperature reaching 68.9°C and minimum temperatures as low as 31.9°C. The highest grain temperatures were found beneath the inlet ducts, while "cold zones" near the walls.

5.3 Predicting the effects of drying on grain quality

The coupled DEM-CFD could be integrated with empirical functions for analyzing the effect of drying on the grain quality, and specifically the germination rate and rate of kernel cracking were predicted in the study. The average predicted germination rate gradually decreased from an assumed initial value of 95% to a stabilized value of 83% after approximately 30 minutes of drying. Grain kernels located beneath the air inlets exhibited the most significant reduction in germination rate, with the worst conditions observed under the lower inlet. This pattern was attributed to slow grain movement, high temperatures, and low moisture content in these areas, where prolonged exposure to excessive heat occurs. Based on the simulated grain temperature and moisture, it was predicted that 18.8% of the grain kernels were at risk of germination loss after 30 minute of drying.

Similarly, the drying process also affected the kernel cracking rate. The average predicted rate of kernel cracking (fissuring) increased gradually from an assumed initial value of 5% to 8.5% after 30 minutes of drying. This increase in cracking rate was attributed to unfavorable drying conditions in localized areas, including high temperature, low moisture content, and restricted grain movement. Model simulations revealed that the kernels most at risk were also located beneath the two air inlet ducts, with the worst conditions under the lower inlet. By the end of the drying process, an estimated 11.2% of the grain kernels were at risk of cracking.

5.4 Design assessment and optimization of mixed-flow grain dryers

The coupled DEM-CFD could be applied for the design assessment for optimization for mixed-flow grain dryers. The design of the duct geometry had a significant influence on dryer performance and the quality of the final product. Simulations of four different duct designs were conducted, evaluating uniformity in moisture content and temperature, germination rate, and kernel cracking. Among the designs, ducts with 60-degree angles were found to be the most favorable. Additionally, while increasing horizontal and vertical distances resulted in a more uniform particle flow pattern, it also led to less uniform temperature and moisture distribution. Of the five layouts simulated, a vertical distance to duct height ratio of 1.35 and a horizontal distance to duct width ratio of 1.5 resulted in the best performance.

6. Recommendations

In the DEM sub-model of grain bulks, it was assumed in the simulations that grain had spherical shape, which is not true for most grains. The non-spherical shape of grain kernels may result in the difference of pore structure in the grain bed and the resistance to airflow in the vertical and horizontal direction of grain bulks. Further research is needed to simulate the pore structure of non-spherical particles and investigate the difference of pore structure and corresponding resistance to airflow through the porous bed.

In the proposed study, the numerical model was validated against experimental data from literature. As conducting an experimental study on grain drying is a very complicated work, no existing study had reported the full-field data (including grain kernel flow, air flow, grain temperature, grain moisture content, air temperature and relative humidity), thus building a "digital-twin" would be more beneficial as the full-field real-time data could provide us more insight into the heat and mass transfer phenomena during grain drying.

When validating the proposed CFD sub-model against an empirical deep-bed study (Zhang, 2014), the phenomenon of condensation was observed near the outlet region of the deep-bed drying system. Even though in practice condensation rarely happens in the mixed-flow grain drying operations and incorporating such phenomena would significantly increase the complexity of the model and consume more computation time and power, introducing a third term of liquid water into the CFD simulations of pore structure within the grain bed would increase the versatility and adaptivity of the proposed model, which would enable the simulation of other critical grain handling processes, such as deep-bed drying and grain storage processes, in which the effect of condensation cannot be neglected.

In the proposed coupled CFD-DEM model, the grain and surrounding air was assumed to be a porous medium, and heat and mass transfer mass transfer was considered only on the kernels surface, but not within the grain kernels. Future research should be conducted to include the inner-kernel heat and mass transfer.

References

ANSI/ASABE. (2021). Moisture Relationships of Plant-based Agricultural Products 3 Wet-basis and Dry-basis Representations Wet-basis moisture content Dry-basis moisture content. *ASABE Standards*. ASABE Standard.

ANSI/ASABE. (2022). Thermal Properties of Grain and Grain Products American Society of Agricultural and Biological Engineers. *ASABE Standards*. ASABE Standards.

ANSI/ASAE. (2014). Revision approved September 2014 as an American National Standard Thin-Layer Drying of Agricultural Crops. *American Society of Agricultural and Biological Engineers*, *2014*(S448.2).

ANSYS Inc. (2006). *Fluent 6.3 User's Guide, Chapter 7.2.3: Porous Media Conditions*.

Babalis, S. J., Papanicolaou, E., Kyriakis, N., Belessiotis, V. G. (2006). Evaluation of thin-layer drying models for describing drying kinetics of figs (Ficus carica). *Journal of Food Engineering*, *75*(2), 205–214. https://doi.org/https://doi.org/10.1016/j.jfoodeng.2005.04.008

Bakker-Aekema F.W., Evans T.Ww, Farmer D.M. (1969). Simulation of Multiple-Zone Grain Drying, 935–938. https://doi.org/10.13031/2013.38424

Ben Nasrallah, S., Perré, P. (1988). Detailed study of a model of heat and mass transfer during convective drying of porous media. *International Journal of Heat and Mass Transfer*, *31*(5), 957–967.

Brooker, D.B., Bakker-Arkema, F.W., and Hall, C. W. (1974). *Drying Cereal Grains.* The AVI Publishing Company Inc., Westport, Connecticut.

Brosh, T., Levy, A. (2010). Modeling of heat transfer in pneumatic conveyer using a combined DEM-CFD numerical code. *Drying Technology*, *28*(2), 155–164. https://doi.org/10.1080/07373930903517482

Bruce, D. M. (1985). Exposed-layer barley drying: Three models fitted to new data up to 150°C. *Journal of Agricultural Engineering Research*, *32*(4), 337–348. https://doi.org/10.1016/0021-8634(85)90098-8

Cao, C. W., Yang, D. Y., Liu, Q. (2007). Research on modeling and simulation of mixed flow grain dryer. *Drying Technology*, *25*(4), 681–687. https://doi.org/10.1080/07373930701290951

Çengel, Y. A., Ghajar, A. J. (2014). *Heat and mass transfer: Fundamentals and applications* (5th ed.). NY: McGraw Hill.

Cenkowski, S. (1985). *Modelowanie Procesu Suszenia Ziarna Zboz. (Modelling of Drying Process of Grains) Habilitation Dissertation*. University of Environmental and Life Sciences in Wroclaw.

Cenkowski, S., Miketinac, M. J., Kelm, A. W. (1990). Airflow patterns in a mixed-flow dryer. *Canadian Agricultural Engineering*, *1*(32), 85–90.

Chandra, P. K., Singh, R. P. (1995). *Applied Numerical Methods for Food and Agricultural Engineers*. Boca Raton, FL: CRC Press.

Conover, W. J., Iman, R. L. (1981). Rank Transformations as a Bridge between Parametric and Nonparametric Statistics. *The American Statistician*, *35*(3), 124–129. https://doi.org/10.1080/00031305.1981.10479327

Crank, J. (1975). *The mathematics of diffusion* (2nd ed.). Oxford, Great Britain: Clarendon Press.

Cundall, P. A. (1988). Formulation of a three-dimensional distinct element model—Part I. A scheme to detect and represent contacts in a system composed of many polyhedral blocks. *International Journal of Rock Mechanics and Mining Sciences & Geomechanics Abstracts*, *25*(3), 107–116.

Cundall, P. A., Strack, O. D. L. (1980). A discrete numerical model for granular assemblies. *Geotechnique*, *30*(3), 331–336. https://doi.org/10.1680/geot.1980.30.3.331

Dai, T., Cao, C. (1965). Structure and Performance Analysis on Mixed—Flow Grain Dryers. *Transaction of CSAE*, *11*(2), 167–172.

Demir, V., Gunhan, T., Yagcioglu, A. K. (2007). Mathematical modelling of convection drying of green table olives. *Biosystems Engineering*, *98*(1), 47–53.

Dexter, J. E., D'Egidio, M. G. (2012). CHAPTER 13 - Grading Factors Impacting Durum Wheat Processing Quality. In M. Sissons, J. Abecassis, B. Marchylo, & M. Carcea (Eds.), *Durum Wheat (Second Edition)* (pp. 235–250). AACC International Press. https://doi.org/https://doi.org/10.1016/B978-1-891127-65-6.50018-0

Diamante, L M, Munro, P. A. (1993). *Mathematical Modelling of The Thin Layer Solar Drying Of Sweet Potato Slices* (Vol. 51).

Diamante, Lemuel M, Ihns, R., Savage, G. P., Vanhanen, L. (2010). new mathematical model for thin layer drying of fruits. *International Journal of Food Science & Technology*, *45*(9), 1956–1962.

Ekechukwu, O. V. (1999). Review of solar-energy drying systems I: An overview of drying principles and theory. *Energy Conversion and Management*, *40*(6), 593–613. https://doi.org/10.1016/S0196-8904(98)00092-2

Elgamal, R., Ronsse, F., Radwan, S. M., Pieters, J. G. (2014). Coupling CFD and Diffusion Models for Analyzing the Convective Drying Behavior of a Single Rice Kernel. *Drying Technology*, *32*(3), 311–320. https://doi.org/10.1080/07373937.2013.829088

Erbay, Z., Icier, F. (2010). A review of thin layer drying of foods: Theory, modeling, and experimental results. *Critical Reviews in Food Science and Nutrition*, *50*(5), 441–464. https://doi.org/10.1080/10408390802437063

Ergun, S., Orning, A. A. (1949). Fluid Flow through Randomly Packed Columns and Fluidized Beds. *Industrial and Engineering Chemistry*, *41*(6), 1179–1184. https://doi.org/10.1021/ie50474a011

Erriguible, A., Bernada, P., Couture, F., Roques, M. A. (2005). Modeling of heat and mass transfer at the boundary between a porous medium and its surroundings. *Drying Technology*, *23*(3), 455–472. https://doi.org/10.1081/DRT-200054119

Erriguible, Arnaud, Bernada, P., Couture, F., Roques, M. (2005). Modeling of Heat and Mass Transfer at the Boundary Between A Porous Medium and Its Surroundings. *Drying Technology - DRY TECHNOL*, *23*, 455–472. https://doi.org/10.1081/DRT-200054119

Fortes, M., Okos, M. R. (1981). Non-Equilibrium Thermodynamics Approach To Transport Phenomena in Capillary Porous Media. *Transactions of the American Society of Agricultural Engineers*, *24*(3), 756–760. https://doi.org/10.13031/2013.34334

Ghazanfari, A., Emami, S., Tabil, L. G., Panigrahi, S. (2006). Thin-Layer Drying of Flax Fiber: III. Influence of Layer Thickness on Drying Parameters. *Drying Technology*, *24*(12), 1643–1648.

Hacıhafızoğlu, O., Cihan, A., Kahveci, K. (2008). Mathematical modelling of drying of thin layer rough rice. *Food and Bioproducts Processing*, *86*(4), 268–275. https://doi.org/https://doi.org/10.1016/j.fbp.2008.01.002

Haghi, A., Angiz, F. (2007). Heat and mass transfer in thermal drying of wool: A theoretical approach (pp. 443–448). https://doi.org/10.1142/9789812771957_0065

Halder, A., Dhall, A., Datta, A. K. (2007). An Improved, Easily Implementable, Porous Media Based Model for Deep-Fat Frying: Part I: Model Development and Input Parameters. *Food and Bioproducts Processing*, *85*(3), 209–219. https://doi.org/https://doi.org/10.1205/fbp07033

Hall, C. W. (1987). The evolution and utilization of mathematical models for drying. *Mathematical Modelling*, *8*(C), 1–6. https://doi.org/10.1016/0270-0255(87)90528-8

Hardke, J., Siebenmorgen, T. (2009). *Arkansas Rice Production Handbook*.

Hasibuan, R., Wan Daud, W. R. (2007). Through drying characteristic of oil palm empty fruit bunch (EFB) fibers using superheated steam. *Asia-Pacific Journal of Chemical Engineering*, *2*(1), 35–40.

Henderson, J. M., Henderson, S. M. (1968). A computational procedure for deep-bed drying analysis. *Journal of Agricultural Engineering Research*, *13*(2), 87–95.

Henderson, S. M. (1974a). Progress in Developing the Thin Layer Drying Equation. *Transactions of the American Society of Agricultural Engineers*, *17*(6), 1–3. https://doi.org/10.13031/2013.37052

Henderson, S. M. (1974b). Progress in Developing the Thin Layer Drying Equation. *Transactions of the ASAE*, *17*(6), 1167–1168.

Henderson, S. M., Pabis, S. (1961). Grain drying theory I: Temperature effect on drying coefficient. *Journal of Agricultural Engineering Research*, *6*(169–174).

Hendorson, S. M., Pabis, S. (1961). Grain Drying Theory (I) Temperature Effect on Drying Coefficient. *Journal of Agricultural Engineering Research*, *6*, 169–174. Retrieved from https://api.semanticscholar.org/CorpusID:208841650

Hii, C. L., Law, C. L., Cloke, M. (2008). Modelling of thin layer drying kinetics of cocoa beans during artificial and natural drying. *Journal of Engineering Science & Technology*, *3*(1), 1–10.

Iroba, K. L., Mellmann, J., Weigler, F., Metzger, T., Tsotsas, E. (2011). Particle velocity profiles and residence time distribution in mixed-flow grain dryers. *Granular Matter*, *13*(2), 159–168. https://doi.org/10.1007/s10035-010-0222-7

Itasca Consulting Group, I. (2019). *PFC 2D, Version 6.0, Theory and Background Manual.* Minneapolis, USA.

Jain, D., Pathare, P. B. (2004). Selection and Evaluation of Thin Layer Drying Models for Infrared Radiative and Convective Drying of Onion Slices. *Biosystems Engineering*, *89*(3), 289–296.

Jamaleddine, T. J., Ray, M. B. (2010). Application of computational fluid dynamics for simulation of drying processes: A review. *Drying Technology*, *28*(2), 120–154. https://doi.org/10.1080/07373930903517458

Jayas, D. S., Cenkowski, S., Pabis, S., Muir, W. E. (1991). Review of thin-layer drying and wetting equations. *Drying Technology*, *9*(3), 551–588. https://doi.org/10.1080/07373939108916697

Jena, S., Das, H. (2007). Modelling for vacuum drying characteristics of coconut presscake. *Journal of Food Engineering*, *79*(1), 92–99. https://doi.org/https://doi.org/10.1016/j.jfoodeng.2006.01.032

Jia, C. C., Sun, D. W., Cao, C. W. (2000). Mathematical simulation of temperature and moisture fields within a grain kernel during drying. *Drying Technology*, *18*(6), 1305–1325. https://doi.org/10.1080/07373930008917778

Kaleemullah, S., Kailappan, R. (2006). Modelling of thin-layer drying kinetics of red chillies. *Journal of Food Engineering*, *76*(4), 531–537. https://doi.org/https://doi.org/10.1016/j.jfoodeng.2005.05.049

Karathanos, V. T. (1999). Determination of water content of dried fruits by drying kinetics. *Journal of Food Engineering*, *39*(4), 337–344.

Kassem, A. S. (1988). Comparative studies on thin layer drying models for wheat. In *Proceedings of the 13th international congress on agricultural engineering*. Morocco.

Kasuya, E. (2001). Mann–Whitney U test when variances are unequal. *Animal Behaviour*, *61*(6), 1247–1249. https://doi.org/https://doi.org/10.1006/anbe.2001.1691

Kaymak-Ertekin, F., Gedik, A. (2004). Sorption isotherms and isosteric heat of sorption for grapes, apricots, apples and potatoes. *LWT - Food Science and Technology*, *37*(4), 429–438. https://doi.org/10.1016/j.lwt.2003.10.012

Keey, R. B. (1972). Introduction. In R. B. Keey (Ed.), *Drying Principles and Practice* (pp. 1–18). Oxford: Pergamon Press.

Keppler, I., Kocsis, L., Oldal, I., Farkas, I., Csatar, A. (2012). Grain velocity distribution in a mixed flow dryer. *Advanced Powder Technology*, *23*(6), 824–832. https://doi.org/10.1016/j.apt.2011.11.003

Kerr, W. L. (2013). Chapter 12 - Food Drying and Evaporation Processing Operations. In M. Kutz (Ed.), *Handbook of Farm, Dairy and Food Machinery Engineering (Second Edition)* (pp. 317–354). San Diego: Academic Press. https://doi.org/https://doi.org/10.1016/B978-0-12-385881-8.00012-4

Khazaei, J., Daneshmandi, S. (2007). Modeling of thin-layer drying kinetics of sesame seeds: Mathematical and neural networks modeling. *International Agrophysics*, *21*(4), 335–348.

Kieviet, F. G., Van Raaij, J., De Moor, P. P. E. A., Kerkhof, P. J. A. M. (1997). Measurement and Modelling of the Air Flow Pattern in a Pilot-Plant Spray Dryer. *Chemical Engineering Research and Design*, *75*(3), 321–328. https://doi.org/https://doi.org/10.1205/026387697523778

Langrish, T A G, Fletcher, D. F. (2001). Spray drying of food ingredients and applications of CFD in spray drying. *Chemical Engineering and Processing: Process Intensification*, *40*(4), 345–354. https://doi.org/https://doi.org/10.1016/S0255-2701(01)00113-1

Langrish, Timothy A G, Zbiciński, I. (1994). The effects of air inlet geometry and spray cone angle on the wall deposition rate in spray dryers. *Chemical Engineering Research & Design*, *72*, 420–430. Retrieved from https://api.semanticscholar.org/CorpusID:102182234

Lawrence, J., Maier, D. E. (2012). Prediction of Temperature Distributions in Peaked, Leveled and Inverted Cone Grain Mass Configurations during Aeration of Corn. *Applied Engineering in Agriculture*, *28*(5), 685–692. https://doi.org/10.13031/2013.42419

Lewis, W. K. (1921). The Rate of Drying of Solid Materials. *Industrial and Engineering Chemistry*, *13*(5), 427–432.

Li, J., Campbell, G. M., Mujumdar, A. S. (2003). Discrete modeling and suggested measurement of heat transfer in gas-solids flows. *Drying Technology*, *21*(6), 979–994. https://doi.org/10.1081/DRT-120021851

Li, J., Mason, D. J. (2000). A computational investigation of transient heat transfer in pneumatic transport of granular particles. *Powder Technology*, *112*(3), 273–282. https://doi.org/10.1016/S0032-5910(00)00302-8

Li, T., Li, C., Li, B., Li, C., Fang, Z., Zeng, Z., … Huang, J. (2020). Characteristic analysis of heat loss in multistage counter-flow paddy drying process. *Energy Reports*, *6*, 2153–2166. https://doi.org/10.1016/j.egyr.2020.08.006

M. Boac, J., E. Casada, M., G. Maghirang, R., P. Harner III, J. (2010). Material and Interaction Properties of Selected Grains and Oilseeds for Modeling Discrete Particles. *Transactions of the ASABE*, *53*(4), 1201–1216. https://doi.org/https://doi.org/10.13031/2013.32577

Madamba, P. S., Driscoll, R. H., Buckle, K. A. (1996). The thin-layer drying characteristics of garlic slices. *Journal of Food Engineering*, *29*(1), 75–97. https://doi.org/10.1016/0260-8774(95)00062-3

Mahmoudi, A. H., Hoffmann, F., Peters, B. (2014). Application of XDEM as a novel approach to predict drying of a packed bed. *International Journal of Thermal Sciences*, *75*, 65–75. https://doi.org/10.1016/j.ijthermalsci.2013.07.016

Mahmoudi, A. H., Hoffmann, F., Peters, B. (2016). Semi-resolved modeling of heat-up, drying and pyrolysis of biomass solid particles as a new feature in XDEM. *Applied Thermal Engineering*, *93*, 1091–1104. https://doi.org/10.1016/j.applthermaleng.2015.10.033

Mao, H., Wang, F., Mao, F., Chi, Y., Lu, S., Cen, K. (2016). Measurement of water content and moisture distribution in sludge by 1H nuclear magnetic resonance spectroscopy. *Drying Technology*, *34*(3), 267–274. https://doi.org/10.1080/07373937.2015.1047952

Mathioulakis, E., Karathanos, V. T., Belessiotis, V. G. (1998). Simulation of air movement in a dryer by computational fluid dynamics: Application for the drying of fruits. *Journal of Food Engineering*, *36*(2), 183–200. https://doi.org/https://doi.org/10.1016/S0260-8774(98)00026-0

Mellmann, J., Iroba, K. L., Metzger, T., Tsotsas, E., Mészáros, C., Farkas, I. (2011). Moisture content and residence time distributions in mixed-flow grain dryers. *Biosystems Engineering*, *109*(4), 297–307. https://doi.org/10.1016/j.biosystemseng.2011.04.010

Mellmann, Jochen, Gottschalk, K., Istvan, F. (2008). *Development of the heat and mass transfer modell for mixed-flow grain dryer*. *IFAC Proceedings Volumes (IFAC-PapersOnline)* (Vol. 17). IFAC.

Menshutina, N. V., Kudra, T. (2001). Computer aided drying technologies. *Drying Technology*, *19*(8), 1825–1849. https://doi.org/10.1081/DRT-100107275

Menter, F. R. (1993). Zonal two equation k-w turbulence models for aerodynamic flows. *AIAA*, *2906*.

Mercier, S. A. (1989). *Dockage and foreign material in the grading standards for wheat exports. Dockage and foreign material in the grading standards for wheat exports*. Washington, DC: U.S. Dept. of Agriculture, Economic Research Service, Commodity Economics Division.

Midilli, A., Kucuk, H., Yapar, Z. (2002). A New Model for Single-Layer Drying. *Drying Technology*, *20*(7), 1503–1513.

Mohseni, M., Peters, B. (2016a). Effects of particle size distribution on drying characteristics in a drum by XDEM: A case study. *Chemical Engineering Science*, *152*, 689–698. https://doi.org/10.1016/j.ces.2016.07.004

Mohseni, M., Peters, B. (2016b). Effects of particle size distribution on drying characteristics in a drum by XDEM: A case study. *Chemical Engineering Science*, *152*, 689–698. https://doi.org/10.1016/j.ces.2016.07.004

Mohsenin, N. N. (1970). *Physical properties of plants and Animal Materials*. New York: Gordon and Breach Science Publishers Inc.

Montross, M. D., McNeill, S. G. (2005). Permeability of corn, soybeans, and soft red and white winter wheat as affected by bulk density. *Applied Engineering in Agriculture*, *21*(3), 479–484.

Moomhorm, A., Verma, L. R. (1986). Generalized Single-Layer Rice Drying Models. *Transactions of the ASAE*, *29*(2), 587–591.

Mujumdar, A. S. (2007). Transport Properties in the Drying of Solids. In *Handbook of Industrial Drying* (pp. 107–146). United Kingdom: CRC Press.

Mukhopadhyay, S., Siebenmorgen, T. J. (2018). Effect of airflow rate on drying air and moisture content profiles inside a cross-flow drying column. *Drying Technology*, *36*(11), 1326–1341. https://doi.org/10.1080/07373937.2017.1402024

Mukhopadhyay, S., Siebenmorgen, T. J., Mauromoustakos, A. (2019). Effect of tempering approach following cross-flow drying on rice milling yields. *Drying Technology*, *37*(16), 2137–2151. https://doi.org/10.1080/07373937.2018.1564760

Norton, T., Sun, D. W. (2006). Computational fluid dynamics (CFD) - an effective and efficient design and analysis tool for the food industry: A review. *Trends in Food Science and Technology*, *17*(11), 600–620. https://doi.org/10.1016/j.tifs.2006.05.004

Nwaizu, C., Zhang, Q. (2021). Computational modeling of heterogenous pore structure and airflow distribution in grain aeration system. *Computers and Electronics in Agriculture*, *188*. https://doi.org/10.1016/j.compag.2021.106315

Olatunde, G., Atungulu, G. G., Sadaka, S. (2016). CFD modeling of air flow distribution in rice bin storage system with different grain mass configurations. *Biosystems Engineering*, *151*, 286–297. https://doi.org/10.1016/j.biosystemseng.2016.09.007

Overhults, D. G., White, G. M., Hamilton, H. E., Ross, I. J. (1973). Drying Soybeans with Heated Air. *Transactions of the ASAE*, *16*(1), 112–113.

Özilgen, M., Özdemir, M. (2001). *A review on grain and nut deterioration and design of the dryers for safe storage with special reference to Turkish hazelnuts*. *Critical Reviews in Food Science and Nutrition* (Vol. 41). https://doi.org/10.1080/20014091091779

Page, G. (1949). *Factors ınfluencing the maximum rate of air drying shelled corn in thin-layers.* (M.S.Thesis). Purdue University, West Lafayette, Indiana.

Parry, J. L. (1985). Mathematical modelling and computer simulation of heat and mass transfer in agricultural grain drying: A review. *Journal of Agricultural Engineering Research*, *32*(1), 1–29. https://doi.org/10.1016/0021-8634(85)90116-7

Parti, M. (1993). Selection of mathematical models for drying in thin layers. *Journal of Agricultural Engineering Research*, *54*, 339–352.

Perré, P. (2010). Multiscale modeling of drying as a powerful extension of the macroscopic approach: Application to solid wood and biomass processing. *Drying Technology*, *28*(8), 944–959. https://doi.org/10.1080/07373937.2010.497079

Peters, B. (2002). Measurements and application of a discrete particle model (DPM) to simulate combustion of a packed bed of individual fuel particles. *Combustion and Flame*, *131*(1–2), 132–146. https://doi.org/10.1016/S0010-2180(02)00393-0

Phillips, J., Durand-Morat, A., Nalley, L. L., Graterol, E., Bonatti, M., Loaiza de la Pava, K., … Yang, W. (2024). Understanding demand for broken rice and its potential food security implications in Colombia. *Journal of Agriculture and Food Research*, *15*, 100884. https://doi.org/https://doi.org/10.1016/j.jafr.2023.100884

Santeramo, F. G., Lamonaca, E. (2021). Food Loss – Food Waste – Food Security : A New Research Agenda.

Schechter, R. S. (1961). Transport Phenomena (Bird, R. Byron; Stewart, Warren E.; Lightfoot, Edwin N.). *Journal of Chemical Education*, *38*(9), A640-.

Sharafeldeen, Y. I., Blaisdell, J. L., Hamdy, M. Y. (1980). A Model for Ear Corn Drying. *Transactions of the ASAE*, *23*(5), 1261–1265.

Shi, J., Pan, Z., McHugh, T. H., Wood, D., Hirschberg, E., Olson, D. (2008). Drying and quality characteristics of fresh and sugar-infused blueberries dried with infrared radiation heating. *LWT - Food Science and Technology*, *41*(10), 1962–1972. https://doi.org/https://doi.org/10.1016/j.lwt.2008.01.003

Shittu, T. A., Raji, A. O. (2011). Thin Layer Drying of African Breadfruit (Treculia africana) Seeds: Modeling and Rehydration Capacity. *Food and Bioprocess Technology*, *4*(2), 224–231. https://doi.org/10.1007/s11947-008-0161-z

Siatkowski, M., Weres, J., Kujawa, S., Szabelska, A., Zyprych-Walczak, J. (2010). Growth curve functions in modeling the thin-layer drying of corn.

Simsek, E., Brosch, B., Wirtz, S., Scherer, V., Krüll, F. (2009). Numerical simulation of grate firing systems using a coupled CFD/discrete element method (DEM). *Powder Technology*, *193*(3), 266–273. https://doi.org/10.1016/j.powtec.2009.03.011

Sokhansanj, S., Lang, W. (1996). Prediction of kernel and bulk volume of wheat and canola during adsorption and desorption. *Journal of Agricultural and Engineering Research*, *63*(2), 129–136. https://doi.org/10.1006/jaer.1996.0015

Soysal, Y., Öztekin, S., Eren, Ö. (2006). Microwave Drying of Parsley: Modelling, Kinetics, and Energy Aspects. *Biosystems Engineering*, *93*(4), 403–413. https://doi.org/https://doi.org/10.1016/j.biosystemseng.2006.01.017

Sripinyowanich, J., Noomhorm, A. (2011). A New Model and Quality of Unfrozen and Frozen Cooked Rice Dried in a Microwave Vibro-Fluidized Bed Dryer. *Drying Technology*, *29*(7), 735–748.

Straatsma, J., Van Houwelingen, G., Steenbergen, A. E., De Jong, P. (1999a). Spray drying of food products: 1. Simulation model. *Journal of Food Engineering*, *42*(2), 67–72. https://doi.org/https://doi.org/10.1016/S0260-8774(99)00107-7

Straatsma, J., Van Houwelingen, G., Steenbergen, A. E., De Jong, P. (1999b). Spray drying of food products: 2. Prediction of insolubility index. *Journal of Food Engineering*, *42*(2), 73–77. https://doi.org/https://doi.org/10.1016/S0260-8774(99)00108-9

Suarez, C., Viollaz, P., Chirife, J. (1980). *Kinetics of Soybean Drying*. (A. S. E. Mujumdar, Ed.). Washington DC: Hemisphere Publishing Company.

Taiwo, A., Oboho, E., Michael, O. (2008). Investigation into the Thin Layer Drying Models of Nigerian Popcorn Varieties. *Leonardo Electronic Journal of Practices and Technologies*, *7*.

Thompson, T. L. (1968). Mathematical Simulation of Corn Drying – A New Model. *Transactions of the ASAE*, *11*(4), 582–586.

Thompson, T. L. (1969). Comparison of Concurrent-Flow, Crossflow, and Counterflow Grain Drying Methods. *Methods. Agricultural Research Service, U.S. Dept. of Agriculture*.

Tsotsas, E., Mujumdar, A. S. (2007). *Modern Drying Technology Edited by Evangelos Tsotsas and Arun S. Mujumdar*.

Tunde-Akintunde, T. Y. (2011). Mathematical modeling of sun and solar drying of chilli pepper. *Renewable Energy*, *36*(8), 2139–2145. https://doi.org/https://doi.org/10.1016/j.renene.2011.01.017

Turgut, S. S., Küçüköner, E., Feyissa, A. H., Karacabey, E. (2021). A novel drying system – simultaneous use of ohmic heating with convectional air drying: System design and detailed examination using CFD. *Innovative Food Science and Emerging Technologies*, *72*(June). https://doi.org/10.1016/j.ifset.2021.102727

Urumović, K., Urumović, K. (2014). The effective porosity and grain size relations in permeability functions. *Hydrology and Earth System Sciences Discussions*, *11*(6), 6675–6714. https://doi.org/10.5194/hessd-11-6675-2014

Valença, G. C., Massarani, G. (2000). Grain drying in countercurrent and concurrent gas flow - modelling, simulation and experimental tests. *Drying Technology*, *18*(1–2), 447–455. https://doi.org/10.1080/07373930008917715

Vega-Gálvez, A., Lemus-Mondaca, R., Bilbao-Sáinz, C., Yagnam, F., Rojas, A. (2008). Mass Transfer Kinetics During Convective Drying of Red Pepper Var. Hungarian (Capsicum Annuum L.): Mathematical Modeling And Evaluation Of Kinetic Parameters. *Journal of*

Food Process Engineering, *31*(1), 120–137. https://doi.org/https://doi.org/10.1111/j.1745-4530.2007.00145.x

Vengaiah, P. C., Pandey, J. P. (2007). Dehydration kinetics of sweet pepper (Capsicum annum L.). *Journal of Food Engineering*, *81*(2), 282–286. https://doi.org/https://doi.org/10.1016/j.jfoodeng.2006.04.053

Verma, L. R., Bucklin, R. A., Endan, J. B., Wratten, F. T. (1985). Effects of Drying Air Parameters on Rice Drying Models. *Transactions of the ASAE*, *28*(1), 296–301.

Vorhauer, N., Metzger, T., Tsotsas, E. (2010). Empirical macroscopic model for drying of porous media based on pore networks and scaling theory. *Drying Technology*, *28*(8), 991–1000. https://doi.org/10.1080/07373937.2010.497088

Wang, D C, Fon, D. S., Fang, W., Sokhansanj, S. (2004). Development of a visual method to test the range of applicability of thin layer drying equations using MATLAB tools. *Drying Technology*, *22*(8), 1921–1948.

Wang, Dai Chyi, Fon, D. S., Fang, W., Sokhansanj, S. (2004). Development of a visual method to test the range of applicability of thin layer drying equations using MATLAB tools. *Drying Technology*, *22*(8), 1921–1948. https://doi.org/10.1081/DRT-200032878

Wang, G. Y., Singh, R. P. (1978). Single layer drying equation for rough rice. Retrieved from https://api.semanticscholar.org/CorpusID:139792414

Weigler, F., Scaar, H., Franke, G., Mellmann, J. (2017). Optimization of mixed flow dryers to increase energy efficiency. *Drying Technology*, *35*(8), 985–993. https://doi.org/10.1080/07373937.2016.1230627

Weigler, Fabian, Mellmann, J. (2014). Investigation of grain mass flow in a mixed flow dryer. *Particuology*, *12*, 33–39. https://doi.org/https://doi.org/10.1016/j.partic.2013.04.004

Whitaker T, Barre HJ, Hamdy MY. (1969). Theoretical and Experimental Studies of Diffusion in Spherical Bodies with a Variable Diffusion Coefficient. *Am Soc Agric Engrs-Trans*, *12*(5), 668–672. https://doi.org/10.13031/2013.38924

White, G. M., Bridges, T. C., Loewer, O. J., Ross, I. J. (1980). Seed Coat Damage in Thin-Layer Drying of Soybeans. *Transactions of the ASAE*, *23*(1), 224–227.

Wu, X. Y., Fu, Y., Xu, Y. (2013). Risk analysis on grain quality in the drying process. In *Applied Mechanics and Materials* (Vol. 397–400, pp. 1078–1082). https://doi.org/10.4028/www.scientific.net/AMM.397-400.1078

Yiotis, A. G., Stubos, A. K., Boudouvis, A. G., Yortsos, Y. C. (2001). A 2-D pore-network model of the drying of single-component liquids in porous media. *Advances in Water Resources*, *24*(3–4), 439–460. https://doi.org/10.1016/S0309-1708(00)00066-X

Yue, R., Zhang, Q. (2017). A pore-scale model for predicting resistance to airflow in bulk grain. *Biosystems Engineering*, *155*, 142–151. https://doi.org/https://doi.org/10.1016/j.biosystemseng.2016.12.007

Zare, D., Ranjbaran, M. (2012). Simulation and Validation of Microwave-Assisted Fluidized Bed Drying of Soybeans. *Drying Technology*, *30*(3), 236–247. https://doi.org/10.1080/07373937.2011.630765

Zhang, H. (2014). *Research on Property and Mathematical Model of the Corn Low Temperature Deep-bed Drying (in Chinese)*. Jilin University.

Zhang, M., Tang, J., Mujumdar, A. S., Wang, S. (2006). Trends in microwave-related drying of fruits and vegetables. *Trends in Food Science and Technology*, *17*(10), 524–534. https://doi.org/10.1016/j.tifs.2006.04.011

Zheng, X., Wang, C. (1999). Experimental study on the relationship between paddy crack additional percentage and drying conditions. *Transaction of the CSAE*, *15*(2), 194–197.